NATIONAL AERONAUTICS AND SPACE ADMINISTRATION

Technical Memorandum 33-369

Photoheliograph Study for the Apollo Telescope Mount

J. D. Allen

R. A. Happe

L. M. Michal

E .H. Rehnborg

L. M. Snyder

JET PROPULSION LABORATORY

CALIFORNIA INSTITUTE OF TECHNOLOGY

PASADENA, CALIFORNIA

November 1, 1967

NATIONAL AERONAUTICS AND SPACE ADMINISTRATION

Technical Memorandum 33-369

Photoheliograph Study for the Apollo Telescope Mount

J. D. Allen
R. A. Happe
L. M. Michal
E .H. Rehnborg
L. M. Snyder

Approved by:

R K Sloan for

H. G. Trostle, *Manager*
Space Instruments Section

JET PROPULSION LABORATORY
CALIFORNIA INSTITUTE OF TECHNOLOGY
PASADENA, CALIFORNIA

November 1, 1967

TECHNICAL MEMORANDUM 33-369

Prepared Under Contract No. NAS 7-100
National Aeronautics & Space Administration

Contents

I. Introduction 1

II. Scientific Objectives 2

III. *Apollo* Applications Program System Constraints 3

A. Mission Description 3

B. Solar Telescope Mission Profile 6

C. *Apollo* Telescope Mount Mission Module Description 6

D. Environment Description 12

IV. General Description of Solar Telescope System 13

V. Optical Description 15

A. Resolution 15

B. Focus Tolerances 15

C. Multiple Reflections 16

D. Vignetting 17

E. Ray Trace Analysis 18

VI. Engineering Considerations 23

A. Camera System 23

B. Structural Description 27

C. Weights, Centers of Gravity, and Moments of Inertia 28

D. Temperature Control 29

E. Materials 41

F. Telescope Alignment 52

G. Power Conversion and Electrical Distribution 52

H. Reliability and Telescope Test Program 55

Appendix A. Proposal for Photographic Exploration of the Sun 63

Appendix B. Basic Optics and Imaging 81

Nomenclature 101

References 101

Bibliography 103

Contents (contd)

Tables

1. Comparative thermal distortions for various metals 44
2. Solar telescope experiment power 53
3. Solar telescope testing program (parts and components) 56
4. Solar telescope testing program (subsystems) 57
5. Solar telescope testing program (telescope system and ATM) 59

A-1. JPL peak manpower 64
A-2. Performance schedule and JPL manpower 65
A-3. JPL procurement and manpower accumulated costs 66
A-4. *Cost summary* ($ × 1000) 67

Figures

1. *Saturn/Apollo* applications cluster 4
2. *Apollo* applications program mission profile 5
3. Solar telescope 13
4. *Apollo* telescope mount; solar telescope 14
5. Sketch of preliminary design 16
6. Construction for determination of re-reflected radiation on secondary mirror 17
7. Re-reflected radiation on primary mirror 17
8. Vignetting curve, on-axis system 17
9. Spot diagram, all surfaces spherical, $K = 0$ 18
10. Spot diagram, parabolic primary, spherical secondary, $K = 0$ 19
11. Spot diagram, parabolic primary, hyperbolic secondary, $K = 0$ 20
12. Spot diagram, parabolic primary, hyperbolic secondary, $K = 0.5$ 21
13. Spot diagram, parabolic primary, hyperbolic secondary, $K = 1.0$ 22
14. Modulation transfer function, aspheric surfaces, $K = 0$ 22
15. Spot diameter vs back focal length, $K = 0$ 23
16. Earth orbital path of spacecraft in relationship to Sun 24
17. *Apollo* telescope mount; telescope camera cassette accessibility and mechanism 25
18. *Apollo* telescope mount/lunar module modification; solar telescope accessibility of cameras 26
19. Rays from full Sun to primary and secondary mirrors 29

Contents (contd)

Figures (contd)

20. Direct solar energy received by primary mirror 30
21. Division of primary mirror into 3 zones 31
22. Zone I of primary mirror 31
23. Zone II of primary mirror 32
24. Zone III of primary mirror 32
25. Final plot of surface temperature vs radial distance from center of primary mirror 34
26. Temperature zones 35
27. Analysis configuration 35
28. Top surface distortion normal to top surface for various boundary conditions 36
29. *Apollo* telescope module; active thermal control 38
30. Primary mirror heaters; method 4 40
31. Schematic presentation of heat distribution; on-axisCassegrainian system . . . 42
32. Schematic presentation of energy incipient on primary mirror for extreme positions of solar observation 42
33. Compatibility of hard-coating materials with invar 48
34. Spectral reflectance of vapor-deposited aluminum and silver 51
35. Electrical power demands during orbiting 54
36. Optics for the collimator 61
A-1. Projected accumulated JPL cost ($ × 1000) 64
A-2. High-resolution solar telescope; functional block diagram 70
A-3. Solar telescope 71
A-4. Schematic diagram of optical system of solar telescope 72
A-5. TV subsystem functional block diagram 73
A-6. Electrical power consumed during hypothetical orbit (total connected load = 503 w) 74
A-7. Solar telescope TCM in 10-ft solar and space simulator 79
B-1. Spherical mirrors 81
B-2. Cassegrainian optical system 82
B-3. Construction for conic mirrors 82
B-4. Construction for tolerance determination 83
B-5. Construction (1) for vignetting by secondary mirror 84

Contents (contd)

Figures (contd)

B-6. Construction (2) for vignetting by secondary mirror 84

B-7. Construction (3) for vignetting by secondary mirror 85

B-8. Intensity distribution of diffraction pattern for circular aperture 86

B-9. Sinusoidal variation of intensity 86

B-10. Example of modulation transfer function 87

B-11. Intensity distribution of diffraction pattern for ring aperture 87

B-12. Contrast curve for ring aperture 88

B-13. Construction for heating factor determination, on-axis system 88

B-14. Tube length vs heating factor, on-axis system 88

B-15. Focal length vs heating factor, on-axis system 89

B-16. Construction for mask diameter determination, on-axis system 89

B-17. Construction for secondary diameter determination, on-axis system 90

B-18. Construction for primary hole diameter determination, on-axis system 90

B-19. Construction for determination of diameter of re-reflected radiation on primary mirror 91

B-19A. Construction for determination of vignetting by primary mirror, on-axis system 91

B-20. Front view, off-axis system 92

B-21. Construction for heating factor determination, off-axis system 93

B-22. Tube length vs primary focal ratio, off-axis system 93

B-23. Focal length vs heating factor, off-axis system 93

B-24. Construction for determination of radius of secondary mirror, off-axis system 94

B-25. Construction for determination of radius of mask, off-axis system 95

B-26. Construction for determination of $R_h = (R'_s + \omega)$, off-axis system 95

B-27. Construction for determination of radius of re-reflected radiation, off-axis system 96

B-28. Rayleigh criterion vs telescope aperture 96

B-29. Design constraint (1), on-axis system 98

B-30. Design constraint (2), on-axis system 98

B-31. Preliminary design, on-axis telescope 99

B-32. Design constraint (1), off-axis system 100

B-33. Design constraint (2), off-axis system 100

Abstract

An optimized flight-telescope system is analyzed to determine the feasibility of conducting a flight program with a moderate size solar telescope on the *Apollo* Telescope Mount (ATM). Information is summarized to obtain high-resolution photography in the near UV, white light, and near infrared. Problem areas are delineated for future study. Appendices review the geometry of the optics and a general plan to conduct the flight program.

Photoheliograph Study for the *Apollo* Telescope Mount

I. Introduction

The activity reported herein was started in December 1966 and concluded in June 1967. The goal was to create a conceptual design of a solar telescope which could be included in the *Apollo* Telescope Mount (ATM) program as part of the *Apollo* extension programs. The task was accomplished under the direction of Prof. Harold Zirin of Caltech as the principal investigator with Dr. Robert Howard of Mount Wilson and Palomar Observatories as co-investigator. Dr. Mitzugu Makita, a research fellow at Caltech, provided valuable consultation in the optical design area. The JPL personnel were: J. D. Allen, task leader; R. A. Happe, materials; L. M. Michal, system design; S. E. Persson, experiment description; E. H. Rehnborg, mechanical design; L. M. Snyder, optical design; Dr. J. M. Vickers, thermal design; and P. F. Gott, scale model testing. We would also like to recognize B. K. Wada who provided consultation and analysis on distortional behavior of mirror materials, and E. F. Dobies who participated in discussions of photographic techniques.

An early conclusion of the study was that a proposal for a flight instrument be prepared and submitted to NASA, OSSA. Such a proposal was written and is included as Appendix A.

The thermal control problem is believed to be the most challenging from an engineering standpoint. For this reason it was concluded that a telescope configuration be selected for detail analysis in an attempt to discover the magnitude of the problem. The optical configuration presented in this report is not necessarily the optimum configuration for the flight instrument, but represents a design which will satisfy the requirements of the experiment and allow detail thermal analysis.

It was discovered early that the final performance of the telescope will depend heavily on the selection of materials, so considerable effort has been devoted to the study of materials compatible with optical figuring.

A section describing a possible mission profile has been included for completeness. It is believed that the auxiliary equipment such as the TV camera, film cameras, and electronic equipment such as the control console are reasonably straight-forward design problems and thus have only been treated lightly in the report.

Areas receiving considerable attention in the follow-on work will include:

(1) In-flight alignment and focus

(2) Optimization of the optical configuration

(3) Ground testing and calibration

(4) Structural design

(5) Thermal design

(6) Material selection

(7) Film utilization and filters

II. Scientific Objectives

In the study of any astronomical body, simple spatial resolution of the morphology of the body has always played an extremely important role. In recent years, this has been graphically illustrated by the great improvement in our knowledge of the Moon and Mars, resulting from vehicles such as Mariner and Ranger which have enabled us to obtain photographs from close range. In the case of the Sun, which may be said to be the most important astronomical body, the same improvement in our knowledge has come from the use of higher resolution. The improvement over the past has not come in such dramatic steps as were produced by the Ranger and Mariner spacecraft. We can safely say that many of the features we are studying today were discussed by careful observers one hundred years ago. This is because the terrestrial atmosphere limits daytime seeing to ½ s of arc at best for a few brief moments at a few selected places. The seeing at most established solar observatories is very poor most of the time, and even at best is not better than a second of arc under typical "good conditions." Still, careful analysis of direct photography and cinematography of the Sun through various filters has provided a wealth of information about the structure of the surface and the physical conditions of the Sun. In the one attempt so far to carry out photography of the Sun from above the terrestrial atmosphere (Schwarzschild's Stratoscope I program), a great advance was made in our knowledge of solar granulation through a relatively short white-light motion picture. Although present techniques enable us to almost duplicate this motion picture from ground based observations, there is no doubt that it provided us with important new information on surface structure.

Our present situation in solar physics is that we see a great many surface phenomena with scales greater than 700 km (1 s of arc). We have some idea of the physical conditions in these phenomena from spectroscopy, although we are never sure because of the difficulty of interpretation and because of producing spectra of a given small element of the surface. The explanation of the behavior of these structures is to be sought in further application of spectroscopy, and in the pursuit of higher resolution down to the mean free path of particles in the solar atmosphere. Several features on the Sun's surface which are presently observed at the Earth with a 1-arc-second resolution will now be described and considered, keeping in mind the 0.15-arc-second resolution attainable with the proposed telescope.

In white light the Sun appears as a sharply defined sphere of diameter 1.39×10^{11} cm, or about 30 min of arc at the distance of the Earth. This "surface," called the photosphere, is mainly composed of hydrogen gas at a mean temperature of about 5750°K, flowing generally radially outwards, but showing a definite oscillatory motion which appears as a granular pattern of bright cells 700–1000 km in diameter on the average, separated by darker lanes about 300 km wide. Thus, these granules and dark lanes are evident at the present limit of resolution. It is possible that greater detail, such as dark lanes 100 or 200 km wide, may exist; the 100-km resolution considered in this report will certainly define it.

Firmly established cell sizes coupled with the time correlation data of granule lifetimes (8 min on the average) to be obtained in continuous photography will define the motion of the granules much more rigorously, and set new constraints on the theory of convective energy transport at the altitude of the photosphere.

Two forms of data, spatial and temporal correlations, will also be useful in studying granulation within and around sunspots. High-resolution extended films of these active areas of the Sun are sorely needed. In particular the penumbrae of sunspots and the photospheric areas around large, complex sunspot groups will give useful information on magnetic field structure and changes as a function of time, in particular before and after periods of intense solar activity. Present data on the changes that take place in photospheric granules, bright areas, and in general a whole sunspot region during a period of enhanced activity are limited in precision by atmospheric seeing and short observation periods. Resolution on the order considered here will certainly help to correct this deficiency.

It will be of great interest also to compare the UV pictures of the photosphere obtained simultaneously with the white light and H_α photographs. A measure of the

UV flux enhancement over an active region will be obtained and will give a clearer understanding of the mechanism, and time sequence as a function of wavelength of the enormous energy release at the surface. Time correlations of the above mentioned type will also clarify possible triggering of one event (such as a flare or surge) by another.

In the H_α wavelength band, several photographic techniques are made possible by the use of a tunable narrow band filter. Simply, the Sun can be photographed in the H_α line and the active regions correlated in the three sets of pictures. The Lyot filter can set a narrow window to one side of the H_α line center, and in this way up and down motions of the gas can be monitored, as the light intensity seen by the camera will vary when the H_α line is doppler shifted back and forth across the narrow window. More sophisticated tuning and switching techniques make possible a very detailed picture of gas motion in high resolution.

The higher resolution of this instrument will be applied to phenomena in the chromosphere, the thin (1500 km) shell of gas overlying the photosphere. A sudden brightening and density increase in the upper chromosphere and lower corona (the bright halo extending millions of miles out from the Sun) is often observed over active regions. This form of energy release, called a flare, is brightest in H_α and is accompanied by enhanced radio emissions, X-ray flux, high energy proton and heavy nucleon flux, and solar wind. These particle and radiation emissions are known, but the flare triggering mechanism and the detailed structure of the flares, which consist of knots and threads of gas, just on present limits of resolution, have not been explained. Magneto-fluid dynamic wave-coupling of flare events at large separations was thought to have been observed. In the H_α wings such transverse oscillations may be detected in greater detail close in to active regions.

Also connected with the magnetically enhanced regions are the thin (800 km) vertical jets of emitting gas (spicules) which occur in groups and extend to 5000-km heights above the temperature minimum of 4500°K in the chromosphere. Up to now the best picture we have of them relies on fuzzy images occupying 10, 20, or 50 film grains on exceptional frames. Studies of spicule lifetimes will lead to a better understanding of this mode of convective energy transport through the upper chromosphere. Cinematography and optical correlations with the other two wavelength regions will also reveal the spicule sources in the low chromosphere. Cinematography in the H_α wings shows a remarkable brightness oscillation similar to that observed in the weaker Fraunhofer lines, but the relationship between the two is at present not clear. In every case, the information obtained with this telescope will be useful from the standpoints of resolution, time and wavelength correlations, and length of observation time. These studies will also generate further and more extensive spectroscopic studies of the features listed above; thus the step taken in this experiment represents a logical one in the sequence of investigations of solar surface phenomena.

III. *Apollo* Applications Program (AAP) System Constraints

A. Mission Description

As a basis for analysis of the solar telescope system requirements, we may presume that the experiment will be conducted in a clustered mission module orbiting the Earth in space at a low altitude. The cluster would contain an Orbiting Workshop (OWS), an *Apollo* Telescope Mount (ATM), an Airlock Module (AM), and a Multiple Docking Adapter (MDA). This arrangement illustrated by Fig. 1 will be serviced by a series of Command Service Modules (CSM) which will provide the logistics support for the missions.

The mission of the cluster involves the activation and re-use of the OWS and ATM and the demonstration of extended station keeping by each astronaut crew for periods up to 56 days. In the low altitude orbit, the lifetime of the cluster is expected to be two years. A subsequent re-use of the experiment's equipment is anticipated. It may imply that certain equipment should have provisions for up-rating by modifications in orbit in order to conduct other experiments. We can analyze the system for this purpose.

The combined mission will use up-rated *Saturn I* vehicles for the four launches to assemble the cluster module. Figure 2 illustrates the combined mission profile for the events.

At the time when the ATM vehicle containing the proposed solar telescope should be launched, the manned orbiting cluster could contain at least one other ATM (AAP-III) in a docked condition, such as shown in Fig. 2. The moment of inertia of the cluster under that condition would be increased; consequently, the oscillating rates will be further reduced, to ease the docking of the solar telescope to the cluster in a *hard docked mode* for performing experiments under this condition. During active

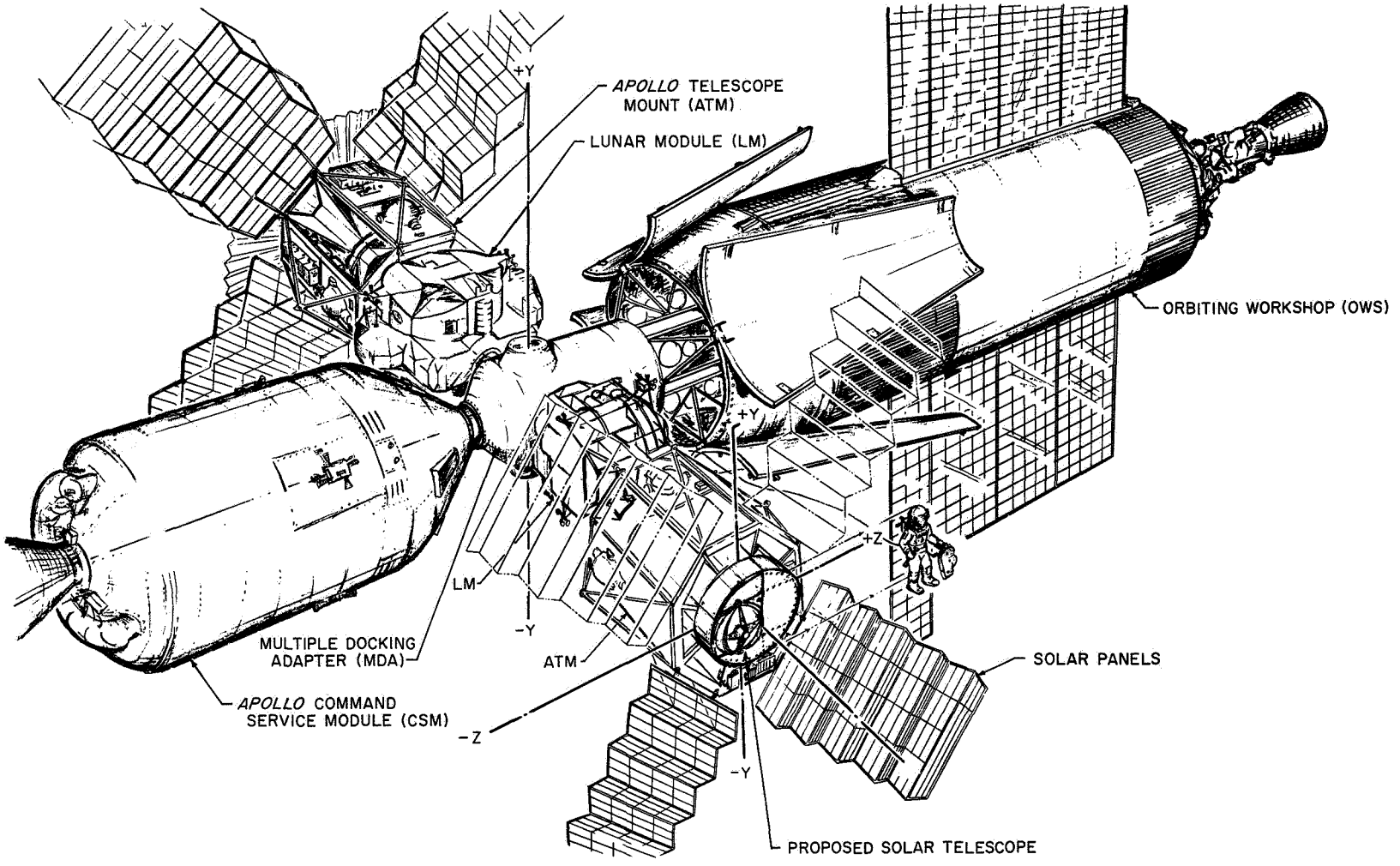

Fig. 1. *Saturn/Apollo* applications cluster

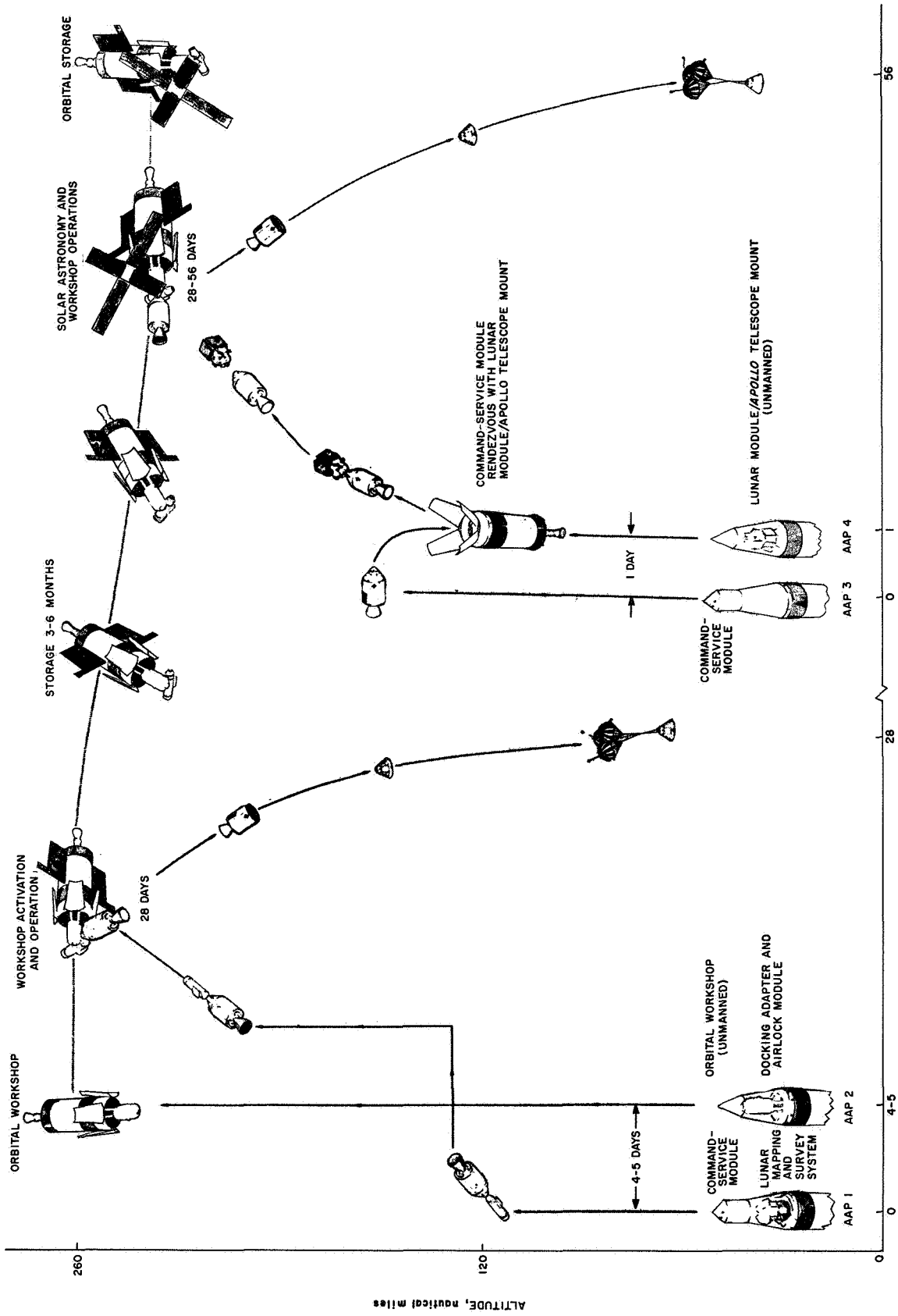

Fig. 2. *Apollo* applications program mission profile

operation, it is expected that the clustered configuration will stay inertially fixed—solar oriented with the longitudinal axis of the cluster constrained to lie in the orbital plane.

Although it is not clear at this writing to what extent the accommodations in the clustered vehicles could service the experiment requirements, at least it is necessary that provisions should exist in the command module, which would be returning to Earth, for stowing the exposed film cassettes after they have been retrieved from the telescope cameras. Prior to the launch for the experiment, the camera cassettes will be loaded with film and installed in place. Requirements will also be analyzed to carry additional reload film or film cassettes to be taken in the *same* launch. It is further considered that the exposed film cassettes should be removed from the cameras and stored in the OWS in the event that the overall mission requirements should be extended beyond the mission phase of the solar telescope. The purpose is to minimize exposure to the radiation hazards.

It is recognized that the design of the cassette shielding cannot become heavy and bulky because the returning command module has limitations of weight and storage space. A possible design approach is to add shielding around the camera structure. Such protective shielding can be moved aside by the crew during an extra vehicle activity (EVA) retrieval of the cassettes.

B. Solar Telescope Mission Profile

The solar telescope and its mission-dependent equipment, installed in an un-manned LM/ATM vehicle, will be carried by an up-rated *Saturn I* vehicle through a direct ascent flight path and injected into a low-altitude inclined, circular, Earth orbit. At the time of launch, all power to the telescope is *off*, the cover is closed and the mirror caging supports are in place. At the injected altitude (200–220 n. mi.), and at the proper phase relationship with a previously launched AAP containing a manned re-supply CSM with the provisions for returning exposed solar telescope film, the CSM will rendezvous with the LM/ATM. All power to the telescope is still off, except the thermal control system is on and mirror caging supports are in place.

The CSM and the ATM will execute a transfer to the orbiting plane of the *Saturn–Apollo* cluster. Upon reaching the rendezvous position, crew members of the CSM will leave and enter the Lunar Module (LM) and proceed to check out the LM/ATM system. The checkout procedure for the solar telescope will include a number of control check points. After the checkout of the LM/ATM and the solar telescope, the solar telescope power will be turned off, except for the thermal control system. The mirror support will be re-caged.

The LM/ATM will separate from the CSM and dock with the *Saturn–Apollo* cluster. All power for the solar telescope remains off, except the thermal control unit. The mirror supports will remain caged.

After the CSM has docked at the MDA port in line with the OWS, the LM crew will proceed to complete the checkout of the entire LM/ATM system. At this time, the ATM solar panels are extended. The solar telescope and all mission-dependent equipment in the LM/ATM will be energized in preparation for functional checkout. All mechanisms will be operated and secured in a stand-by mode. The mirror supports will be un-caged and an alignment check of the optics will be conducted to see if launch and docking loads have changed the optics alignment. In the event that a primary mirror adjustment is required, a member of the crew will conduct the EVA procedure, using the adjustment tool from the solar telescope kit.

As soon as the solar telescope has been prepared for an experiment, all operating units will be placed in a stand-by mode. At the direction of the principal investigator, who is located at the ground laboratory but in voice communication with the LM/ATM crew, all solar observation experiments using the telescope will proceed under his direction.

When the observations and photography of the Sun have been completed, the telescope system will be placed in the orbiting storage mode. A member of the crew will leave the *Saturn–Apollo* orbiting cluster and remove the exposed film cassettes. The cassettes will be transferred to the command module for storage. Subsequently, the CSM will un-dock from the *Saturn–Apollo* orbiting cluster and return the film to Earth.

After spacecraft (CM) recovery, the sealed cassettes will be removed and safely stored in the recovery vessel, later being transferred under a controlled environment to the principal investigator. Under *no* conditions will the cassettes be opened prior to delivery to the principal investigator.

C. *Apollo* Telescope Mount Mission Module Description

On the basis of the requirements which would influence the design and operational requirements of the solar telescope, the ATM mission module definition is reviewed.

The ATM mission module is understood to contain the following vehicles and mission arrangements:

(1) An LM vehicle which will be a modification of the ascent stage, with the provisions to carry an ATM and conduct the solar observations.

(2) An ATM which will contain the experiment package.

As a further constraint on the design, it is understood that the LM/ATM with the solar telescope may be operated in a CSM docked mode, or in a free-flight or tethered mode, in the event a hard dock to the orbiting cluster cannot be performed.

The LM ascent stage is to provide the crew volume and provisions for operations of the ATM system. These would include a thermal control of the LM electronic systems, the necessary guidance, navigation communications, telemetry and control, including a Radio Command System (RCS) for the various mission requirements which have been described. The integrated ATM system shall withstand the induced environment of the up-rated *Saturn I* launch vehicle during launch and orbital operations.

The total lift-off weight of the AAP mission containing an ATM/LM payload at the 240-n. mi. altitude is anticipated not to exceed 28,300 lbs. (12,837 kg).

Maintenance, repair and replacement activities are being considered in the design of the ATM. The work would be scheduled during an orbital storage period.

The ATM system is composed of the following subsystems:

(1) Structural and mechanical

(2) Pointing control

(3) Electrical power

(4) Instrumentation and communications

(5) Experiment (solar telescopes)

1. Structural and mechanical subsystem.

a. Rack. The rack which will carry the ATM systems is an octagonal truss structure, 97.5 in. (247.65 cm) deep. It provides structural support for the gimballed ATM experiment package and support equipment (such as batteries and control-moment gyros), and for the LM ascent stage. It attaches to the launch vehicle at the four SLA/LM support points and provides the lateral stiffness required by the SLA.

The structure for both the forward and aft planes of the rack is a shear web beam running around the periphery of the octagon, giving a clear area [inscribed circle diameter of 112.8 in. (286.512 cm)] in the center of the plane to provide clearance for the ATM experiment package.

A 102-in. (259.08-cm)-diameter experiment package support ring is carried at the center of the rack and supports the gimbals required for fine pointing. Loads on the experiment package support ring are distributed through the structure by a shear web system connecting the corner fittings to the support ring.

b. Experiment package. The structure of the ATM experiment package is an 82-in. (208.28-cm)-diameter cylinder with a length of about 130 in. (330.2 cm). A cruciform spar extends the length of the configuration and divides the cylinder into four equal parts. A nonstructural shroud encompasses the package for thermal and contamination control. The proposed solar telescope with other ATM experiments would be mounted on a modified cruciform spar similar to the ATM-A design. The outside edges of the cruciform are tied together locally by a girth ring in the plane of the support ring of the rack (coincident with the c.g. plane of the experiment package). The girth ring is required to resist out-of-plane inertia loads on the cruciform and to introduce pitch and yaw vernier control moments into the package.

The experiment package is attached to the support ring by a gimbal system. The gimbal system consists of a gimbal ring, two inner and two outer flexure pivots, and a bearing ring. The bearing ring is attached to the support ring and provides a $\pm$95-deg roll capability for the experiment package. The gimbal ring connects the two inner flexure pivots to the two outer flexure pivots, and provides a maximum of $\pm$3-deg pitch and yaw motion.

The ATM experiment package is mounted parallel to the thrust axis of the rack, and its c.g. is located in the plane of the support ring. The experiment package extends aft to the maximum distance allowable for clearance of the forward bulkhead of the *S-IV B* stage. It partially extends forward into the engine bay of the LM ascent stage.

c. Thermal control. ATM thermal control requirements fall into two general categories: (1) the telescopes and related equipment located within the experiment package, and (2) rack-mounted components, such as control moment gyros, and batteries, etc. Rack-mounted components and individual quadrants of the experiment package receive varying amounts of radiation depending on their location relative to the Sun, Earth, solar arrays, OWS, and CSM. All components will be designed for operation in the various mission modes.

It is understood that rack-mounted components, with the possible exception of the batteries and pointing control system (PCS), electronics will be passively thermal controlled. Case temperatures of $70 \pm 5°F$ will be provided. Provisions for stability over 15-min exposure times are available. The proposed solar telescope will require stability over a 30-min period for certain observations.

The pointing stability requirements of ± 2.5 arc seconds dictate the maximum allowable spar distortion during an exposure period, defining spar thermal control requirements. To meet these requirements, it is anticipated that the cruciform (spar) be fabricated of a thick, highly conductive material, and that the skin of the experiment package be structurally connected to the spar only with low conductance attachments. Thermal studies have been based on a mounting spar of 1-in. (2.54-cm)-thick aluminum plate. These studies show that spar stability of 1 to 2 arc seconds can be maintained over a 15-min exposure period, provided that the total mount conductance per telescope does not exceed 0.6 Btu/h °F. Spar stability studies have not considered the effect of heat transfer through the gimbal structure, but it is believed that adequate spar stability can be maintained through the use of insulation and/or local heaters on the gimbal structure.

Spar stability is maintained by limiting the spar temperature gradients. These gradients are controlled by (1) thermally isolating the spar through the use of low conductance nonredundant mounts and high performance insulation, (2) using a thick, highly conductive spar material, and (3) minimizing the connections between the cruciform and the surrounding structure and shroud.

The experiment temperature is controlled by radiant transfer of heat from the experiment to the inside wall of the thermal shroud. The shroud is designed to transfer all heat generated by the experiments to the outer skin which radiates to space. The shroud's inner and outer surface will have a black coating. Telescope mounted heaters should be used to prevent the experiment temperature from falling below 65°F. Variable thickness insulation around the telescope can be used as required to control temperature gradients within the experiment.

2. Pointing control subsystem (PCS). A System for Inertial Experiment Pointing and Attitude Control (designated SIXPAC) has been selected for use in the PCS design.

The PCS consists of two basic parts: the coarse, and the fine pointing control subsystems. The PCS will be designed to meet the following requirements:

Pointing accuracy:	± 2.5 arc seconds (pitch and yaw) ± 10 arc min (roll)
Pointing stability drift area:	± 2.5 arc seconds/15-min period (pitch and yaw)
	± 7.5 arc min/15-min period (roll)
Jitter rate:	± 1 arc second/second (pitch and yaw)
	± 1 arc min/second (roll)
Pointing offset:	Repositioning capability from any point to any other point within a ± 21-arc-min square nominally centered on the solar disc. The time to accomplish the maneuver, including settling time at the new point, shall not exceed one minute.
Roll orientation:	± 95 deg from zero roll reference

The coarse control subsystem will be designed to be capable of solar acquisition, orbital plane acquisition, automatic hold operation, and manual operation. It will be capable of maintaining control of the cluster configuration or optional modes of operation.

The fine pointing control subsystem will be designed to be capable of acquisition, offset pointing, automatic attitude hold operation, and manual operation.

a. Coarse pointing control. Based on the SIXPAC Control Moment Gyros (CMG) configuration and a two-axis fine suspension system, three double-gimballed CMG's are aligned with the axes of the Lunar Module (LM). The CMG's provide all vehicle attitude stabilization functions during those phases of the mission required to meet the ATM mission objectives. The CSM RCS will be used for CMG momentum dumping when the LM/ATM is docked to the cluster. During LM/ATM free-flight or tethered

operations, the LM RCS will be used for momentum dumping. It is presently anticipated to keep each CMG at full momentum capacity after startup.

When the vehicle passes from sunlight into the Earth's shadow, pitch and yaw utilize the same attitude hold mode capability as for roll. Within the gyro and inertial attitude integrator drift capability, the vehicle remains nominally pointing in the direction maintained before passing into the Earth's shadow (i.e., remains approximately solar oriented). Assuming this attitude hold mode to be maintained when the Sun is reacquired upon passing out of the Earth's shadow, small attitude maneuvers (either manual or automatic) would be necessary to again boresight the pitch and yaw fine pointing sensors on the solar disc.

To allow maximum utilization of the time while in daylight for experiment data collection or solar monitoring, it is anticipated that all CMG momentum dump phases take place while the vehicle is in the Earth's shadow. Dumping may be performed at any point in the orbit if required.

b. Fine pointing control. Fine pointing control will be provided in the pitch and yaw axes to isolate the telescope package from the disturbance torques in the cluster. A closed-loop torque system operating from a fine Sun sensor package and gyro package mounted on the spar will provide necessary stabilization to insure required stability.

The boresight accuracy of both pitch and yaw will be ± 1.25 arc seconds. The experiment package can be offset pointed in pitch and yaw within a ± 24-arc-min square centered on the solar disc. The fine pointing control design will have an offset rate command capability of at least 80 arc seconds/second and a null pointing accuracy of $< \pm 2$ arc seconds.

The basic line of sight reference for fine pointing will be provided by the fine Sun sensor. However, all observations and offset pointing decisions made by the astronaut will be made using the experiment boresight or H_α telescope displays.

Whenever the experiment optical axis must be aligned to a solar target closer than the alignment tolerances permit ($< \pm 1$ arc min), the astronaut must manually correct the pointing as determined from the boresight display.

Roll positioning is accomplished by manual control of the roll drive mechanism in increments of 6 arc min to any desired positions up to ± 95 deg. Fine adjustment of the roll position is accomplished by manual control of the CMG system. The zero roll reference (North ecliptic or solar North) is provided by the star-tracker system. The longitudinal axis of the cluster is maintained in the orbital plane by utilizing the star-tracker system.

A fine Sun sensor provides the attitude information necessary for fine pointing control of the ATM experiment spar. The fine Sun sensor package contains four single axis trackers for experiment spar pitch and yaw attitude information. Four detectors provide complete redundancy in the package and enhance the reliability of the system. The associated electronics package contains the required electronics to condition the detector outputs into useful attitude error signals, provides the digital pulse rates for offset and scanning operation, and provides the digital readout information for accurate offset pointing.

*3. **Electrical power subsystem.*** The electrical power system being designed for ATM system will provide the power for the LM ascent stage as well as the ATM systems. A combination of solar cells and rechargeable batteries will be utilized. The solar arrays (panels) will be deployed in each quadrant from the Sun end of the ATM, as shown in Fig. 1.

a. Power distribution. Solar power from the four wings is routed through the solar power distributor to each of the 24 power modules. Each power module contains a battery charger, a battery, a regulator, and sensing and control circuitry. Power module outputs are connected in the main power distributor to form two 28-v direct current (Vdc) buses.

The solar power and main power distributors provide interconnection for supplying power to the 28-Vdc buses from electrical support equipment (ESE) during prelaunch checkout. Each power module can be switched on or off by the switch selectors; one command operates the charger and regulator, and one command operates the charger only.

Each ATM load receives power from both buses. Protective circuitry is included between the buses and the loads. Failure of either of the buses and associated circuitry will not degrade the system. The two LM/Ascent stage buses are regarded as two separate loads and receive

power from both ATM buses. The two LM/Ascent buses are also diode isolated from the ATM buses.

b. Solar power. A solar cell power system utilizing a modular approach will be used to meet the ATM mission requirements. The modular approach provides design flexibility, unit replaceability, and convenient item size for testing, shipment, and handling.

By using 6 cells in parallel and 114 in series, the module will have 684 2×2-cm cells. They are 0.015-in. (0.0381 cm) thick and will be protected from micrometeorite erosion by 0.12-in. (0.0305-cm) spectrally selective quartz cover slides. The module substrate will be honeycomb material. The module in-space power rating at the beginning of the mission will be 23.00 w at 70°C and is expected to degrade to 21.50 w at 70°C at the end of one year in a 260-n. mi. (481,520-m) orbit.

The solar array will supply a sufficient amount of power at the beginning of the mission to meet the total load requirement. The average power required is anticipated to be approximately 3200 w.

At the beginning of the mission this solar array could supply as much as 9200 w at 70°C, and at the end of the mission could still supply 8600 w at 70°C.

c. Networks. The ATM networks will be designed to minimize the number and size of wires connecting the ATM to the control panels in the LM ascent stage. The networks design will also provide remote checkout capability and maximum design flexibility when interfacing with experiments.

Command signals to the ATM from the control panel are classified as coded command signals and manual command signals.

The coded command signals drive a switch selector which provides a discrete output to the control distributor. A system utilizing three switch selectors can provide 336 discrete outputs with only 22 input wires. The switch selectors interface with the command decoder to provide remote checkout and control.

Manual command signals will be limited to those that control crew safety items or involve the crew as part of the control loop, and commands that switch ATM control panel meter readings. Manual command signals will also be used for those commands which would require excessive time if they were coded.

d. Controls and displays. The control and display panel located in the LM ascent stage will serve as the experiment work station. The panel will be used by an astronaut to control and monitor the experiments, the pointing control system (PCS), and the power system. Panel controls for these three major functions are divided into hardwire commands and binary-coded commands. Hardwire is used for those functions affecting crew safety, having high repetition rates, requiring quick reaction times, or using analog systems.

To conserve panel space, all displays and controls are time-shared between systems when possible. All commands not hardwired are originated on a time-shared basis by the use of a digital keyboard which stimulates *Saturn*-type switch selectors. Almost all of the panel functions can be accomplished by RF command during remote checkout.

The power control switch selector keyboard provides individual power modules control. Status monitoring of power module temperature, voltage, and current is on a time-shared basis.

The PCS controls are used for system activation, vehicle pointing, and station-keeping by experiment Sun acquisition, and manual pointing and associated PCS "housekeeping" monitors and controls. The manual pointing mode utilizes a hand control unit with visual reference provided by vidicon and digital displays.

Experiment controls will share the keyboard used by the PCS and the power system. Other commands and displays will be time-shared between experiments whenever possible, with task analyses and detailed time lines being the major determining factors.

An astronaut's display of the solar disc will be obtained from the ATM H_α telescope. The system will include a telescope, H_α filter, and vidicon camera. By astronaut commands the system will provide displays in H_α and white light.

Experiment pointing will utilize the PCS manual mode when offset pointing from the Sun's center is required. The offset coordinates will be displayed so that areas of interest may be noted for repeated investigation. The video displays will be switched to the appropriate TV camera for each experiment.

4. Instrumentation and communications. The instrumentation and communications subsystem (I & C) for

ATM will be located within the rack and will be essentially independent of the LM ascent stage. It consists of measuring, telemetry, command, antenna, and TV subsystems which will be designed to provide the following functions. There will be approximately 400 ATM measurements telemetered. These measurements are related to vehicle checkout, environmental control, electrical, electronic, and pointing control systems, and experimental scientific and housekeeping data. A command link will be provided for checkout and activation of systems. A closed circuit TV subsystem for experiment monitoring will be provided. Voice communications between the LM and CSM and the LM and ground will be provided by the basic LM communication subsystem when operating separately. When the LM is docked to the MDA, the primary voice communications will be provided by hard-line audio circuits to the CSM. Similarly, after docking, primary communications between the LM and the MSFN will rely on the hard-line audio link to the CSM and the CSM radio frequency links to the MSFN.

a. Measuring. The measuring subsystem consists of transducers and signal conditioners. Transducers are located at selected measuring points and electrically connected to measuring racks. A modular signal conditioning arrangement provides compatibility between the various transducer outputs and the input characteristics of the telemetry subsystem.

b. Telemetry. The telemetry subsystem consists of equipment for analog and digital multiplexing, encoding and formating, storage and playback, and VHF transmission. The electrical support equipment (ESE) associated with telemetry consists of a digital data acquisition system (DDAS) station and a telemetry receiving station for testing, checkout, and prelaunch activities.

The telemetry subsystem utilizes a pulse code modulation (PCM) technique which provides a variety of sampling rates. All measurements are routed directly or via multiplexer to the Model 301 PCM/DDAS assembly where a 75 k bit per second serial wavetrain is generated to frequency modulate a 10-w VHF transmitter.

A parallel output from the Model 301 Assembly is routed to the Auxiliary Storage and Playback (ASAP) unit where 4 k bit per second of experiment data is extracted and recorded for 90 min. The stored data are then played back, by astronaut or ground command, in 5 min over one ground station. During playback, the ASAP provides a 72 k bit per second PCM serial wavetrain which frequency modulates a second 10-w VHF transmitter.

The use of two transmitters precludes loss of scientific data during playback. Partial transmission redundancy in case of contingencies is provided by connecting the modulation inputs to the two transmitters through a switching arrangement located in an electrical distributor. If one transmitter fails, the other can be time-shared by the two PCM serial wavetrains, with some resulting loss of data. Both the Model 301 Assembly and the ASAP unit provide a 600-kHz FM carrier, modulated by the 72 k bit per second wavetrains, as the DDAS output for use during testing, checkout, and prelaunch activities.

c. Command. The digital command subsystem is composed of an MCR-503B command receiver and command decoder to provide the required command inputs to the switch selectors and ATM control computer.

The command receiver (carrier frequency 450 MHz) is modulated by a phase shift keyed composite baseband waveform containing binary intelligence. The receiver separates the baseband data from the carrier and feeds it to the decoder where it is demodulated. The decoder recovers the transmitted 35-bit command word, performs an error check, and presents 18 information bits to be used as required by the switch selectors and flight control computer.

d. Antenna subsystem. An antenna subsystem will be designed to accommodate the 450-MHz command subsystem and the VHF telemetry subsystem. It will provide adequate gain and angular coverage to satisfy operational requirements. These antennas are located on separate panels located on the ends of two of the solar panel wings. Studies are being performed to determine the possible detrimental effects, on the antenna patterns, caused by the clustered configuration.

5. Experiment (solar telescopes). Five TV cameras and control units, one sync generator, and two video switches and display monitors are available in the ATM design. It is understood that any one of these cameras could be used in the proposed solar telescope experiment for fine pointing as well as monitor.

Based on the present ATM-A experimenter, these cameras are proposed as:

(1) TV Camera I: H_α with field of views of 35 and 7 arc min

(2) TV Camera II: H_α or near white light FOV's 35 and 7 arc min

(3) TV Camera III: Extreme UV (150 Å–600 Å) with FOV of 40 arc min. This camera contains a converter to convert XUV to a sensitive portion of the spectrum.

(4) TV Camera IV: White light with an FOV of 3 arc min

D. Environment Description

The solar telescope and the mission-dependent equipment will experience unusual environments in the course of handling and mission operations. Exposed film to be handled and returned to Earth, and transported to the principal investigator, may be subjected to many other potential hazards, even at the time it would be processed for the images. Considering the possible events, sequence and environments, the following would be constraints on the telescope apparatus and the experiment:

(1) Ground handling, initial storage and shipping

(2) Ground testing and pre-launch operations

(3) Launch and injection

(4) Rendezvous with the CSM

(5) Rendezvous with the orbiting *Saturn/Apollo* cluster

(6) Docking with the orbiting *Saturn/Apollo* cluster

(7) Experiment operations

(8) CMG dump activity

(9) EVA operations

(10) Instrument orbital storage

(11) Post operations recovery, handling and storage

The many environments which could be experienced have not been sufficiently identified to determine their characteristics and probabilities of effects on the telescope, components and film. Certain significant environments can be mentioned with respect to their influences on the telescope:

(1) During ground handling, storage and shipping, all elements of the assembled or disassembled telescope must be safely protected under established and controlled temperatures, humidity, dust, corrosive materials, electrical potentials, and shock and vibration loads.

(2) Ground testing of the flight units will be controlled within the planned abbreviated mission profile for which the levels of the temperature, shock, vibration and space simulated pressures can be specified.

(3) The launch and injection environments will constrain the telescope to withstand the acoustic pressures, shock and vibration during *Saturn* burn, and the thermal-vacuum conditions of space. During launch, no equipment will be energized with high voltage potentials to prevent corona during the critical pressure conditions of the Earth's atmosphere. The telescope cover is closed to protect the unit from contamination by dust and from the products of combustion of the launch vehicle propellants.

(4) Rendezvous with the CSM will subject the telescope to shock loads and the vibrations of the RCS burn. The telescope cover must be closed to protect the unit from contamination during the RCS burn.

(5) During station-keeping at the rendezvous plane of the orbiting *Saturn/Apollo* cluster, the telescope must be protected from contamination by the particles trailing the vehicles in the cluster.

(6) The docking maneuver will subject the telescope to RCS burn vibrations and docking loads when the LM/ATM is being attached to the *Saturn/Apollo* orbiting cluster.

(7) During the mission, the film cassettes and other ATM provisions must protect the film from space particle effects.

(8) Whenever the RCS burn is required to execute CMG dump, the solar telescope must be protected from the vibration shocks and contamination from combustion particles. During RCS burn, the telescope mirrors must be caged.

(9) During EVA operations, the cover of the telescope must be closed to protect the optics from collecting particles disturbed from the ATM and telescope exterior.

(10) For the orbiting storage mode, the telescope will be secured so as to provide the following:

  (a) Thermal survival of the H_α filter

  (b) Thermal survival of the electronics

  (c) Contamination protection of the optics

(11) During the film storage period within the command module, the film cassettes must be protected from the corrosive environment of the CM. Upon recovery, further protection will be required from sea water, temperature extremes, cassette fracturing loads and electrostatic conditions.

IV. General Description of Solar Telescope System

The flight system which has been selected for detail study will consist of a folded Cassegrainian telescope, three film cameras, one TV camera, and associated mission-dependent equipment which are constrained and located in the ATM and corresponding vehicles of the orbiting cluster. Figure 3 is an artist sketch of the

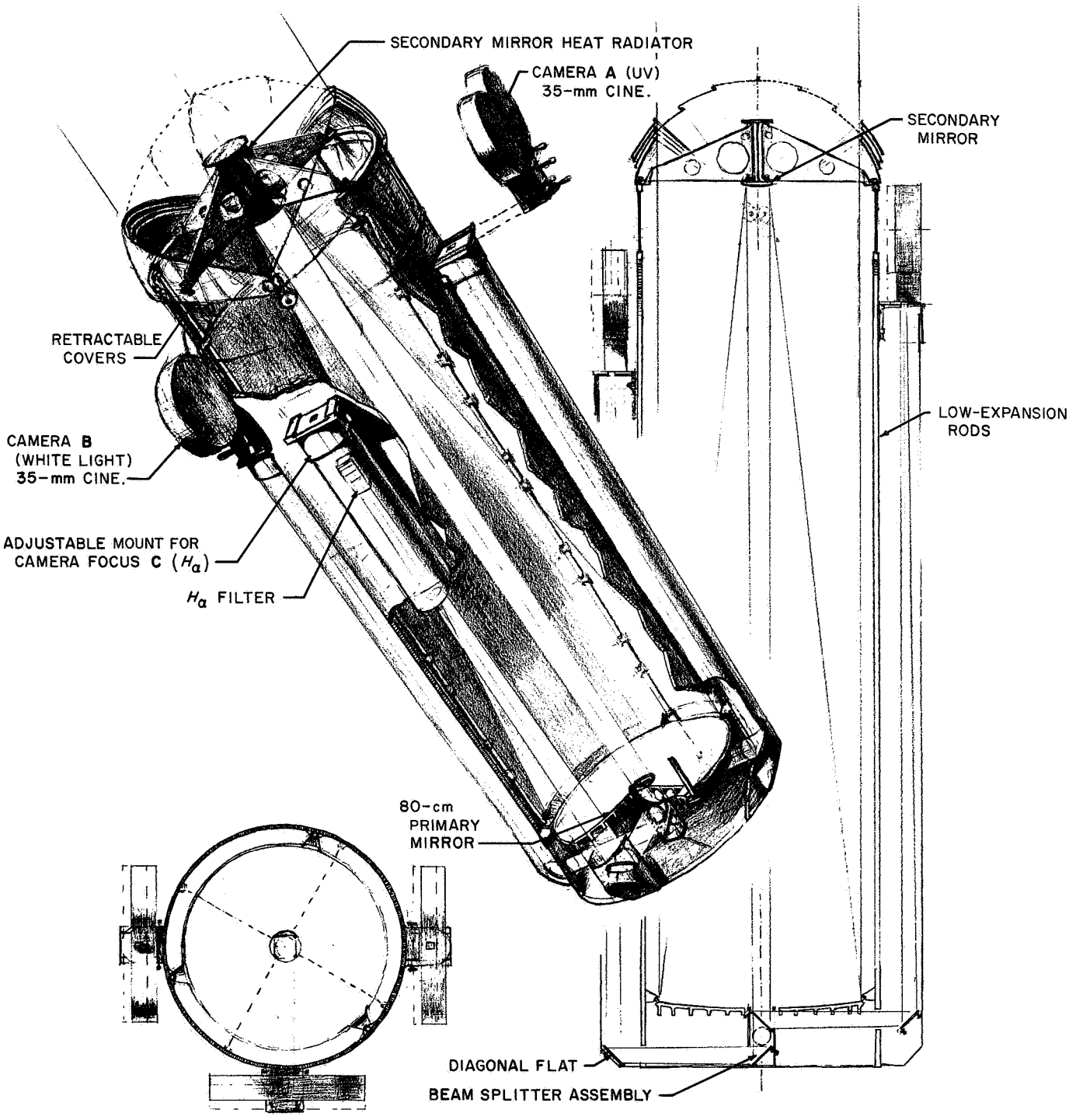

Fig. 3. Solar telescope

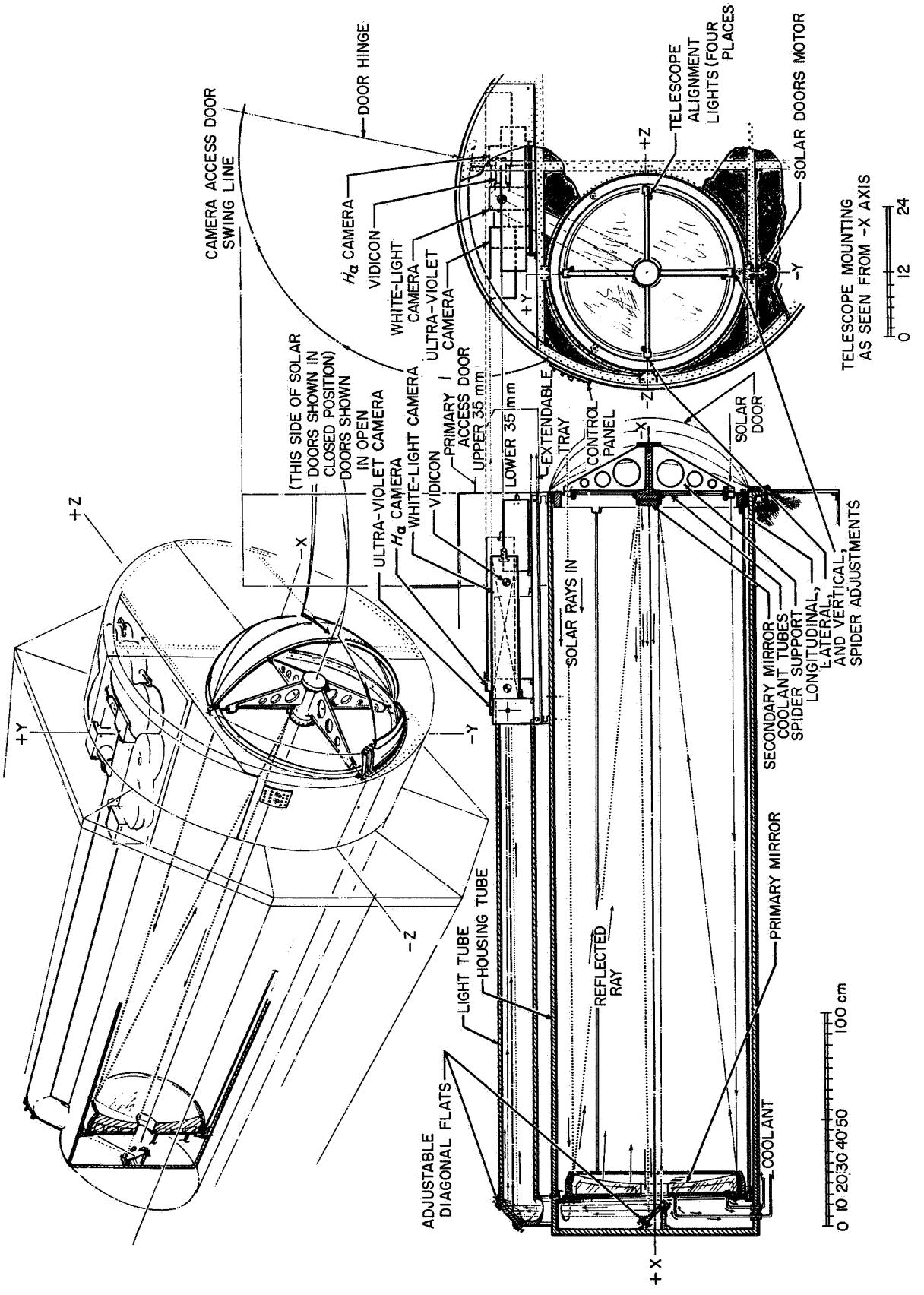

Fig. 4. *Apollo* telescope mount; solar telescope

telescope with the separate film cameras for each of the three spectral bands, namely white light, UV and H_α, located at the focal planes of the divided beams. Figure 4 is another design which conveniently combines the cameras as a group at the end of a single light tube. The latter configuration presents an easier arrangement of cameras for servicing during EVA. A TV camera is mounted in the white light film camera to be used primarily to provide the crew with optical performance information. By observing the signal characteristics on an "A" scope displaying a signal TV line, they will be able to adjust the position of the cameras for optimum focus at the film plane. A field monitor will also be provided which will show them which TV line is being viewed on the "A" scope. A slow scan TV mode will be provided to allow a selected TV frame to be telemetered to Earth and displayed to the investigators. It is assumed that the transmitter for such purposes is provided by the ATM. Detail information of the camera system is provided in Section VI of this report.

An active thermal control system will be used to stabilize system performance during data acquisition and minimize stabilization time at the beginning of the solar observation period. This Cassegrainian telescope has critical temperature distributions in viewing the Sun. Analyses of the optics and thermal characteristics of the design are described in Sections V and VI of this report.

An optical alignment system is provided so that the crew can adjust the alignment of the mirrors and maintain cognizance of the alignment during the operations of the telescope. The preservation of alignment is assured by a caging mechanism which secures the mirrors from the disturbances of launch and subsequent mission maneuvers. Mirror supports are designed to minimize thermal distortions.

The mirrors are housed in a thermally insulated enclosure about the primary supporting structure. A cover is provided at the mouth to minimize contamination and to maintain thermal equilibrium of the telescope when closed. Utilizing power from the ATM, an integral conversion and distribution system is used to energize all of the electronics and electrical networks of mechanism actuators, monitors, and thermal control systems.

The development and checkout of the system will be conducted with ground support equipment which would simulate an ATM and solar telescope modified mission profile.

V. Optical Description

A. Resolution

In the case of the on-axis telescope the angular resolution for a diffraction limited system is

$$\widehat{RL} = \frac{1.22\lambda}{D}$$

$$= \frac{1.22 \times 5000 \times 10^{-8}}{80}$$

$$= 76.1 \times 10^{-8} \text{ radians}$$

$$= 0.157 \text{ s}$$

The corresponding linear resolution is

$$\overline{RL} = \widehat{RL} f$$

$$= 76.1 \times 10^{-8} \times 6 \times 10^{3}$$

$$= 450 \times 10^{-5} \text{ cm}$$

$$= 45 \text{ microns}$$

B. Focus Tolerances

Knowledge of maximum incremental changes that may be applied to p and q is necessary for successful construction and operation of the telescope. Equations developed in Appendix B are repeated for convenience of reference here.

$$\Delta q_{\max} = \pm F\overrightarrow{RL}$$

$$\Delta p_{\max} = \pm\left[\frac{p + f_s}{f_s - q}\right]\Delta q_{\max}$$

Thus, for the on-axis telescope:

$$\overrightarrow{RL} = 45 \text{ microns}$$

$$\Delta q_{\max} = \pm 75 \times 45$$

$$= \pm 3370 \text{ microns}$$

$$= \pm 0.34 \text{ cm}$$

and

$$\Delta p_{\max} = \pm\left[\frac{-34.4 + 36.6}{36.6 + 646}\right]3370$$

$$= \pm 11 \text{ microns}$$

It can be concluded from these results that moving the focal plane is preferable to moving the secondary for focusing the telescope.

C. Multiple Reflections

Because of limitations on D_h only a small portion of the cone of light reflected from the secondary mirror passes through the primary to the focal plane. The remainder is re-reflected by the primary mirror and forms a real image at an intermediate position between the primary and secondary mirrors. Since, however, a real surface is lacking on which to form the image, the radiation continues on toward the mouth of the telescope. It is important, at this point, to determine that portion of the re-reflected radiation that is intercepted by the secondary, since the energy absorbed forms an unwanted contribution to the temperature of the mirror. An analysis of this situation for the on-axis system follows.

A sketch of the optical system is given in Fig. 5. The diameter of the reflected radiation intercepted by the primary mirror was found (Appendix B) to be

$$D_a = D_s + \left(\frac{I - D_s}{q}\right) L$$

$$= 29.5 \text{ cm}$$

for this system. This radiation is re-reflected and forms an intermediate image 26.4 cm in diameter at a distance 170 cm from the front of the mirror.

A schematic diagram depicting the graphical construction necessary to determine the amount of re-reflected radiation that is intercepted by the secondary is shown in Fig. 6. Rays A and A' from the primary converge on a point at the top of an imaginary image at the prime focus. Rays B and B' are drawn from the points where the primary rays are intercepted by the secondary to the corresponding point on the focal plane. Finally, rays C and C' are drawn from the points where the reflected radiation is intercepted by the primary to the corresponding point at the top of the intermediate image. These rays may be continued to outline a cone of radiation that passes unintercepted out of the mouth of the telescope.

This construction process may be repeated at intermediate starting points on the primary image to find an envelope for the cone of rays that is actually intercepted by the secondary. The result is depicted in Fig. 7. $A = 40$ cm is the radius of the primary mirror. $B = 14.75$ cm is the radius of reflected radiation on the primary. $C = 7.5$ cm is that portion of the reflected radiation that is re-intercepted by the secondary and $D = 8$ cm is the radius of the hole in the primary.

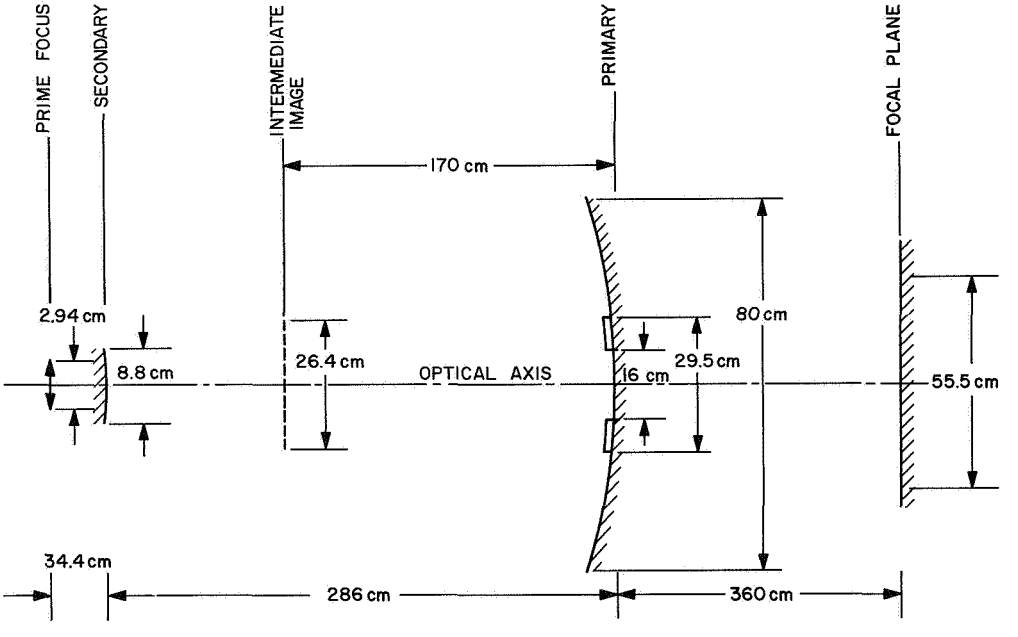

Fig. 5. Sketch of preliminary design

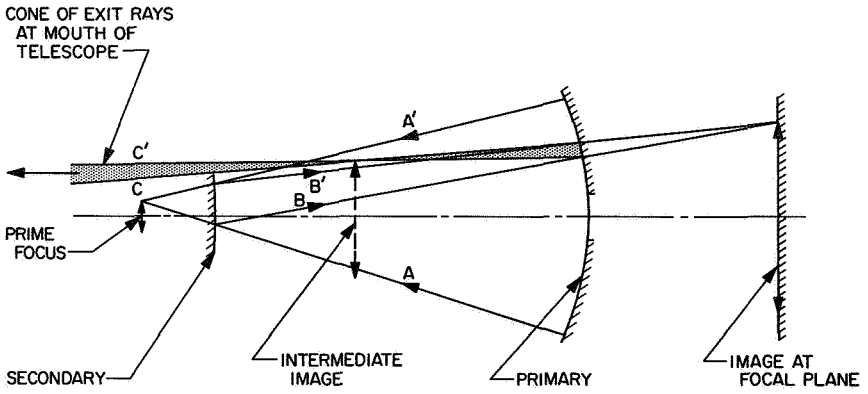

Fig. 6. Construction for determination of re-reflected radiation on secondary mirror

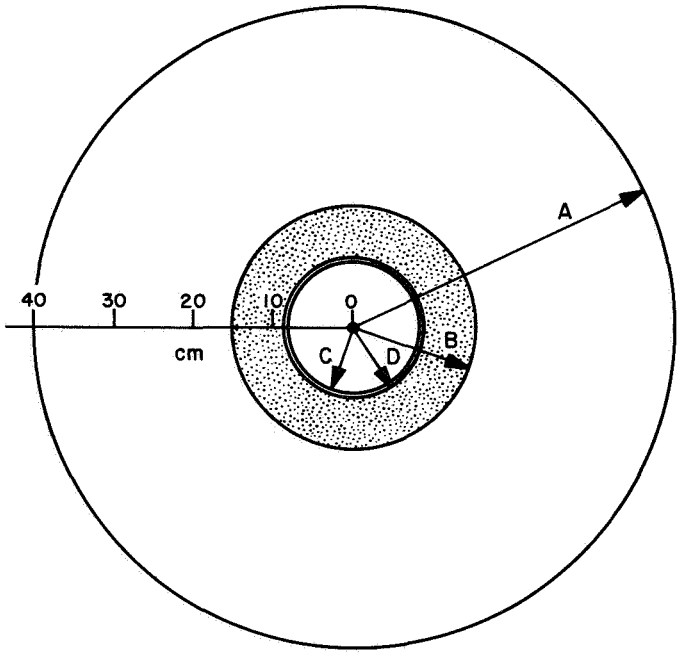

Fig. 7. Re-reflected radiation on primary mirror

It is now possible to trace the radiation through the optical system. Area A initially collects 1 Sun and, since $H = 9.3$, reflects 87 Suns back to the secondary. The secondary reflects $87 \times (4.4/15)^2 = 7.5$ Suns back to area B on the primary. Hence in annular space $B - D$, the total radiation is $1 + 7.5 = 8.5$ Suns. Because $C < D$, there is no portion of the primary which re-reflects the light to the secondary again.

D. Vignetting

A method for determining the approximate vignetting curve at the focal plane is developed in Appendix B. When these equations are applied to the on-axis design,

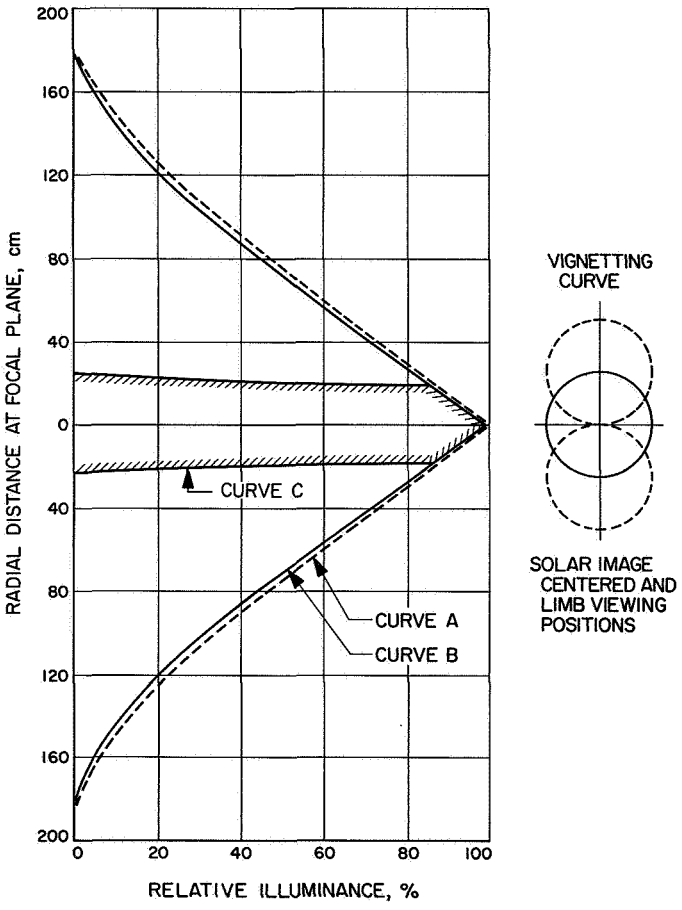

Fig. 8. Vignetting curve, on-axis system

the distances of the extreme points are calculated as follows:

$x_0 = 180$ cm (Appendix B)

$x_1 = 15.9$ cm (Appendix B)

$x_2 = 23.7$ cm (Appendix B)

Curve *A* in Fig. 8 depicts vignetting at the focal plane due to the secondary mirror. Curve *B* results when a small correction for the effect of telescope tilt is applied. Vignetting at the focal plane caused by the 16-cm hole in the primary is depicted by Curve *C*. Finally, the resultant vignetting curve is denoted by continuous cross-hatching of the appropriate curve.

It is evident from this analysis that the available field is centered within a radius of approximately 20 cm at the focal plane. The maximum vignetting within this area is less than 15%. No vignetting, it is recalled (Appendix B), occurs within the 35-mm picture frame.

In Fig. 8, Curve *B* forms a useful approximation of the vignetting of the bright area on the primary caused by reflected radiation from the secondary mirror.

E. Ray Trace Analysis

Evaluation of the on-axis Cassegrain telescope was conducted by use of the Aerospace Corporation Image Evaluation Program [TDR-469 (5540-20)-3]. The runs were carried out on an IBM 7094 computer at JPL. The model system had the following parameters (Appendix B).

Diameter of primary	D_p	80 cm
Focal length	f	6000 cm
Focal ratio telescope	F	$F/75$
Focal ratio primary	F_p	$F/4$
Tube length	L	286 cm
Back focus length	d	360 cm
Magnification	m	18.8x
Diam. central obscuration	D_m	16 cm
Eccentricity primary	e_p	1
Eccentricity secondary	e_s	1.11249

For this system, the diameter of the auxiliary disc is 92μ at $\lambda = 5000$ Å, and 0.15 arc sec corresponds to a linear distance of 46 μ at the focal plane.

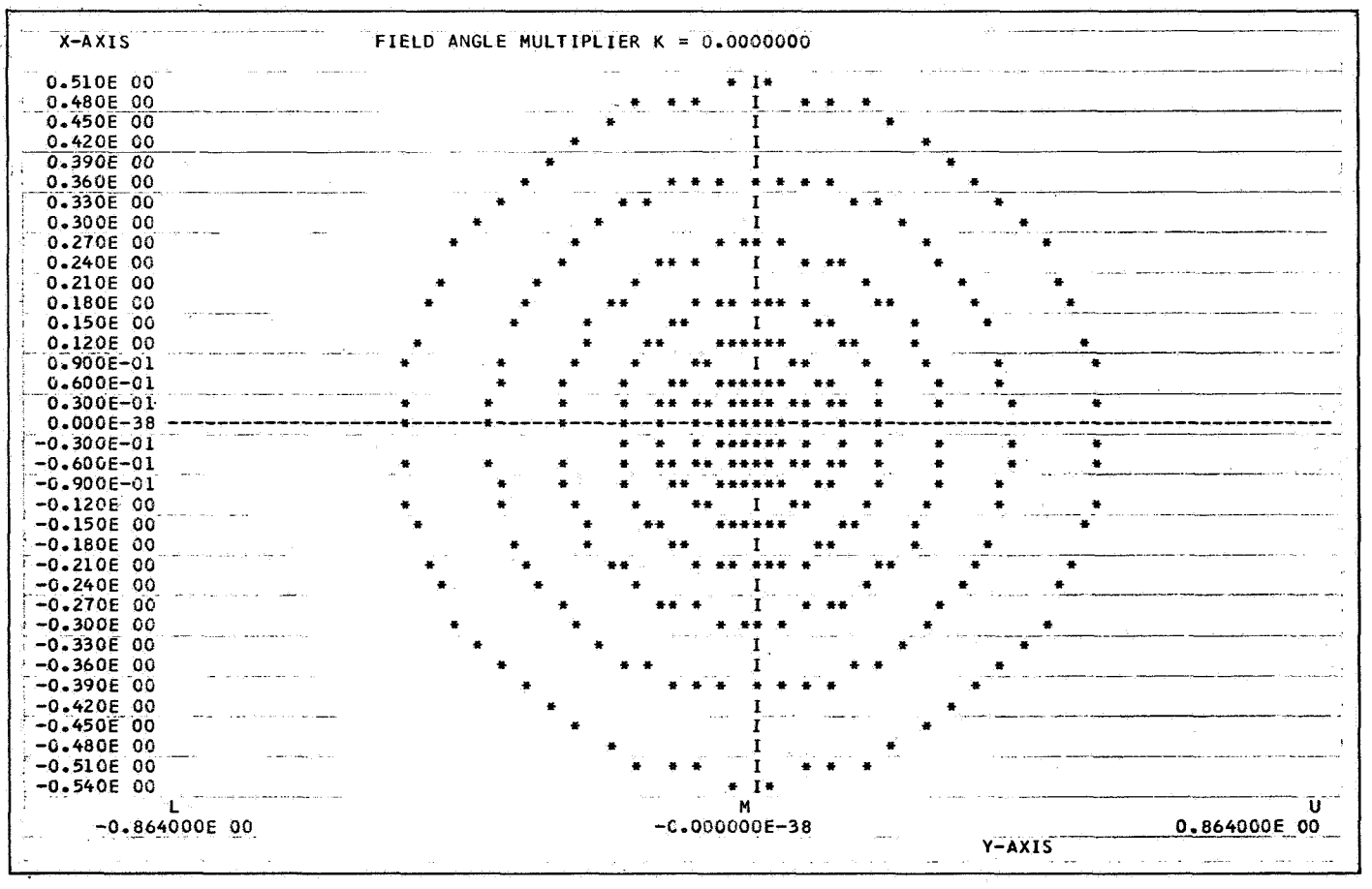

Fig. 9. Spot diagram, all surfaces spherical, $K = 0$

Results of the computer analysis are shown in Figs. 9 through 14. It is important to observe that the effect of diffraction is included along with geometric considerations in the MTF calculation, but not in the determination of spot size. The latter is a function of the geometry of the system only. In the diagrams, $K = 0$ corresponds to a location at the center of the focal plane, $K = 0.5$ is a point 3.7 cm from the center, and $K = 1.0$ is a point 7.4 cm off center. In the latter two cases, distances are taken along the +y axis. All dimensions given in the diagrams are in inches.

Figure 9 shows the spot diagram for the case of spherical primary and secondary mirrors. The 2.5-cm spot size clearly eliminates this combination of surfaces for the telescope. The result of using a parabolic primary and spherical secondary is shown in Fig. 10. The diameter of the spot is about 3.5 mm; hence, the requirement for an aspheric secondary as well as primary is indicated.

All of the remaining diagrams (Figs. 11 through 14) are for a system consisting of a parabolic primary and hyperbolic secondary. Figure 11 depicts the spot size at the center of the focal plane ($K = 0$). Its size (a fraction of a micron) and odd shape are believed to be due to numerical noise in the computer. At $K = 0.5$, the spot size is approximately 24 μ (Fig. 12) and at $K = 1.0$ (Fig. 13) it is about 93 μ. The feasibility of using a 35-mm picture frame is definitely apparent.

The MTF for this system is given in Fig. 14. Here the vertical axis is the image modulation and the horizontal axis is the normalized spatial frequency $\bar{\nu} = \nu(\lambda f/2\beta_0)$

where

ν = sinusoidal spatial frequency

λ = spectral wavelength = 0.59 μm

β_0 = radius of entrance pupil

f = focal length of system.

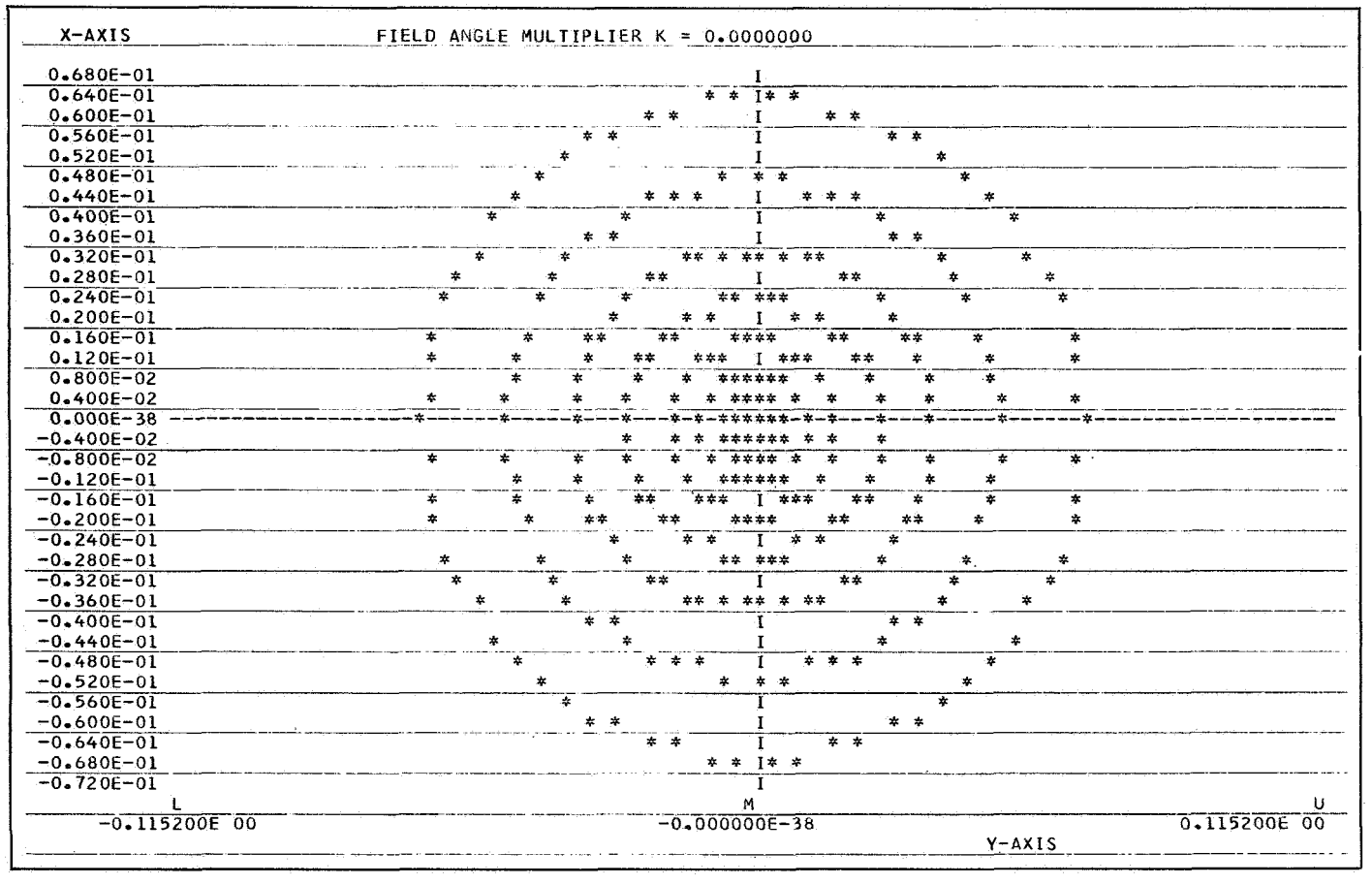

Fig. 10. Spot diagram, parabolic primary, spherical secondary, $K = 0$

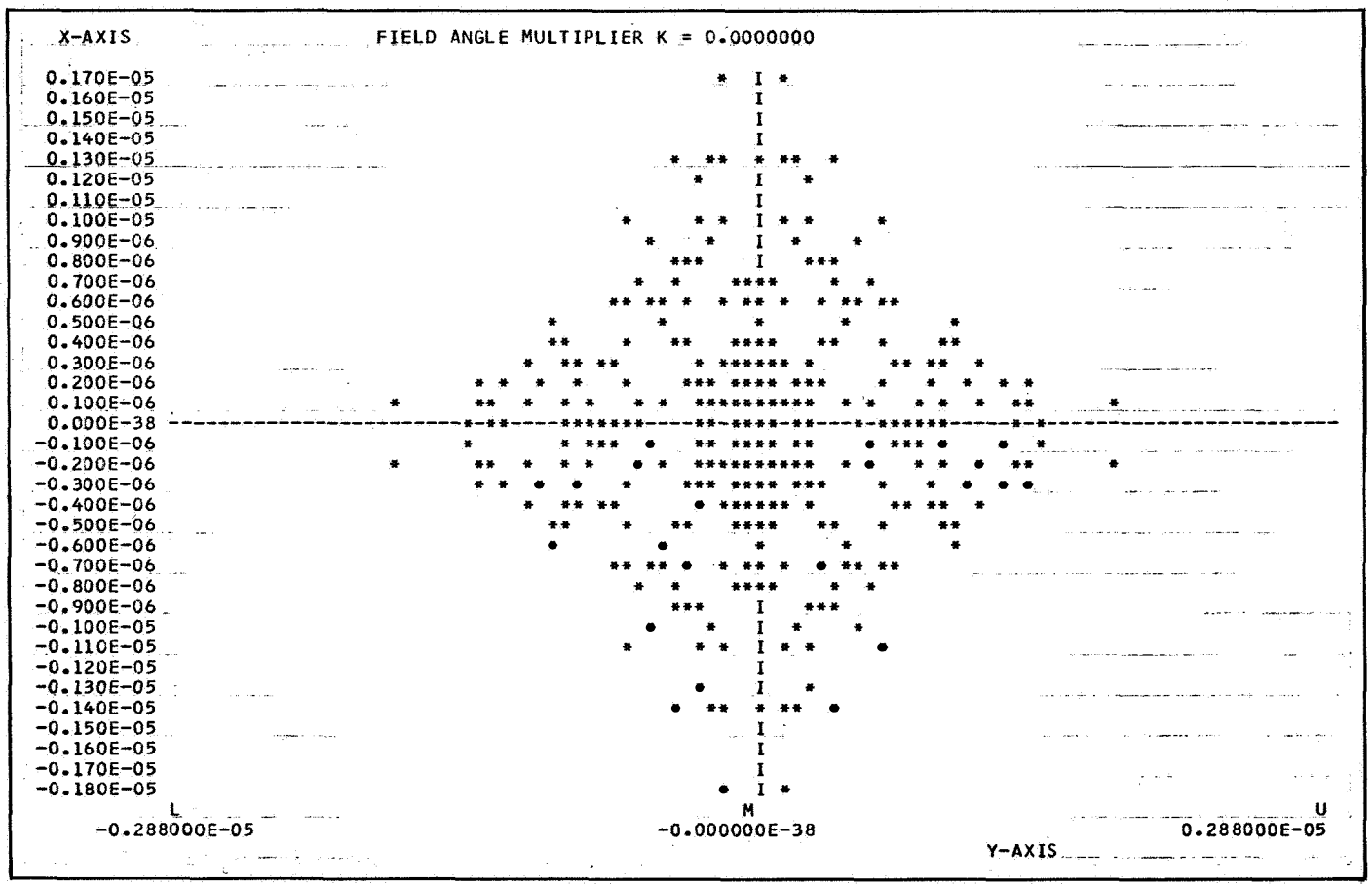

Fig. 11. Spot diagram, parabolic primary, hyperbolic secondary, $K = 0$

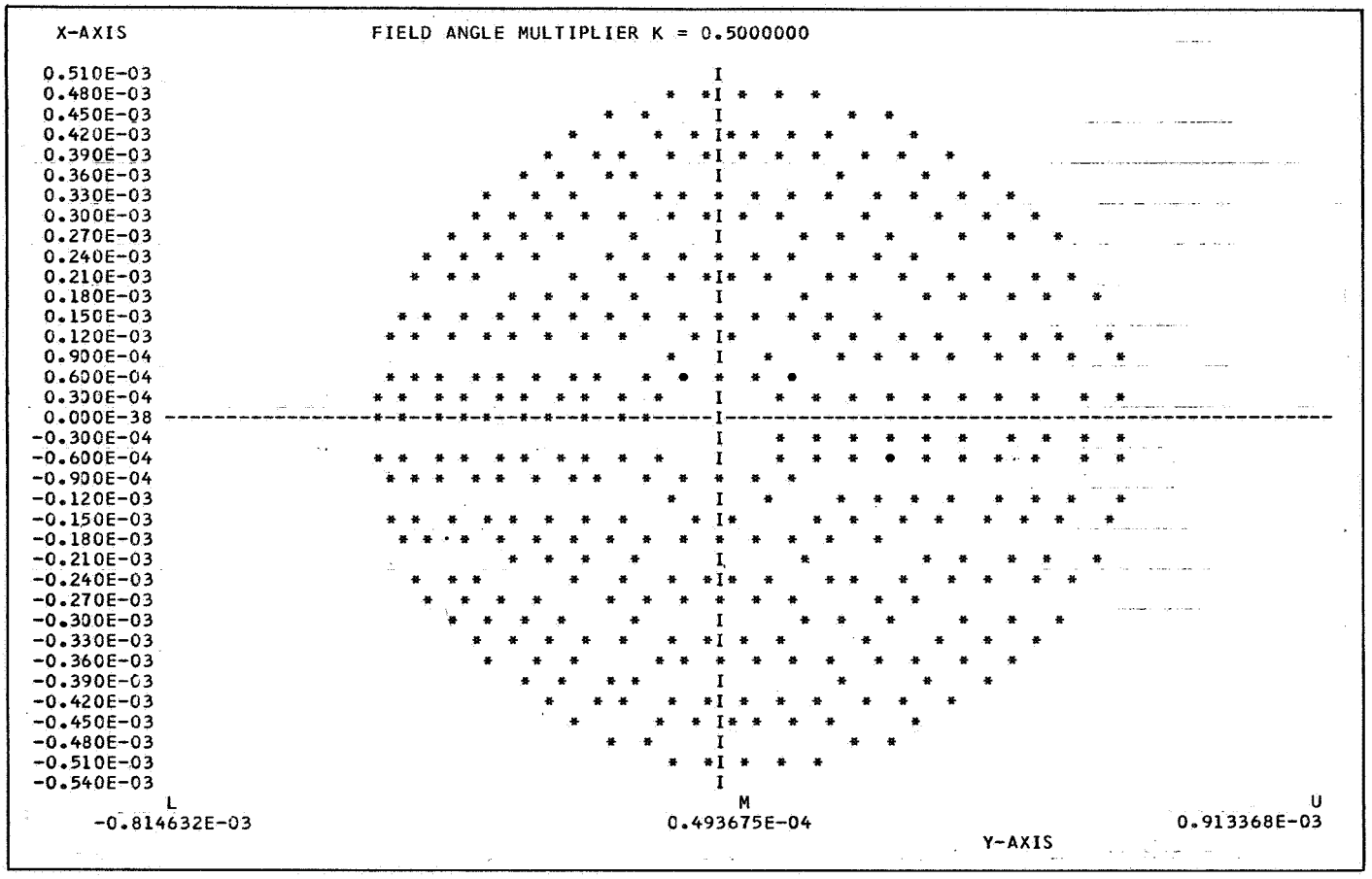

Fig. 12. Spot diagram, parabolic primary, hyperbolic secondary, $K = 0.5$

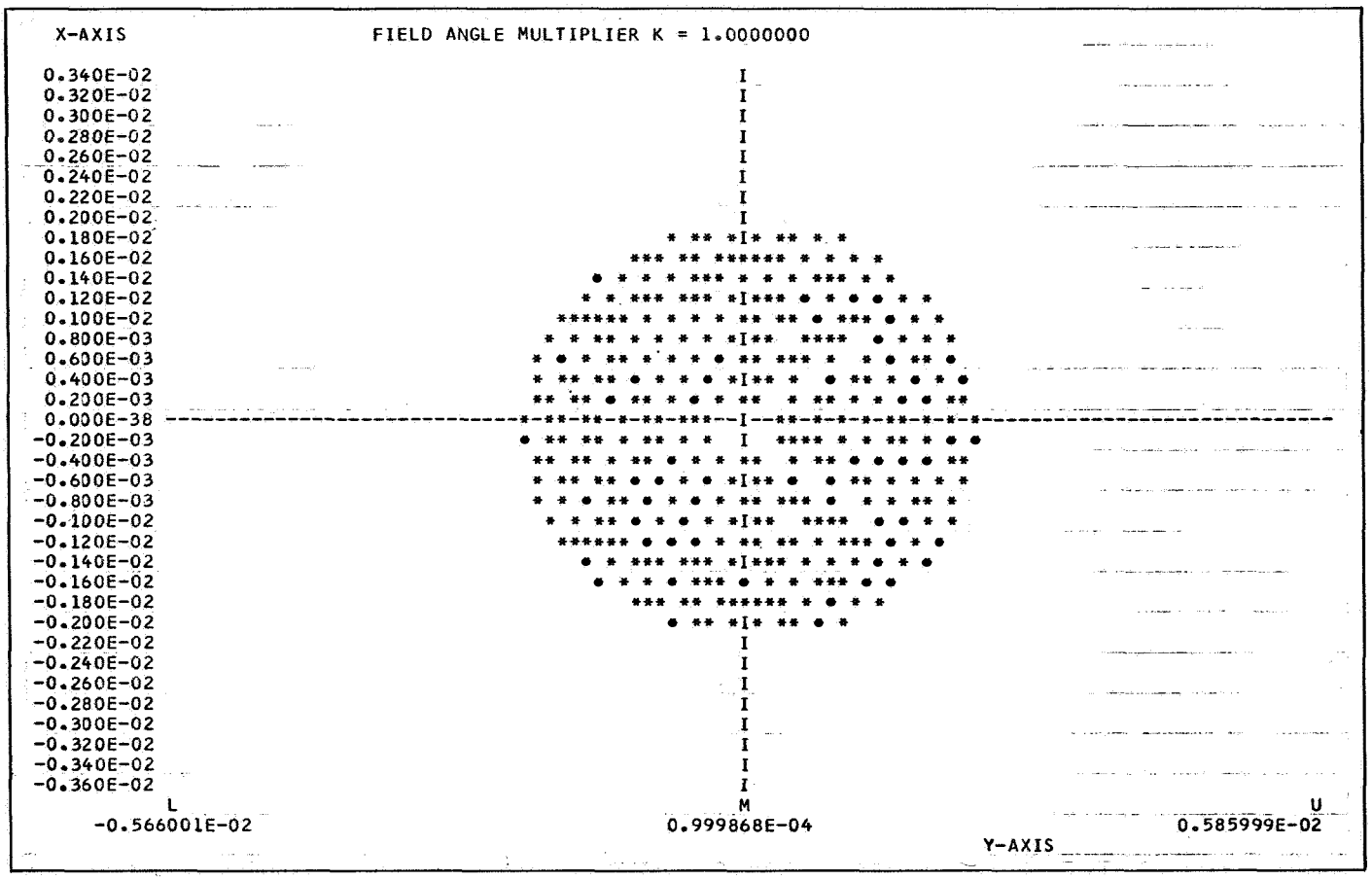

Fig. 13. Spot diagram, parabolic primary, hyperbolic secondary, $K = 1.0$

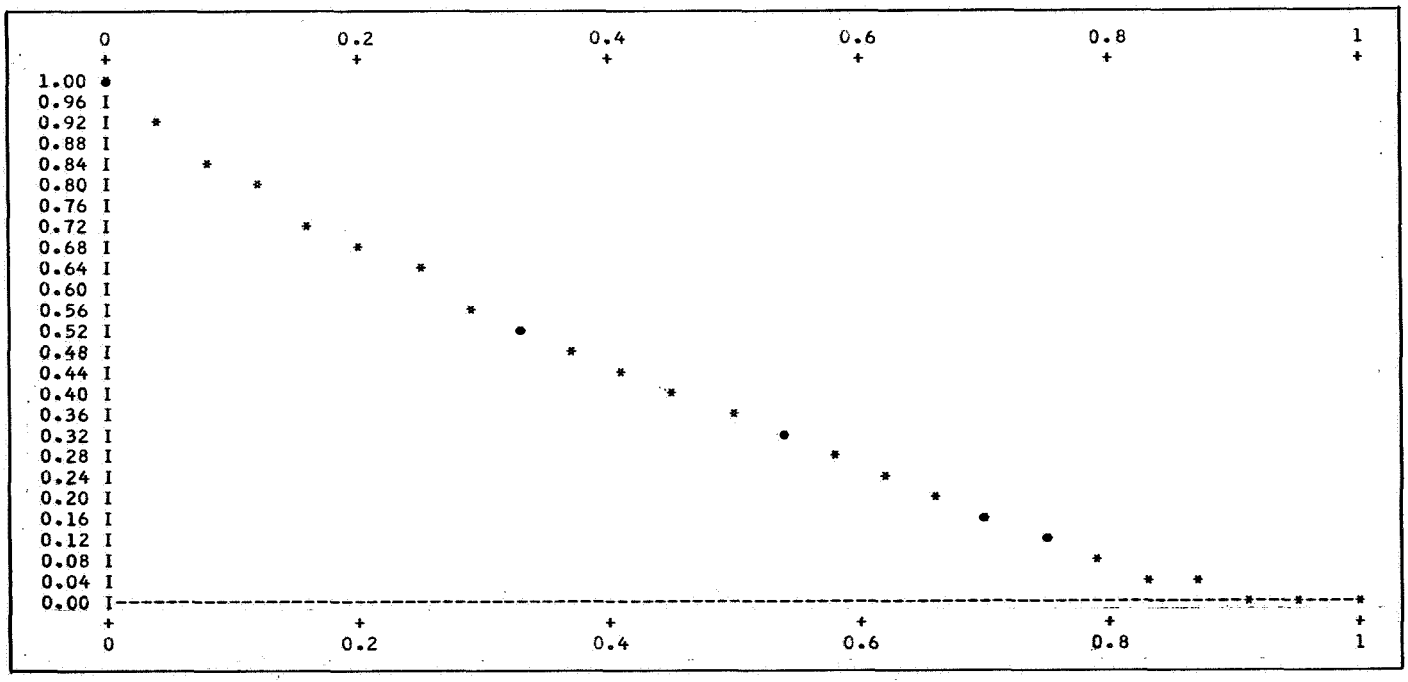

Fig. 14. Modulation transfer function, aspheric surfaces, $K = 0$

For this particular system the value of $(\lambda f/2\beta_0) \approx$ Rayleigh limit is 44.2 μ. At a spatial frequency in the image plane of 10 cycles/mm $\bar{\nu} = 0.44$, the value of the MTF (Fig. 15) is 0.42. Hence, 100% modulation in the object will produce 42% modulation in the image at this frequency. For the same scene, 10% modulation in the object will produce 4.2% modulation in the image. The MTF for this system is 0.15 at a spatial frequency of approximately 20 cycles/mm (0.15 arc sec).

The result of the concluding series of computer is depicted in Fig. 15. Here, the depth of focus was determined by varying the position of the focal plane in increments of 0.25 cm. For each position, the diameter of the spot size was measured and plotted against total distance from the secondary mirror. A line corresponding to 0.15 arc sec (42μ) has been superimposed on the chart. The points of intersection of this line with the focus curve indicate the depth of focus is approximately $\pm$0.32 cm. The computed back focal length is 645.965 cm.

The focus tolerance of $\pm$0.32 cm as determined from computer runs, it is observed, is in excellent agreement with the calculation of Appendix B.

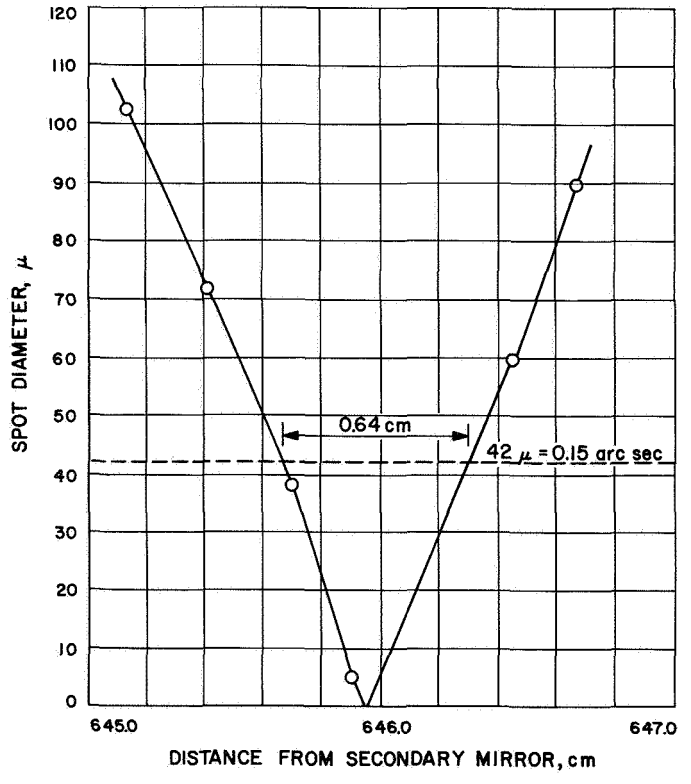

Fig. 15. Spot diameter vs back focal length, $K = 0$

VI. Engineering Considerations

A. Camera System

1. General. The primary objective for this solar telescope is to obtain photographs, especially in near ultraviolet light, of selected areas and events on the Sun during the extent of the mission. All optics, coating, windows, filters and film will be selected with this in mind. Much work must still be done on film types, filter attenuation and bandpass, exposure times and film development. All these have to be balanced with the amount of solar energy available, on a shared basis, via the beam-splitter.

Three camera systems will be included: white light, UV and H_α. For improved reliability, these will operate independently from one another, except, possibly, for TV monitoring and the use of a common focusing mechanism. Independent operation will ensure that not all information will be lost, should one or two cameras fail. The shared components are, in general, the more reliable. These include the diagonal mirrors, the beam-splitter, the thermal control system, and obviously, due to other restraints, the telescope, in addition to the above.

The three cameras will share the same view and incident solar energy. The simplest picture-taking arrangement will be used, namely, having all three take photographs simultaneously; shutters and film advance mechanisms will be synchronized at whatever frame exposure rate is selected. In this way, maximum information will be recorded for each event photographed.

Also, film will be expended at the same rate for each camera, which will minimize EVA time by the astronaut for film changing.

2. Basic cameras. The three camera systems have been specified by the principal investigator as follows:

(1) *Ultra-violet:* A relatively broad-band arrangement covering the region from 3000 to 2000 Å or lower. This system will incorporate special UV sensitive film and one or more Fabry-Perot interference-type filters, probably on a wheel for remote selection of different cut-off points and different pass-bands. This is the most important of the three cameras because of the wavelength concerned. Components and materials used in common by the other cameras are controlled by the requirements of this system.

(2) *Hydrogen H_α* (Balmer Series): A narrow-band system for the deep red at 6563 Å. This includes a single Lyot-type bi-refringent filter for a pass-band

of ½ Å remotely tunable over ±2 Å to permit photographing both advancing and receding prominences. The filter incorporates two heaters for stability of its optical elements. The tuning adjustment, also by varying the temperature of the filter elements, will be necessary to compensate for the orbital velocity of the telescope, which can shift the ½ Å pass-band of the H_α intensity peak. The magnitude of this doppler shift is computed as follows (see Fig. 16):

Orbital velocity

$$\text{of spacecraft} = \frac{24{,}000}{90 \times 60} = 4.44 \text{ mi/sec.}$$

$$\text{Frequency shift } \frac{\Delta\lambda}{\lambda} = \frac{V}{C}$$

$$\Delta\lambda = \frac{4.44}{186{,}000} \times 6563 = 0.157 \text{ Å shift}$$

Total shift is 0.313 Å between the start and end of the lighted half of each orbit.

Panchromatic or special red-sensitive film such as Kodak S0-375 can be used. The basic camera mechanism will be the same as in (1) above, and pictures will be taken both simultaneously and of the same solar region as the other cameras.

(3) *White Light:* This is the last in line of the three cameras relative to the beam-splitter. The camera mechanism and film type will be the same as for (2) above. Photographs will be taken in various bands of the visible spectrum. For this, a four-color filter wheel will be incorporated with, perhaps, red, yellow, blue and polaroid filters. Neutral density filters will also be included as required, so that correct exposures are obtained in each of the colors, using a constant, pre-set, exposure time. The filter wheel is motorized so that any filter can be remotely selected on command.

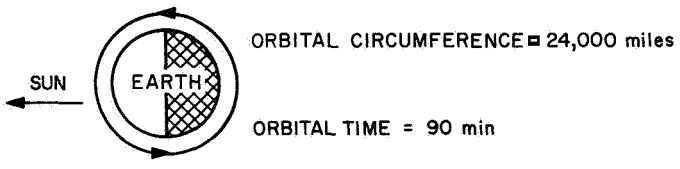

Fig. 16. Earth orbital path of spacecraft in relationship to Sun

3. Camera arrangement. For operational convenience, and for simplicity and strength of the installation, the preferred arrangement for the cameras is a cluster near one of the spars of the ATM cruciform. Each camera is mounted on a face of the central, movable base which contains the beam-splitters and the focus adjustment mechanism (see Fig. 18). This rides on tracks attached to the side of the telescope housing (see Figs. 4 and 18). A single light tube contains the image and the diagonal mirrors at the base of the telescope. Adjustments to the diagonals and beam-splitters, if necessary, may be made through the side of the ATM. The cameras and film cassettes are accessible through doors at the top face of the ATM.

During initial installation, the cameras are mounted relative to the beam-splitters such that the UV and H_α cameras are at right angles and the white light camera is axially above. Alignment with, and distance from, the beam-splitters are thus pre-established and held fixed. During focus adjustment, the cluster moves as a unit parallel with the light beam so that the individual alignment does not change and focusing can be done for the cluster as a whole. A single TV vidicon, located in the white light camera, will be a representative monitor for all cameras.

4. Camera mechanism. The basic camera of all three units includes the shutter mechanism and drive, the filter and controls or change mechanism, the film cassette, shifting motor and gears, a light mask to define the picture frames, a time or frame identification number imprinter, thermal control provisions as required, power distribution wiring, connectors and sensors, and the basic box housing the above and to which the film cassette is secured.

The shutter will consist of a disk with an adjustable slot for varying the exposure time, and a motor-activated mechanism for rotating the disk once per signal pulse. On the white light camera, the disk will also carry one or more mirrors for reflecting the image to the vidicon face plate between exposures. All cameras will have provisions for two exposure rates, one for time-lapse photography (one frame each 10 seconds), and the other for a high-speed mode (10 frames per second) lasting for up to 15 min. The power required for the driving motor is thus uniquely determined. Both the mode and the start-stop times are selectable from the command console. Exposure time (slot width) will be pre-selected prior to launch but may be changed, if required, by the astronaut during EVA.

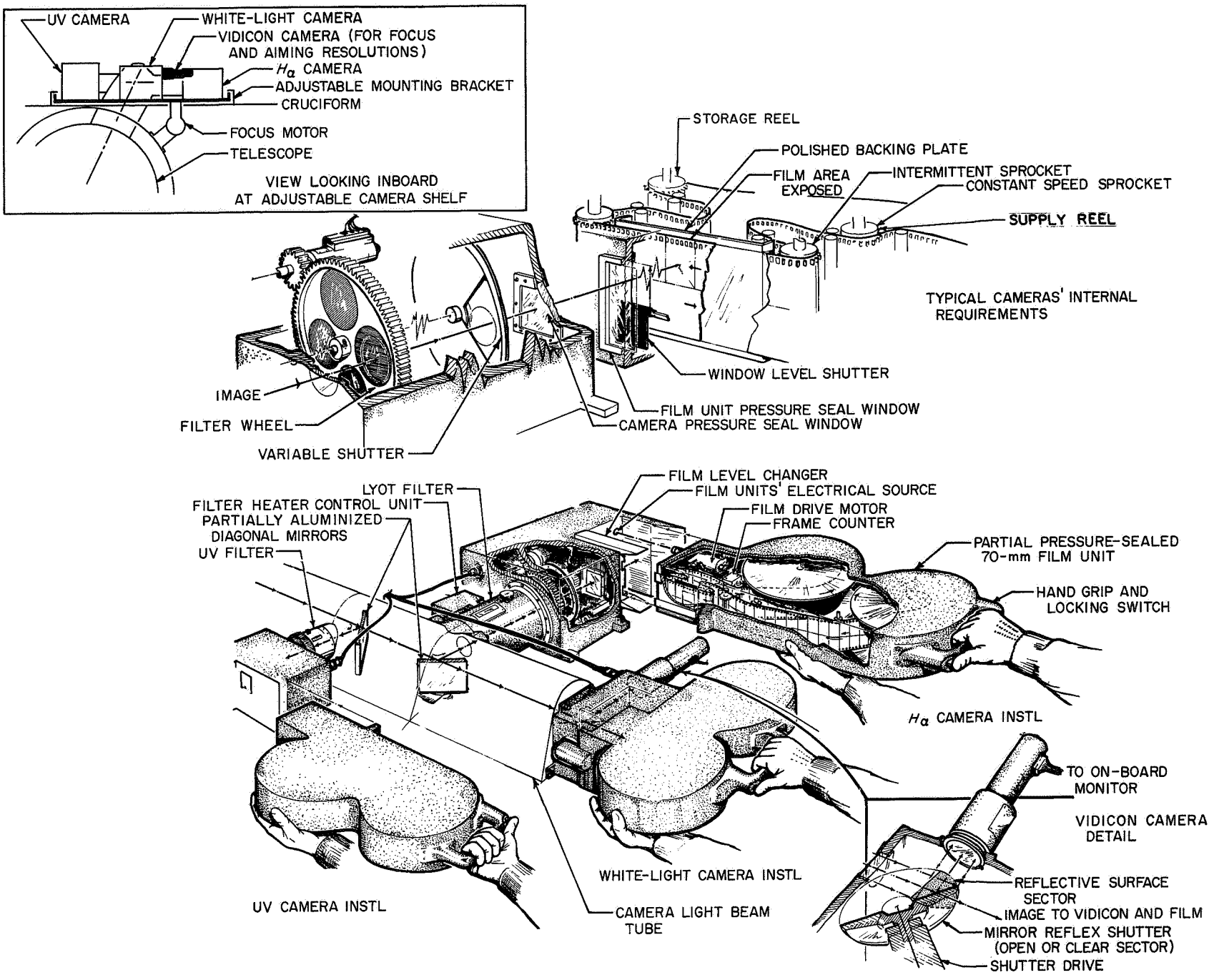

Fig. 17. *Apollo* telescope mount; telescope camera cassette accessibility and mechanism

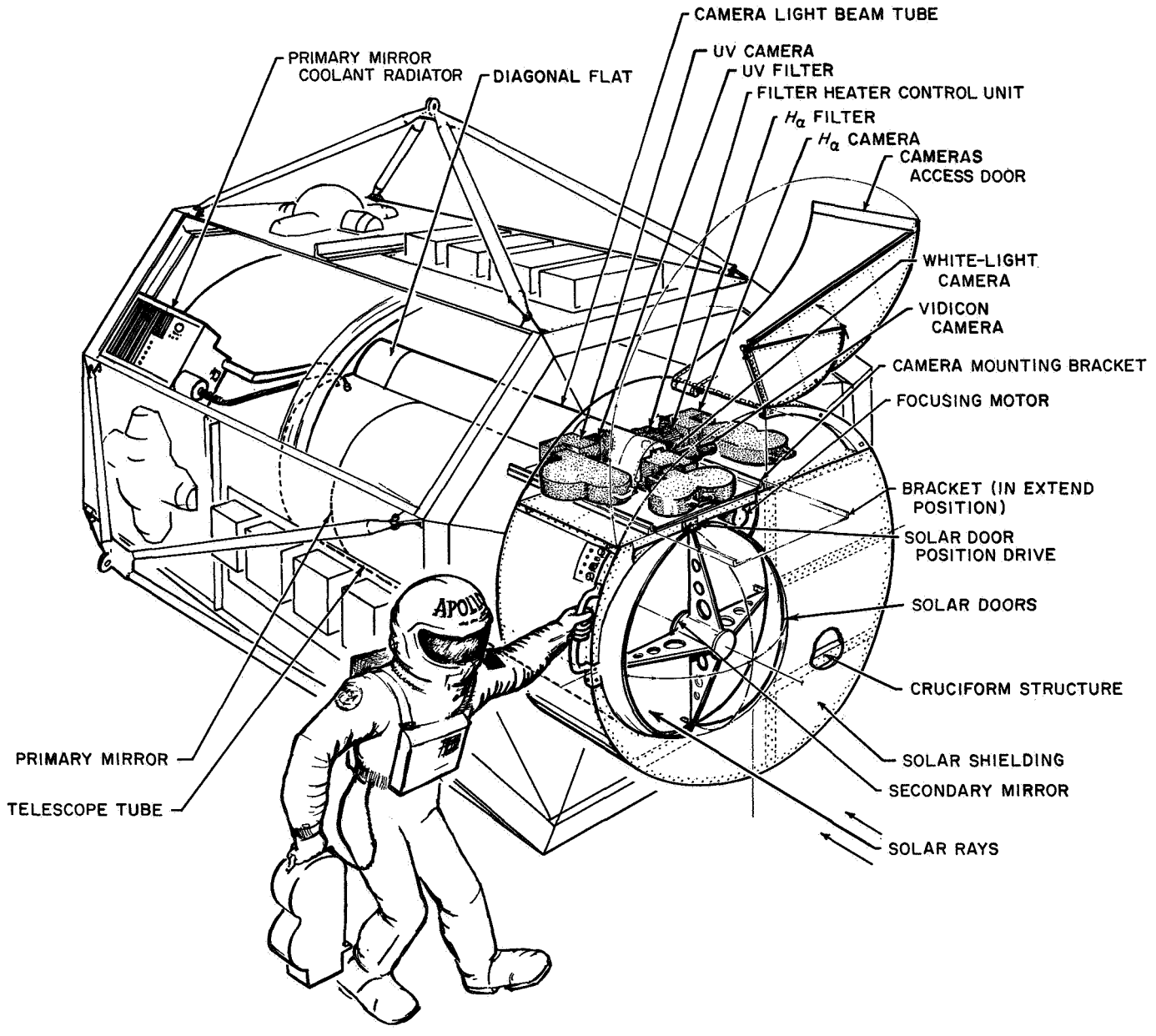

Fig. 18. *Apollo* telescope mount/lunar module modification; solar telescope accessibility of cameras

5. Films and cassettes. 70-mm movie film will be used in all cameras. This is pre-loaded on 1000-foot reels in sealed cassettes. Tentatively, Kodak type S0375 has been selected for the H_α camera and type 649GH for the white light camera. No film has yet been selected as entirely satisfactory for the UV camera. Additional work must be done on the light intensities required for proper exposure in different wavelengths considering the restraints present on exposure time and amount of light available after passing through the system.

The cassettes are lightweight, pressure-sealed, self-contained packages. Each includes the supply and take-up reels, film advance mechanism and drive motor, and a transparent window through which the exposures are made. Gamma ray shielding may be needed as part of the cassettes or may be supplied by the ATM enclosure. Further investigations must be made on the expected magnitude of this problem considering that the mission will occur during the active part of the sunspot cycle, and that, at present, little is known about the degree of film fogging which may occur during a mission of this duration.

At present, it is planned to have all film cassettes, both initial and EVA replacements, pre-loaded and sealed prior to launch. This will ensure that the proper amount of clean air and moisture is present to preserve the film emulsion and base. Because it would be impractical to build the cannister sufficiently strong to hold either an internal or external pressure differential of 1 atmosphere, a two-way relief valve will be incorporated. Only 1 or 2 psi internal air pressure is needed during the mission, provided the relative humidity is maintained. Dry lubrication of the film advance motor and mechanism will also be aided by this partial atmosphere.

The 70-mm film provides for two track widths of 35-mm picture frames. This gives 2000 ft of equivalent 35-mm film with the minimum of weight and complexity. The double length means one-half the required EVA film changing time. After one track has run through (and this will occur simultaneously for all three cameras), the shift mechanism will translate the film cassette laterally so that the mask will be over the second track for the return run of the film. "Up" and "Down" do not exist in these pictures, so with solar "North" and time identified, the photographing can proceed in either direction on the film. Thus, the motor and film advance mechanism can be, for example, a reversible geneva gear. No fast re-wind provisions are needed, which simplifies the operation at the 1000-ft shift point.

During the next phase of work on the camera systems, an investigation will be made of the light (energy) absorption in the mirror, beam-splitter, filter train. The various factors of mirror reflectance, beam-splitter and window absorption, filter absorption, and film sensitivities will be balanced against the solar irradiance curve as now known for space operations. From this, firm decisions will be made on the types of film, filters and surfaces which must be used for the specified exposure times (to freeze the motion) and frame rate.

B. Structural Description

The telescope structure consists of a main housing or tube, a primary mirror cell, the secondary mirror support and spider, a movable cover or dust-hood, the camera mounting structure, and a system of supports for attaching the telescope assembly to the ATM. The assembly thus comprises a self-contained package with interfaces for mechanical support, electrical power, command and data channels, and mirror cooling fluids as required. Weight and thermal control are the primary constraints, modified by the functional requirements of strength, dimensional stability and ease of adjustment.

Due to the large and intermittent heat input, local temperature gradients of considerable magnitude are expected. Where these may affect alignment, special low coefficient of expansion materials or active cooling systems will be used. The mechanical and optical supports will be separate structures joined together in a single area near the base. The optical support is designed to operate in a weightless environment where stability is more important than strength; it will be inherently weak and flexible. Clamps are thus included at both the primary and secondary mirrors for securing them to the telescope housing during launch and maneuver operations.

Figure 4 shows the general arrangement of the telescope. At the base is the principal load-carrying structure which will be attached to the ATM. To this is fastened the housing and the primary mirror cell. Provisions are included in the bolted joints for alignment of the primary mirror axis with the ATM spotting telescope. The housing tube is sufficiently oversize so that its alignment is not critical. Attached to the upper surface of the primary mirror cell are three rods of low-expansion material. These extend the length of the housing and at the upper ends are attached to the secondary mirror and spider assembly. Each attachment includes adjustment screws for initial fine adjustments or realignment of the secondary mirror relative to the primary. This is important

for proper operation of the telescope and may be required during EVA following docking of the ATM.

The mechanical structure including housing, hood, clamps and camera rack, also attaches to the base load-carrying bracket. Additional attachments are provided near the upper end of the housing for lateral support. The camera rack may be a part of the main housing or may be attached directly to the ATM cruciform, whichever appears to be most advantageous from both load-carrying and EVA film changing points of view. Figure 18 shows one possible arrangement where the entire camera rack is on tracks attached to the cruciform. Film changing and camera adjustments are then possible external to the ATM wall.

During load-producing maneuvers such as launch, docking or reorientation of the cluster, the optical structure will be automatically clamped to the mechanical structure. In fact, this operation will occur each time the telescope system is placed in the stand-by mode with the dust cover closed. A set of arms, which may be a part of the cover or may deploy out from the housing, will clamp onto the heat radiating tube at the back of the secondary mirror. This will neither load nor unload the three secondary supporting rods, but will prevent any additional loading of the rods or the spider assembly. When the cover is opened, the clamps will release the secondary and fold back into the housing.

At the bottom, the primary mirror will simultaneously be clamped during stand-by maneuvers. During operations, the mirror is unloaded but restrained from moving by a ring of soft-padded segments located in a groove around its outside circumference. During stand-by maneuvers, the segments which have a tapered cross-section would be pressed firmly into the groove and clamped by a mechanism in the mirror cell. The mirror itself has sufficient strength to withstand all specified shock and vibration loads when supported in this manner.

C. Weights, Centers of Gravity, and Moments of Inertia

1. Weight. The telescope weight has been estimated on the basis of refinements to a number of designs which have been studied. In some detail, certain design features, such as in the camera subsystem can be approximated very well. The estimated weight of 220 lbs for the primary mirror attempts to optimize a probable weight whether glass or metal might be used. This assumes that the structure of the mirror will be a cellular form to take advantage of a weight reduction, i.e., if the thermal distortions are not prohibitive. In the materials section of this report are representative weights for solid and cellular designs of the primary mirror. For super invar which is a likely candidate, the probable weight would be nearer the 200-lb figure for a maximum lightened structure. In the case of aluminum, the chances are that a mirror could weigh as little as 100 lbs. For Cervit, it would probably be about 150 lbs. It is likely that the estimated 220 lbs is a conservative figure.

There is considerable experience in the fabrication and utilization of small beryllium mirrors. The low weight and excellent thermal conductivity of beryllium make it a good candidate for the secondary mirror. The heat radiator, which is attached to the mirror, could also be made of the same material. In this case, the weight of the assembly would be at a minimum estimate. An aluminum assembly on the other hand would weigh about 2 or 3 lbs more.

Generally, the estimates of weights for the telescope supporting structure and housing can be based on typical aerospace designs.

The total weight of the telescope designed with a unified camera arrangement including all of the mission dependent equipment installed in the ATM and LM is about 1425 lbs. If the cameras are separately located around the telescope, an additional 80 lbs would be required for such an arrangement containing another diagonal mirror, two more light tubes, camera supports, separate focusing mechanisms and electrical harnesses.

The following is a detailed breakdown of the estimated weights:

Primary Mirror Assembly	*lbs*
Primary mirror (optimum for metal or Cervit)	220
Mirror cell	20
Support structure to housing	50
Secondary Mirror Assembly	
Mirror (Be)	1
Heat radiator (Be)	4
Spider and standoff structure assembly	118
Beam Splitter and Diagonal Assembly	
Diagonal flats	12
Assembly support (Be)	15

Telescope	*lbs*
Housing (main tube)	190
Insulation	25
Telescope aperture cover	25
Cover motor drive and mechanism	15
Thermal control system	25
Beam splitter housings	15
Camera focusing system	25
Mounts to ATM structure	(ATM furnished)
Truss structure, telescope mounting to housing	50
Diagonal assembly support and light tube	20
Control electronics housings	10
Camera (3 Cine and 1 TV)	
Film cassettes and film advance systems (3)	200
Film, 70 mm, 3000 ft	30
Camera base and shutter housing (3)	60
Cassettes, 35-mm format, shifting mechanisms (3)	40
Vidicon (1-in. incl. yoke)	10
Interference filters, stepping motor turrets and mechanism	15
H_α monochromator and temperature control	30
Electrical Harness and Distribution	
Telescope, internal distribution and cable assembly	25
LM monitor and control cable assembly	10
Relays, junctions, switches, electronics	30
ATM/Telescope 28 VDC bus	20
Inverters, converters, regulators (high dc voltage)	50
Controls	
Temperature sensors and indicators	5
Command display (TV, LM installed)	15
Camera sequencer and shutter controls, switches, logic and electronics	20
Meters, indicators, relays, sensors (LM installed)	10
Optics alignment provisions	15
Total:	1425 lbs

2. Centers of gravity. The centers of gravity of the 3 camera group system and the system of 3 separately located cameras were computed using total masses of 1400 lbs and 1483 lbs, respectively. The origin of coordinates was chosen on the plane of the base of the telescope, the $-X$ axis along the symmetry axis of the housing, $+Y$ in the direction of H_α light tube, and $+Z$ in the direction of the UV light tube. These axes are parallel to the axes chosen for the ATM. The positions of the components of the telescope system were estimated using a scale diagram, and the masses were taken from the list of estimated weights. The results are given below.

3. Moments of inertia. The moments of inertia about the centers of gravity were computed for the two systems in each case by approximating structures in the system by simple geometrical shapes. For example, the primary mirror was treated as a thin circular disk, the telescope housing as a thin-walled tube, the cameras as point masses, etc. In several cases, the small moments of inertia of components about their own centers of gravity were ignored in comparison with the moments given about the system center of gravity. The moments quoted in the table below are approximate, and under-estimate the true moments of inertia.

Parameters	*3 Camera group*	*3 Separately located cameras*
Center of Gravity:	$-X$ 6.48 ft	6.48 ft
	$-Y$ 0.529	0.205
	$-Z$ 0.000	0.034
Moment of Inertia (around axis):	$-X$ 2845 ft² lb	3434 ft² lb
	$-Y$ 21370	22250
	$-Z$ 22435	22120

D. Temperature Control

1. Primary mirror temperature distribution. In the following, only the concentric case will be considered (telescope pointing at the center of the solar disk). The off-center case, where the solar limb is being viewed, is considerably more complex and would add very little to this initial estimate of the thermal situation. Figure 19 shows the rays from the full Sun. One solar unit is directly

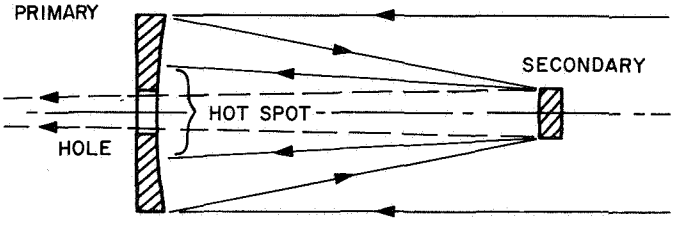

Fig. 19. Rays from full Sun to primary and secondary mirrors

incident on the primary. Some of this is absorbed, depending on the absorptance of the mirror coating, and the balance is reflected to the secondary which intercepts the full beam. The secondary mirror also absorbs a portion of the incident beam and reflects the balance back to the primary where a small amount passes through the central hole and the rest strikes a small area of the primary around the center. This forms a "hot-spot" on the primary mirror. With any appreciable thickness to the mirror, radial heat flow from the hot spot will occur in addition to the overall axial flow from the front absorbing surface to the heat sink at the rear.

2. Assumptions.

(1) 90-min orbit; 45 min with full solar input (442 Btu/ft²-hr) and 45 min with both zero input and zero radiated loss (Earth in field of view or cover closed).

(2) Mirror material properties are constant with time and temperature.

(3) Fully effective heat sink, maintained at 70°F, covering back surface of mirror and both inner and outer edges.

(4) 7.56% of incident energy absorbed by mirror.

(5) Mirror construction—solid, circular plate: CER-VIT, Owens-Illinois.

(6) Three concentric zones considered as approximating the average temperature distribution.

3. Dimensions and constants.

Primary outside diameter	= 80 cm = 31.5 in.
Hole in primary	= 12.0 cm = 4.72 in.
Secondary outside diameter	= 12.1 cm = 4.8 in.
Image of secondary on primary	= 31.2 cm = 11.8 in.
Solar constant, S = 2 gm-cal/cm² min	= 442 Btu/ft²-hr
Cervit: (C-101)	P = 0.090 lbs/in.³
k = 0.97 Btu/hr ft°F	C_p = 0.21 Btu/lb °F
Aluminum (5052)	P = 0.097 lbs/in.³
k = 80 Btu/hr ft°F	C_p = 0.23 Btu/lb°F
Absorptivity of mirror surface	= 7.56%

The primary mirror receives direct solar energy over the full surface except for the area shadowed by the secondary mirror (see Fig. 20). Of this incident energy, 7.56% is absorbed and the rest reflected to the secondary.

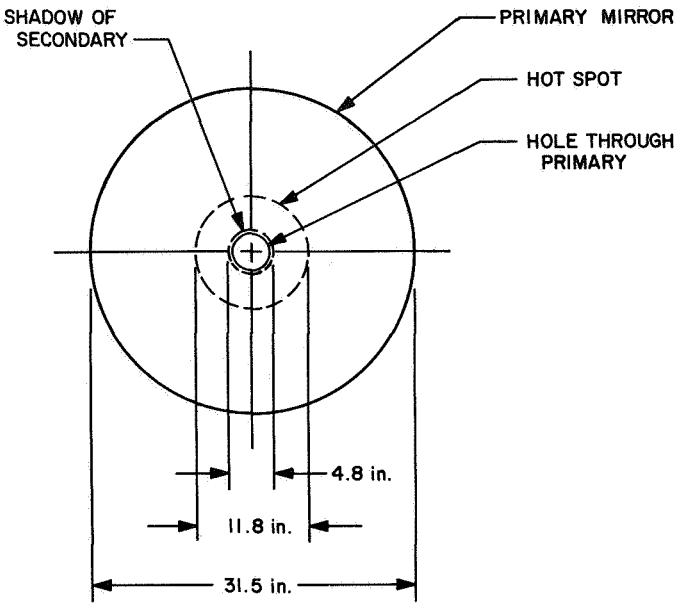

Fig. 20. Direct solar energy received by primary mirror

Again, 7.56% is absorbed and the balance reflected back to the primary where it strikes a small area or hot-spot while part passes through the central hole and on to the camera system. Additional reflections are not considered even though ray tracings show that not all of the final reflection passes out into space.

The areas affected are as follows (these apply to the primary mirror only):

Total primary mirror illuminated	761.9 in.²
Area of secondary illumination	109.4 in.²
Area of hole in primary	17.5 in.²
Net primary outside of hot spot	670.0 in.²

Energy absorbed and reflected, considering the shadow, hole and reflections, is then calculated as being:

Initial on primary	2337 Btu/hr
Absorbed by primary	177
Reflected to secondary	2160
Absorbed by secondary	163
Reflected back to primary	1997
Absorbed by hot spot	127
Passing thru central hole	320
Reflected back to space	1550

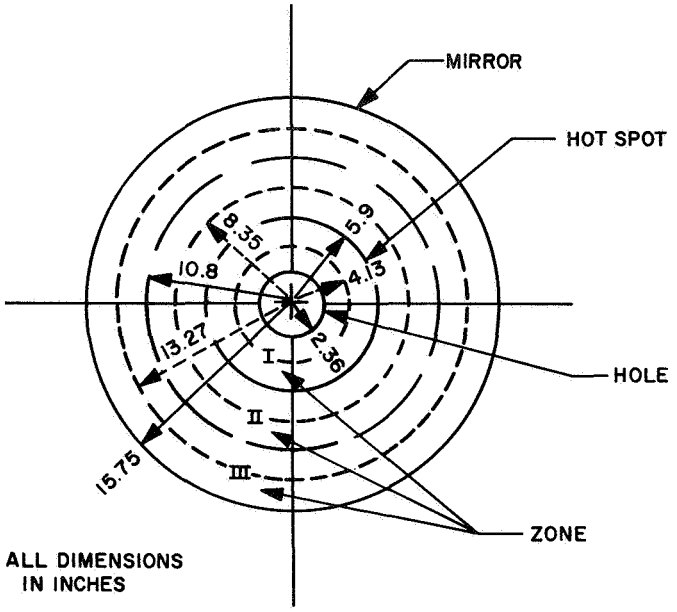

Fig. 21. Division of primary mirror into 3 zones

The absorbed heat flux by the primary mirror (less central hole) is thus 177 Btu/hr over the entire area plus 127 Btu/hr over the hot spot. This amounts to:

Outer annulus	33.4 Btu/ft²-hr
Hot-spot	232.1

For thermal conductivity and temperature-time computations, the primary mirror is divided into three zones as shown in Fig. 21. Zone I (Fig. 22) is the hot-spot around the central hole. Zones II (Fig. 23) and III (Fig. 24) are the outer annulus of the mirror with an arbitrary boundary at the midpoint. The temperatures at the average radii (dotted circles), and along the mid-thickness plane, are considered to be representative of the zones as a whole. At any time, (θ), these temperatures, with the assumed constant 70°F of the back surface and the inner and outer edges, determine the upper (input) surface temperature distribution.

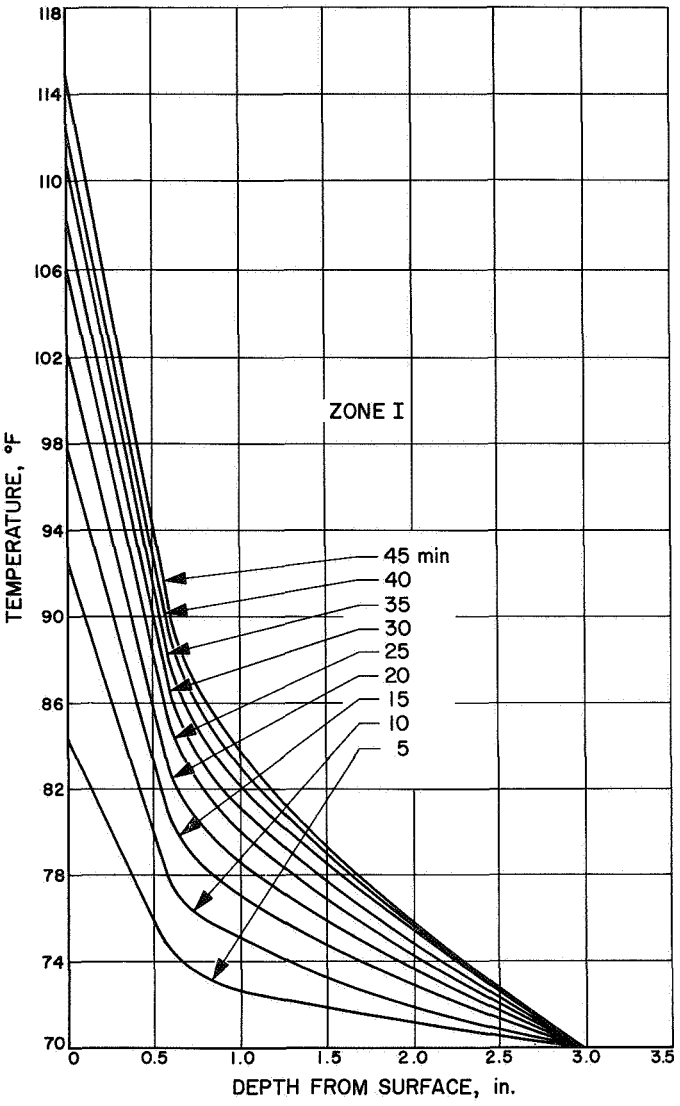

Fig. 22. Zone I of primary mirror

The heat-sinks on the back surface and along the inner and outer circumferential edges are assumed to maintain those surfaces at 70°F. Then, at any time, θ, the zone temperatures can be determined for mid-point layers within the full slab and within upper layers.

The following example is for a Cervit mirror, 80-cm outside diameter, 12-cm central hole, and 3 in. thick. The constants for the three zones are:

Zone	IR (in.)	OR (in.)	A (in.²)	Input (Btu/hr)	Volume (in.³)	Weight (lbs)	Wc_p (Btu/°F)	Input (Btu/5 min)
I	2.36	5.9	91.9	148.1	276	21.9	4.37	12.34
II	5.9	10.8	257.1	59.7	771	61.2	12.23	4.97
III	10.8	15.7	412.7	95.8	1238	98.2	19.64	7.98

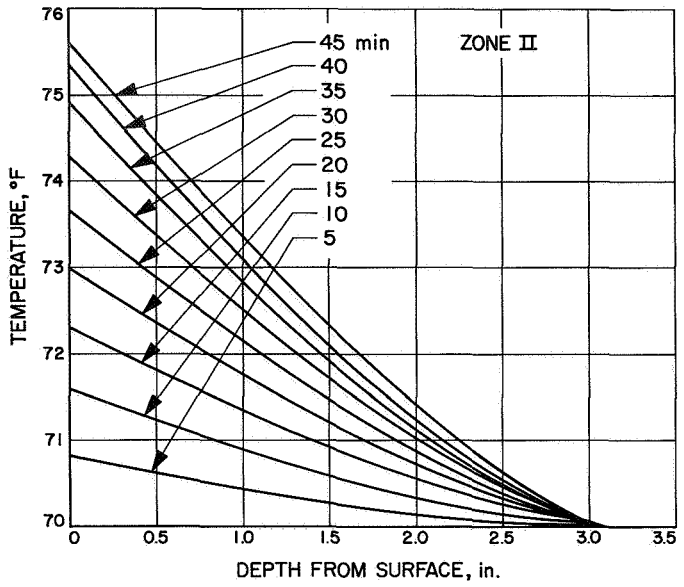

Fig. 23. Zone II of primary mirror

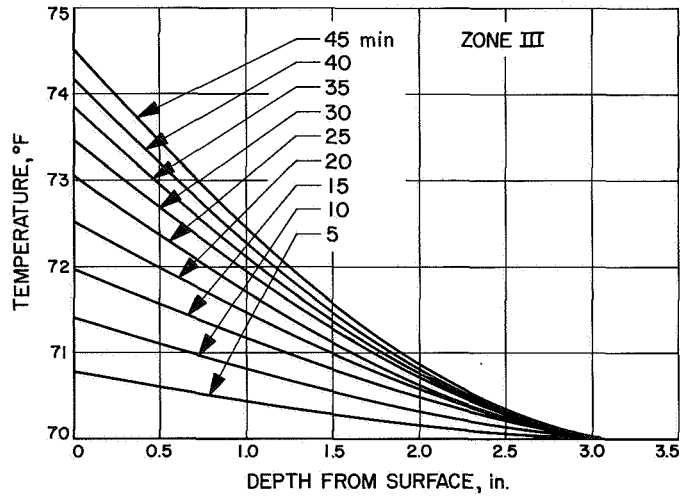

Fig. 24. Zone III of primary mirror

Consider successive time increments of $\Delta\theta = 5$ min. The procedure is to find t at the mid-thickness of the mid-point radius of each zone. The process is then repeated for upper-half thickness using the values of t just calculated as the new "back" temperatures. This gives mean temperatures at ¼ depth. Repeating this a third time for the top ¼ thickness then gives three points in depth for each zone. Extrapolating the curves through these points gives the surface temperature distribution for each 5-min interval during the 45 min of sunlight.

The nomenclature is as follows:

q = heat flow, Btu/hr

t_n = final temp. in zone n, °F

t'_n = starting temp. in zone n, °F

t_0 = initial temp. and heat sink temp., °F

L = slab thickness

$\bar{x}_n$ = radial distance to zone n midpoint, ft

x_n = radial distance to zone n outer boundary, ft

x_i = inside radius, ft

W_n = weight of zone, lbs

c_p = specific heat, Btu/lb-°F

k = thermal conductivity, Btu/hr-ft-°F

θ = time, hrs

q_{in} = q absorbed + q to inner edge + q to back + q to outer edge

$$q_n = W_n C_p (t_n - t'_n) + \frac{\Delta\theta k 2\pi L (t_n - t_{n-1})}{\ln\left(\frac{X_n}{X_{n-1}}\right)}$$

$$+ \frac{k A_n (t_n - t_0)}{L/2} + \frac{\Delta\theta k 2\pi L (t_n - t_{n+1})}{\ln\left(\frac{X_{n+1}}{X_n}\right)}$$

Zone I:

$$q_1 = W_1 C_p (t_1 - t'_1) + \frac{\Delta\theta k 2\pi L (t_1 - t_0)}{\ln\left(\frac{X_1}{X_0}\right)}$$

$$+ \frac{kA_1 (t_1 - t_0)}{L/2} + \frac{\Delta\theta k 2\pi L (t_1 - t_2)}{\ln\left(\frac{X_2}{X_1}\right)}$$

Zone II:

$$q_2 = W_2 C_p (t_2 - t'_2) + \frac{\Delta\theta k 2\pi L (t_2 - t_1)}{\ln\left(\frac{X_2}{X_1}\right)}$$

$$+ \frac{kA_2 (t_2 - t_0)}{L/2} + \frac{\Delta\theta k 2\pi L (t_2 - t_3)}{\ln\left(\frac{X_3}{X_2}\right)}$$

Zone III:

$$q_3 = W_3 C_p (t_3 - t'_3) + \frac{\Delta\theta k\, 2\pi L (t_3 - t_2)}{\ln\left(\frac{X_3}{X_2}\right)} + \frac{kA_3 (t_3 - t_0)}{L/2} + \frac{\Delta\theta k\, 2\pi L (t_3 - t_0)}{\ln\left(\frac{X_0}{X_3}\right)}$$

Substituting numerical values, these become for case A, the full thickness slab:

Zone I:

$$12.342 = 4.372 (t_1 - t'_1) + 0.23443 (t_1 - 70) + 0.4255 (t_1 - 70) + 0.18626 (t_1 - t_2)$$

Zone II:

$$4.973 = 12.232 (t_2 - t'_2) - 0.18626 (t_1 - t_2) + 1.1903 (t_2 - 70) + 0.28262 (t_2 - t_3)$$

Zone III:

$$7.983 = 19.636 (t_3 - t'_3) - 0.28262 (t_2 - t_3) + 1.9106 (t_3 - 70) + 0.76608 (t_3 - 70)$$

Combining and rearranging terms:

$$t_1 = 11.459 + 0.8382t'_1 + 0.03145t'_2 + 0.00063t'_3$$

$$t_2 = 6.535 + 0.8808t'_2 + 0.01768t'_3 + 0.01341t_1$$

$$t_3 = 8.65 + 0.8690t'_3 + 0.0125t_2$$

Solving these equations for each time increment yields the following:

Case A (full thickness, mid-point mean temperatures):

θ	t_{1A}	t_{2A}	t_{3A}
0 min	70°F	70	70
5	72.38	70.41	70.36
10	74.39	70.79	70.68
15	76.08	71.16	70.96
20	77.51	71.51	71.21
25	78.72	71.84	71.43
30	79.75	72.15	71.63
35	80.62	72.44	71.80
40	81.36	72.71	71.95
45	81.99	72.95	72.09

Now taking the half thickness with the "back" temperatures equal to the above (t_{nA}) and using half $W_n C_p$, but the same (X_n/X_{n+1}), etc., and the same input heat, the equations for the three zones, for *Case B*, become:

$$t_1 = 6.3296 + 0.6734t'_1 + 0.0201t'_2 + 0.003218t'_3 + 0.2621t_{1A} + 0.00783t_{2A} + 0.000125t_{3A}$$

$$t_2 = 0.6094 + 0.7006t'_2 + 0.11122t'_3 + 0.2727t_{2A} + 0.004366t_{3A} + 0.10668t_1$$

$$t_3 = 2.457 + 0.6932t'_3 + 0.26979t_{3A} + 0.009976t_2$$

Case B (half thickness quarter-point mean temperatures):

θ	t_{1B}	t_{2B}	t_{3B}
0 min	70°F	70	70
5	74.01	70.62	70.57
10	77.35	71.21	71.07
15	80.15	71.77	71.51
20	82.49	72.29	71.90
25	84.45	72.78	72.24
30	86.11	73.23	72.54
35	87.51	73.65	72.81
40	88.69	73.74	73.04
45	89.68	74.19	73.24

Repeating this a third time, using the top quarter-thickness of the mirror slab, the equations for *Case C* become:

$$t_1 = 5.68 + 0.37691t_1' + 0.00618t_2' + 0.000056t_3' + 0.58692t_{1B} + 0.081008t_{2B} + 0.0000852t_{3B}$$

$$t_2 = 0.64149 + 0.38533t_2' + 0.00341t_3' + 0.59995t_{2B} + 0.00531t_{3B} + 0.005867t_1$$

$$t_3 = 1.6693 + 0.38311t_3' + 0.59643t_{3B} + 0.005514t_2$$

Case C (quarter thickness, eighth-point mean temperatures):

θ	t_{1C}	t_{2C}	t_{3C}
0 min	70°F	70	70
5	79.26	70.68	70.63
10	85.16	71.36	71.21
15	89.38	72.00	71.73
20	92.68	72.61	72.20
25	95.34	73.17	72.61
30	97.54	73.70	72.96
35	99.38	74.19	73.30
40	100.93	74.64	73.59
45	102.22	74.88	73.84

The following three curves show temperature vs depth below the top surface of the Cervit mirror for each 5-min interval. The extrapolated values for average surface temperature (°F) *vs* time in minutes are:

θ	Zone I	Zone II	Zone III
0	70	70	70
5	84.2	70.8	70.7
10	92.3	71.6	71.4
15	97.7	72.3	72.0
20	102.1	73.0	72.5
25	105.9	73.6	73.1
30	108.1	74.3	73.5
35	110.4	74.9	73.9
40	112.3	75.3	74.2
45	114.6	75.7	74.5

A final plot of surface temperature vs radial distance from the center of the mirror, for each 5-min interval of time, is shown in Fig. 25.

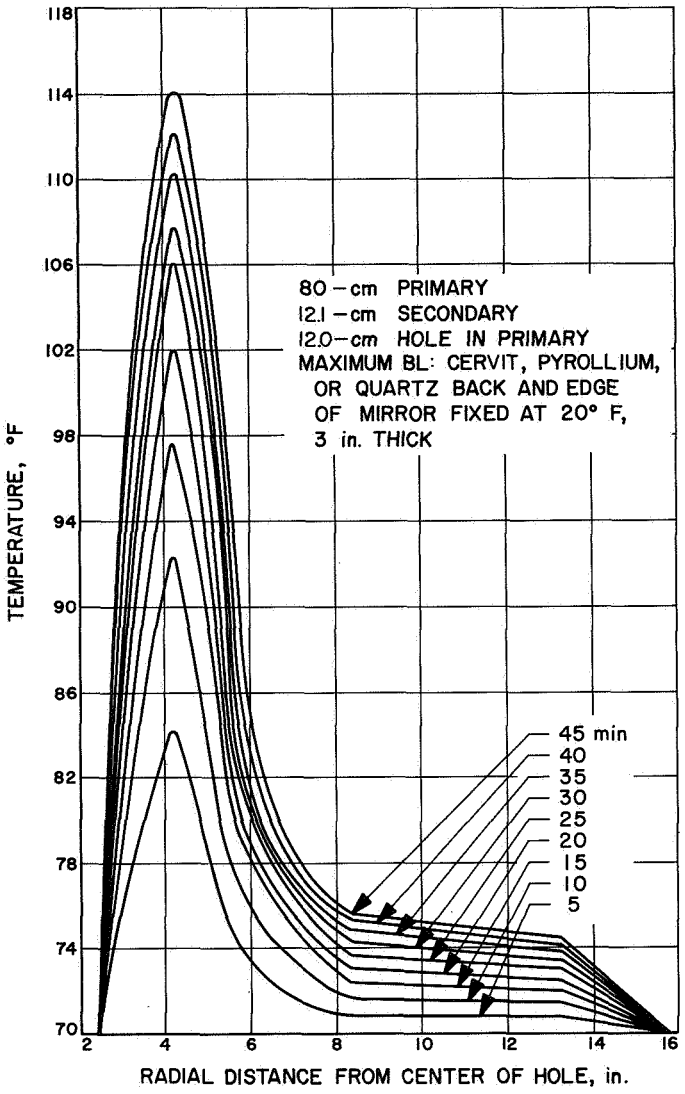

Fig. 25. Final plot of surface temperature vs radial distance from center of primary mirror

4. Thermal distortion of primary mirror. The purpose of this study was to determine the top surface distortion (reflecting surface) of the primary mirror caused by temperature gradients. To represent the worst case, the final body and surface temperatures of the concentric hot-spot case were used (see Section on Temperature Distribution). To maximize distortions, fused quartz was taken as the material rather than CER-VIT as the temperature distribution would be approximately the same.

The assumptions for the analysis were as listed below. These are consistent with the objectives of the study and with the known parameters of the environment, geometry and material.

(1) Both surfaces of the mirror are essentially flat.

(2) Deflections at 29 nodes on the mirror surface are adequate to describe the surface distortion. The smallest distance between adjacent nodes is 0.25 in., and the density of the nodes is directly related to the magnitude of the thermal gradient. (See Fig. 26 for nodal distribution).

(3) Three different boundary conditions were considered. These indicate the influence of method of mirror support on the distortion.

  (a) Axial restraint (no radial) at the inner and outer edges only.

  (b) Axial and radial restraint at the inner edge, axial restraint only at the outer.

  (c) Axial restraint only at the inner edge.

The analysis technique is based on the computer program "ELAS" (Reference: JPL IOM from F. Akyuz and S. Utku to Distribution, "ELAS Computer Program," dated 3/9/67). The accuracy of the analysis is dependent on the material properties and on the temperature distribution used. Non-isotropic material properties and asymmetrical temperature distribution can be solved if a coarse finite element representation is acceptable.

Other axisymmetric temperature distributions and other mirror materials can be handled using the existing finite element representation. Any other modification will require considerably more effort. The definition of tolerances is vital to the method of analysis. The allowable distortions must be defined for the overall surface as well as local variations because the finite element technique provides displacements at discrete points.

The analysis procedure can be briefly described as follows:

(1) A geometric and loading symmetry about the axis of revolution reduces this problem to a two-dimensional case. A 30-deg sector (any sized sector could be used) is selected for the analysis. This size has resulted in good solutions to other similar problems. (See Fig. 27.)

(2) The 30-deg sector of the mirror is approximated by 140 tetrahedrons defined by the nodes selected to represent the temperature distribution.

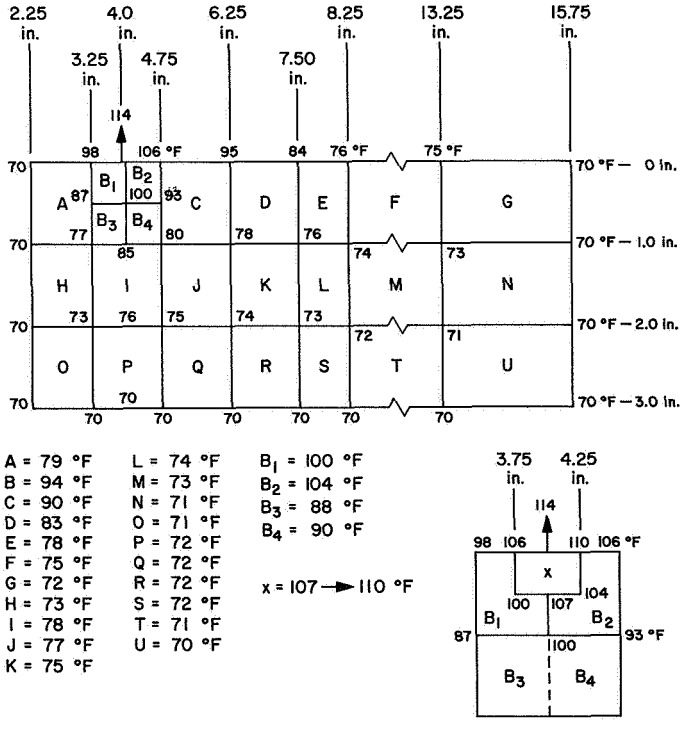

Fig. 26. Temperature zones

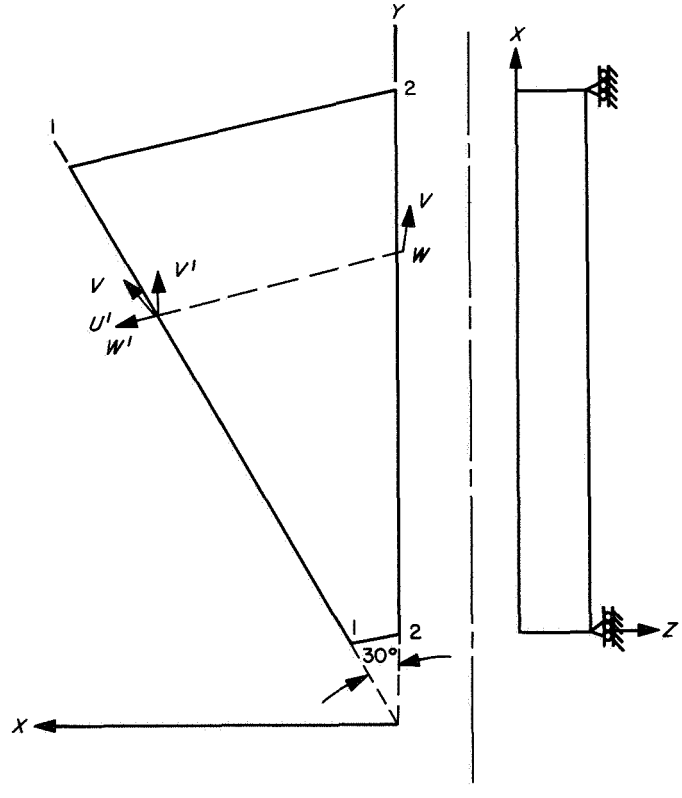

RELATION BETWEEN DISPL. ON SURFACE 1-1 TO 2-2:

$V' = V \cos\theta = 0.867\,V$
$U' = U \sin\theta = 0.500\,V$
$W' = W$

Fig. 27. Analysis configuration

(3) A stiffness formulation for each tetrahedron is used to define the elasticity of the mirror. Since displacement continuity of all edges of each element is assured, a lower limit in the displacement is obtained.

The resulting distortion of the top surface of the primary mirror is shown in Fig. 28 for the three assumed boundary conditions. The distortion along one radial plane completely describes the problem because of symmetry. The resolution of the distortions is only as good as the smallest distance between nodes, which in this case is 0.25 in.

For future studies, the analysis will be extended to include: (1) surface curvature, (2) non-isotropic materials, (3) various different boundary conditions (methods of support), (4) non-symmetric temperature distribution, for which a coarser grid can be used to obtain surface distortions, and (5) different materials.

Temperature Breakdown (Refer to Fig. 26):

Temp. Code	Temp., °F
1	110
2	104
3	100
4	89
5	83
6	78
7	75
8	72
9	70

Zone	Code	Zone	Code
A	6	J	6
B_1	3	K	7
B_2	2	L	7
B_3	4	M	8
B_4	4	N	9
C	4	O	9
D	5	P	8
E	6	Q	8
F	7	R	8
G	8	S	8
H	8	T	9
I	6	U	9
		X	1

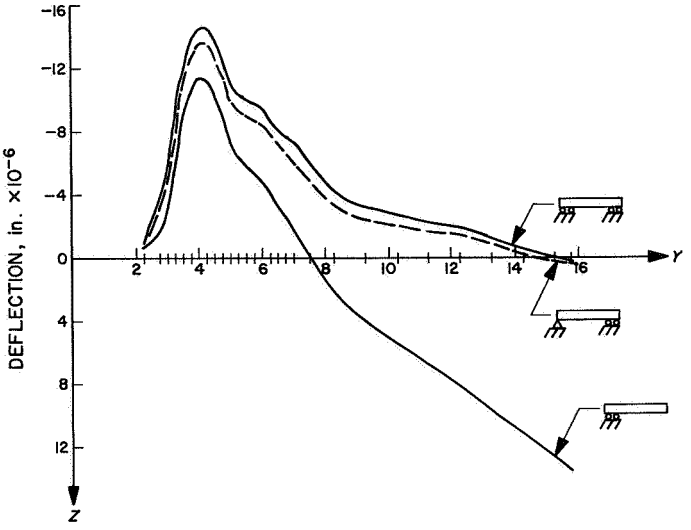

Fig. 28. Top surface distortion normal to top surface for various boundary conditions

5. Mirror active thermal control systems. The analysis of the heat loads and thermal behavior of the telescope optics has shown the need to dissipate the heat which both the primary and secondary mirrors would accumulate during the periods of solar observation. As long as the heating is uniform, producing no thermal gradients, the net effect on the mirrors will be merely a change in size and, hence, a change in focal length. This may be compensated easily by refocusing the telescope system which can be done continuously during orbit by remotely controlled motors. However, the primary mirror is also nonuniformly heated by a hot spot which can appear on any part of the mirror depending on the region of the Sun which is under observation. (See Fig. 20.) The secondary mirror becomes greatly heated as a result of the intensely concentrated light which is collected on it during solar observations. This heating is uniform, but if the temperatures become excessive, the reflecting surface may be damaged.

In addition to the problem of heating, the properties of the optics are also affected by cooling whenever the telescope is not in observation. Such is the case when the passage in orbit is in the Earth's shadow and whenever the telescope cover is closed.

In the ideal situation, the mirrors should be maintained at a constant temperature and thermal gradients in any direction should be zero. This would give no thermal distortions in the mirrors' surfaces other than those which might arise from the mounting cell or telescope structure. For constant temperature during the orbit cycle of full

sunlight and darkness, the mirrors would require a heating system as well as cooling.

Without an active cooling system, the heat absorbed by the mirrors will be greater than the losses through natural conduction and radiation to the surrounding ATM structure. The temperatures, then, will continue to rise during each successive orbit. It is possible that the resulting equilibrium temperature can go well above 200°F. This is the upper limit for insulators which would release volatile condensible materials, for certain cooling fluids, and for available photographic materials.

The zero thermal gradients, both axially and radially, considering the high energy input at the hot-spot image on the primary mirror, can not be attained with available materials in a practical mirror configuration even with an active cooling system. The exact degree to which the gradients, and distortions, could be reduced has yet to be examined in detail for all material and structural arrangements. Conceptually, there are three possible methods of minimizing distortions in the primary mirror: (1) select a material with a high thermal conductivity such that the temperature gradients are held down to an acceptable level, (2) select a mirror material with a near-zero thermal expansion coefficient over the range of temperatures expected such that distortions are negligible even with thermal gradients, and (3) build in an active temperature control system, with both heating and cooling, so that the temperature distribution remains constant during the picture-taking sequence. The first two are considered in detail in the Section on Materials. The third approach is discussed below.

6. Primary mirror temperature stabilization. The supposition of temperature stabilization considers that the primary mirror would require heat to be added as well as removed during the course of the mission. Four possible methods are described:

(1) A system in which water is circulated through the sealed cavities of the mirror structure.

(2) A system in which water is circulated through coils of piping which can be attached to the underside of the mirror.

(3) A system in which a low melting temperature solution of solids is contained within the cavities of the mirror structure.

(4) A system of heaters which is placed under the mirror.

Method one proposes that the mirror could be fabricated as a back-ribbed structure composed of hollowed out sections to form a grid or "wheel spoke" pattern. The base of the mirror can be welded with an aluminum plate which seals the cavities as cells shown in Fig. 29. Various heat conduction fluids could be used, but from a fail-safe point of view, it must not be an oil or one which would leave a film or residue on the mirror surfaces in case of a leak. Water is still one of the more efficient fluids and has the advantages of low vapor pressure, compatible operating temperature range, and, when pure, low corrosion activity and lack of residues. Heat carried away by the water would be dumped by a radiator remotely located on the side of the ATM. Plumbing radiator and pump could be easily sized to give a broad range of flow rates. Such a system could also transfer heat from the hot spot of the mirror over the cooler zones to reduce radial thermal gradients.

During periods when the telescope will be in a standby mode, either on the dark side or with the cover closed, the temperature of the mirror can be maintained at near the selected ambient condition by utilization of a heater in the loop. A single valve which can be operated by temperature sensors could cause fluid to bypass the radiator and pass through the heater. A limiting temperature sensitivity for the sensors can be established to maintain the figure constraints of the optics.

This is an efficient method of heat transfer in the sense that all of the surfaces of the cells in the mirror are wetted to promote immediate response to the requirements of heating or cooling. There are possibilities however, for stagnation regions to appear in the flow characteristics of some mirror cell patterns. A rectangular grid arrangement would be a complex pattern to manifold. A "spoked wheel" grid would be easier to manifold allowing a flow pattern to be directed radially toward the periphery of the mirror where the cooler regions would be present. This cooling system would be equally applicable to a metal or CER-VIT, etc., mirror material.

The second method is a variation of the above system with coils of tubing brazed to the back of the metallic mirror. Water would be circulated through the tubing for heating and cooling. Controls, plumbing, pump and radiator would operate in a similar manner. This is shown in Fig. 29. Generally, this is a favorable design because it is simple and direct. The tubing would confine the fluid independent from the body of the mirror material. Joints of a piping system are much easier to seal than the larger surfaces used in the above design. Also, there

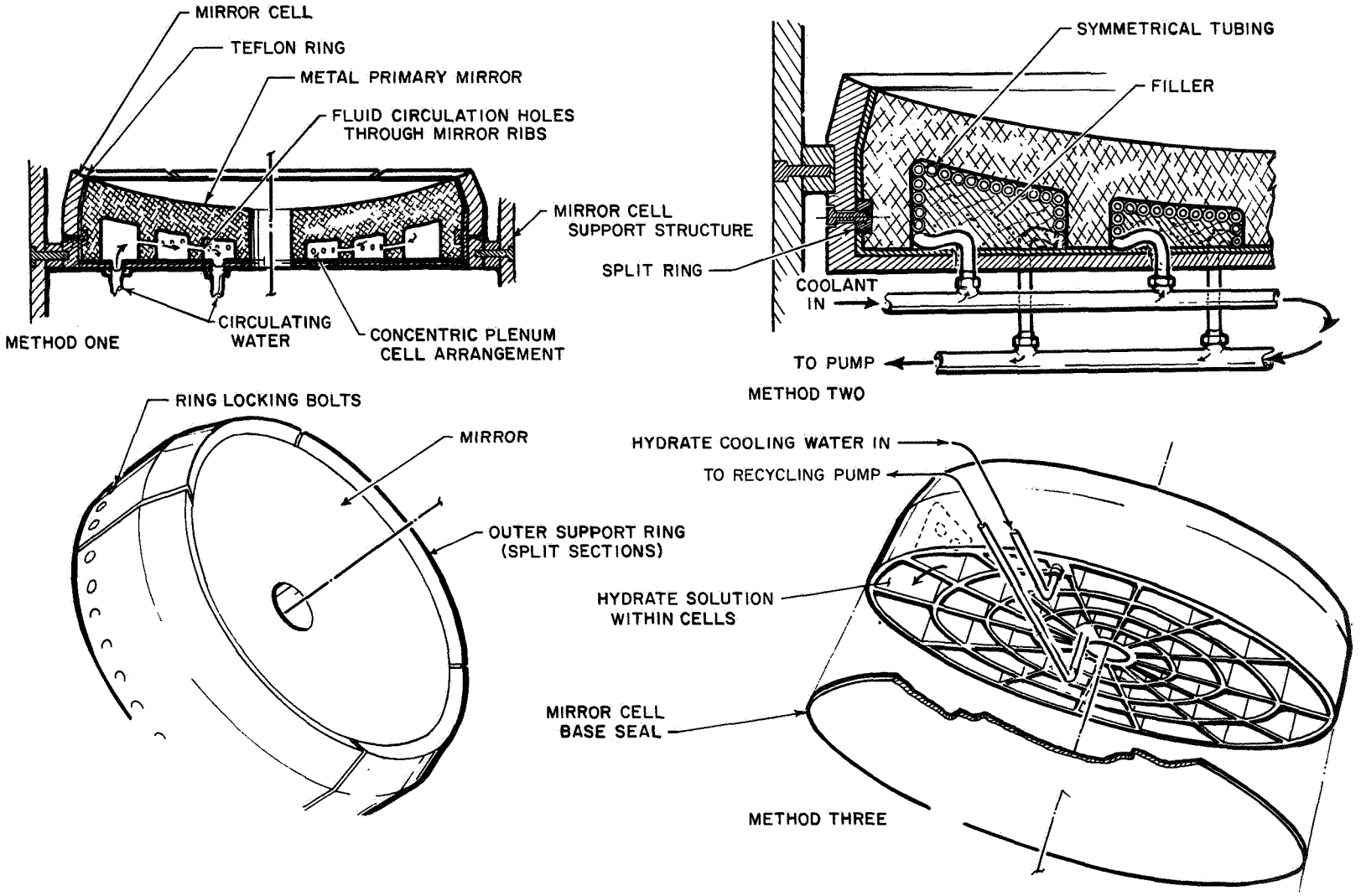

Fig. 29. *Apollo* telescope module; active thermal control, method 3

would be no stagnant regions, all of the fluid in the tubing would be moving at relatively uniform velocity, which is not the case in the first design. An added advantage is that a multiplicity of systems could be arranged. Each would cover a limited area of the mirror back, and each would be independently controlled with its own sensor, pump and heater or radiator.

A disadvantage is that the rate of heat transfer from the mirror to the fluid would be materially inferior to the first method. It may be necessary to lay a part of the coils along the walls of mirror ribs in order to stabilize their temperatures as well. Variations in sizes of the coils may be an approach to resolving the problems of local hot spots. This would, however, complicate the fabrication of piping and would be vulnerable to flaws of fabrication.

Of the possible failure modes in the two described methods of stabilizing the primary mirror temperature, the most serious would be in the water circulating apparatus. Failure would occur with any of the following:

(1) A joint leak, resulting in loss of water. Operation of the pump would increase the loss rate.

(2) Blockage of the flow by foreign matter or ice in the tubing. The latter condition would only be temporary.

(3) Failure of pump or pump motor. Water would cease to flow in the absence of gravity.

(4) Failure of valve. Same result as (3), or could flow too freely.

(5) Micro-meteoroid puncture of external lines and radiators. Same result as (1).

(6) Failure of heat sensor or control. Same result as (4).

Conditions (3) and (4) could be minimized by reliable designs and establishment of confidence by reliability testing procedures. Condition (5) could be minimized by locating the radiators in protected areas of the ATM rack. The mechanical design and coupling practice of reliable pipe joints (1) can reduce the probabilities of leakages at these places. The failure probabilities of heat sensors and the associated electronic and electrical parts (6) can be minimized by designing redundancy in the control. Boiling water due to excessive heat inputs in the case of failed circulation should not cause failure of the system, as an adequate expansion provision could be included with a water accumulator and pressure relief valve.

With any of these failures, the cooling system would change from active to passive. The telescope would continue to operate satisfactorily if the heat input could be reduced to balance the conduction and radiation losses, particularly during the dark-side half of the orbit.

A third method for active thermal control is also shown schematically in Fig. 29. This consists of a heat stabilizing fluid sealed in the cell space behind the mirror. The fluid is a salt-hydrate formulation with a high latent heat of fusion such as Cyro-Therm "Transit Heat" which is allowed to melt during the hot half of the orbit and is refrozen during the dark half.

The primary mirror construction could include a rib pattern and back cover welded or fused together such that a series of interconnecting cells is formed. These cells can be filled with a salt-hydrate with suitable expansion chambers to allow for the small increase in volume when liquid. Throughout the cell space would be a series of metal tubes carrying the refreezing coolant (probably distilled water) which would be pumped in a closed path from the mirror assembly to an external heat radiator on the side of the ATM, and back to the mirror.

A typical operating cycle (single Earth orbit) would be as follows: Starting with the first sighting of the Sun, the water coolant pump would be turned off, the salt-hydrate would be 90+% frozen and the mirror assembly would be uniformly at a specified temperature, say 120°F. As the picture-taking sequence progressed, the illuminated surface of the primary mirror would receive solar energy. This heat would be conducted to the back where it would melt the salt-hydrate material. However, as long as the material included both solid and liquid phases, and it can be sized to accomplish this for the 45-min illuminated portion of the orbit, it would remain at a constant temperature thus tending to hold the mirror temperature constant also. During the dark half of the orbit, the coolant pump would be turned on and refreeze the salt-hydrate back to 90+% solids. The cooling rate, the amount of telescope insulation, and the timing of the cycle could be adjusted so that the primary mirror remained at the same specified temperature during the dark half of the orbit.

An example of a salt-hydrate type of heat absorbing material is sodium-thiosulfate pentahydrate ($Na_2S_2O_3 \cdot 5H_2O$). Crystals of this material melt at 120°F, dissolving completely in the water of crystallization ($5H_2O$). This material shrinks about 8% as it solidifies, which means that expansion chambers would only be needed to protect

against the possibility of melting the entire charge and subsequently heating the solution above its melting point. The properties of this material are as follows:

Density, solid	115 lbs/ft^3
Density, liquid	104 lbs/ft^3
Specific heat, solid	0.43
Specific heat, liquid	1.79
Heat of fusion, weight basis	90 Btu/lb
Heat of fusion, volume basis	9360 Btu/ft^3

Thermal calculations which indicate approximately 300 Btu/hr will be absorbed by the primary mirror. Thus, 4 lbs of the salt-hydrate would accomplish our purpose leaving a margin of residual solids at the end of the illuminated (heating) half and residual liquid at the end of the dark (cooling) half of the orbit.

The hydrate, being a stable chemical compound, is not a subject for reliability estimates. Should a leak occur, the transition temperature would not be affected but some water of hydration could be lost. This would result in a reduction of the effective amount of salt-hydrate in the system. On the other hand, the refreezing system contains piping, a radiator and a pump, any of which may fail. Should failure occur, the telescope system would still be operable, but at a reduced level or duty cycle, as the heat loss method would be passive rather than active.

Assuming 120°F for the melting point of the salt-hydrate, the total conduction loss from the mirror to the ATM structure, at 70°F, would be approximately 50 Btu/hr. This neglects radiation to the structure or out of the tube to the dark sky, both of which would be negligible at these temperatures. Total heat absorbed has been calculated at 300 Btu/hr maximum. Operations could then continue with balanced input and loss if the telescope cover were open to the Sun for 50/300 = 1/6 of the illuminated half of the orbit. Thus, with 45 min of dark-side cooling, there would remain 7.5 min of satisfactory solar observation for each orbit without overheating the primary mirror.

A fourth method considers the possibility that the heat load on the mirror could be satisfactorily conducted by the mirror and mounting material to appropriate heat sinks without the assistance of cooling fluids and without exceeding some specified maximum temperature. It compensates for the hot spot by adding additional heat to the regions of the mirror which are cooler. In this manner, the thermal gradient, radially and through the mirror, is reduced and maintained at a steady low level. Figure 30 illustrates a typical pattern of heaters which can be individually turned on or off, as required. A pattern of temperature sensors in the mirror would provide the control and monitoring signals.

The heaters can be controlled by thermal sensors for automatic compensation. By maintaining a plot of the photographs taken, the Sun image position could be anticipated for the next orbiting observations. It would then be possible to pre-heat a pattern in the mirror to match the next hot-spot location. This can have a manual override on the heaters and place the system in a stand-by mode.

This method is very simple, requiring no moving parts or circulating fluids. The system can be provided with

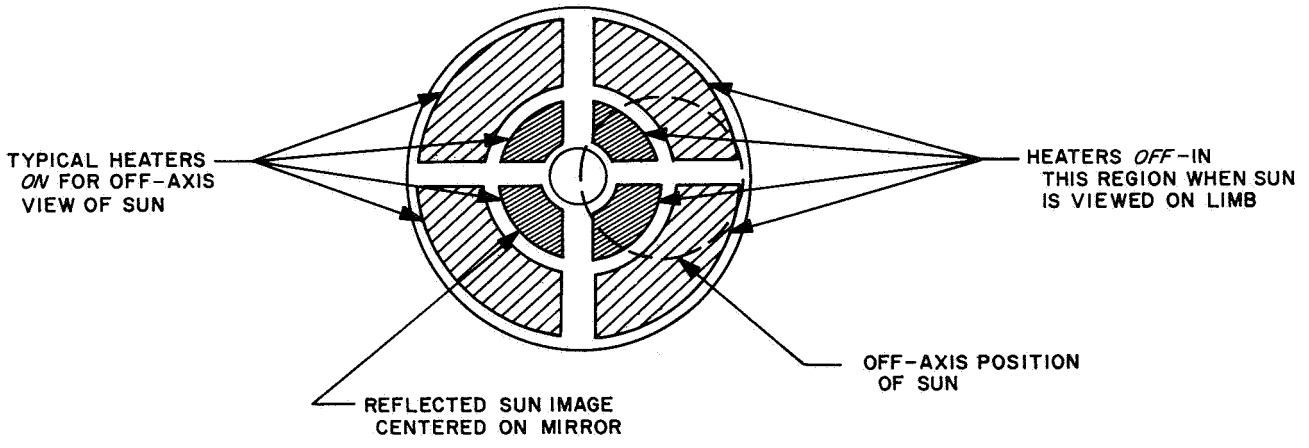

Fig. 30. Primary mirror heaters; method 4

a timer to cycle the 45-min period for cooling when in the dark side of the Earth. Such a timer can be reset by the astronaut. A sampling sequence can be scheduled to monitor each thermocouple during the dark side of the orbit as an operational procedure in preparation for the next period of observation.

All of the above described methods will be analyzed to determine an optimum design for the telescope. An evaluation of these methods can be conducted with thermal scale models containing optical flats as substitutes for the mirrors.

E. Materials

1. Introduction. In a near-diffraction-limited system, such as the one proposed, the ultimate success of the design necessarily hinges on the proper choice and fabrication of the optical elements. This is an area considered pacing from a materials point of view. Limited time has dictated a larger concentration of effort during the study on mirror materials than any other area.

Satisfactory non-flight mirrors for stellar observation have traditionally been fabricated from glasses, usually low-expansion pyrex or fused silica (quartz). In recent years, metal mirrors have been gaining importance, especially for solar telescopes. Most of the efforts along the latter lines have utilized aluminum (usually cast). Because of the difficulty of figuring an aluminum surface, a thick coating of hard nickel (electroless) is applied. Such a surface can be figured in a manner similar to that used for the glasses.

Since the advent of the "space age" considerable effort has been devoted to the development of lightweight flight mirrors. Because of their low densities and fabricability into relatively thin sections, aluminum and beryllium have been the favored choices. Most of the effort has been concentrated on mirrors of relatively low optical quality, for example, for infra-red detection systems. Small electroless nickel-coated beryllium mirrors were used in the *Mariner-Mars* Cassegrainian-type television camera telescope.

The presently proposed telescope requires lightweight mirrors of extremely high optical quality, able to survive the strenuous launch environment and retain their figure under non-uniform solar heating conditions during service in orbit. It is, therefore, judged that the mirror requirements for the proposed system are somewhat beyond the current state of the art. It is felt, however, that satisfactory mirrors can be fabricated using available materials and taking advantage of much of the experience gained to date in fabricating lower quality flight mirrors. Much of the present report is devoted to a discussion of this subject including selection of reflective surfaces and overcoating for the mirrors.

Other subjects which will be discussed include materials for filters, the telescope structural housing, cameras, and electronic equipment. It is felt that generally satisfactory choices can be made within the current state of the art in these applications. Areas where more information is needed to ensure satisfactory choices will be indicated.

2. Mirror materials. The solar telescope considered* is an on-axis Cassegrainian type with an 80-cm-diameter primary parabolic mirror and a 9-cm-diameter hyperbolic secondary mirror. The image of the Sun is focused "behind" the primary, passing the light through a 12-cm hole in the center of the mirror. The system is a folded one utilizing a pair of 45 deg flat mirrors to place the focused image in a position near the mouth of the telescope. Suitable devices for splitting the beam to place images in several cameras placed on the outside of the housing at various positions in the focal plane will be provided.

The proposed design imposes non-uniform heat loads on the primary mirror during solar observation. This is illustrated schematically in Figs. 31 and 32. The right-hand diagram of Fig. 32 illustrates the worst-case condition, i.e., when viewing the limb of the Sun. About 5 to 10% of the incident energy is absorbed** into the mirror giving rise to unsymmetrical heating effects. Unless proper materials are chosen and fabrication is done with care, the heating effects could give rise to unacceptably large thermal distortions. The factors which must be considered in making satisfactory choices will be discussed in subsequent sections.

In addition to thermal distortions, which are reversible, other factors which must be considered include (a) dimensional stability, i.e. freedom from irreversible changes resulting from time-dependent phenomena such as relief of residual stresses and metallurgical instability (aging), (b) weight, and (c) fabricability. The last includes the adaptability of the material to brazing or welding techniques to build up lightweight and/or sealed** mirror

*See Refs. 1 through 27.

**In the event an active temperature control system must be used to stabilize mirror temperatures, provision must be made for sealing the mirror structure to contain a heat transfer fluid.

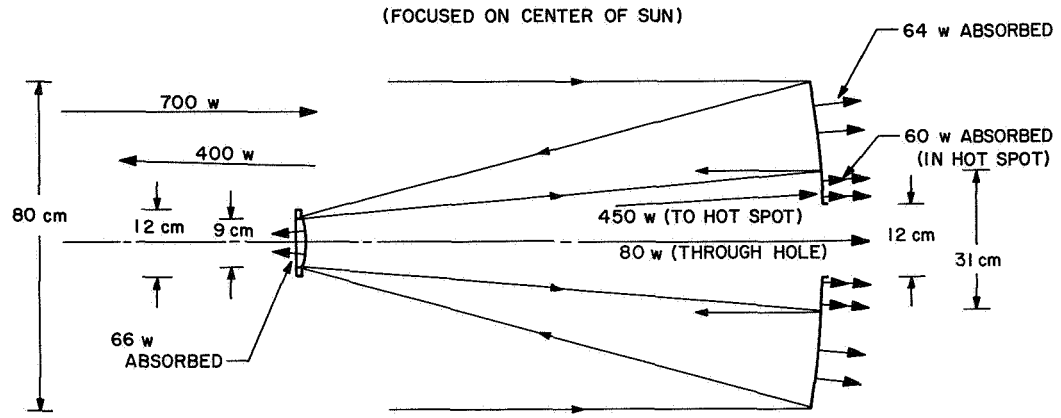

NOTES:

1. BOTH PRIMARY AND SECONDARY COATED WITH ALUMINUM
2. α_s OF Al = 0.11 (ρ_s = 0.89)

Fig. 31. Schematic presentation of heat distribution; on-axis Cassegrainian system

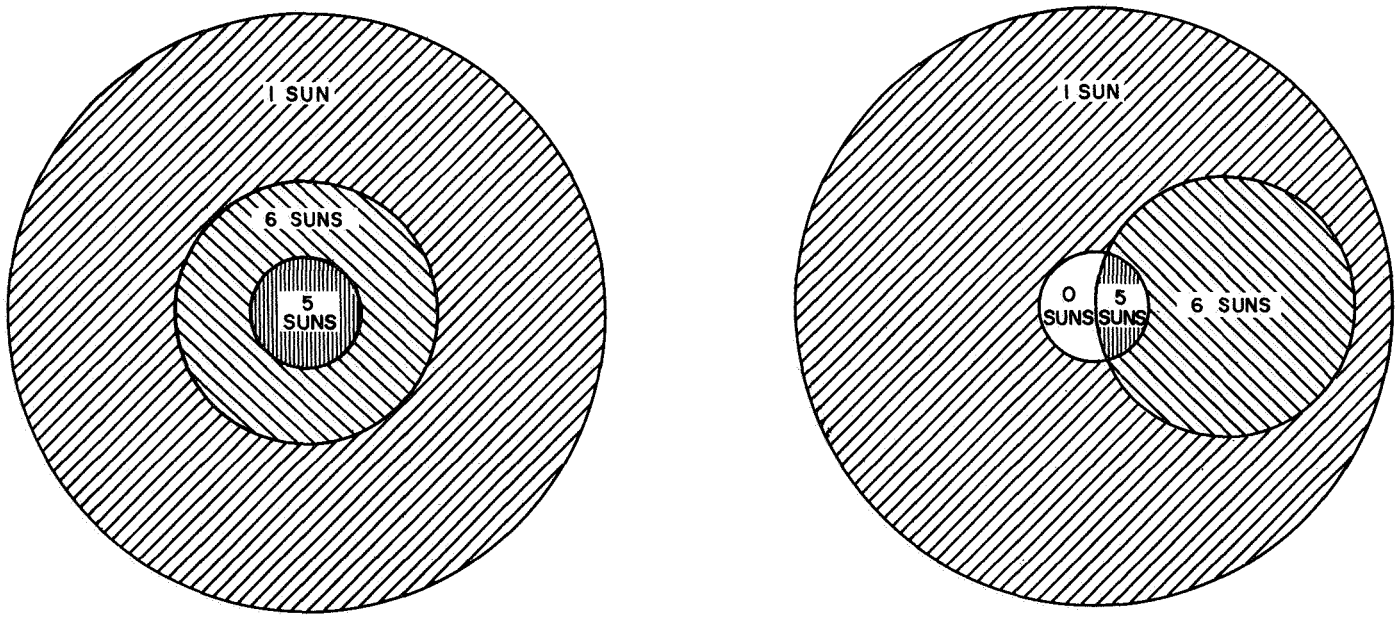

OBSERVATION OF CENTER OF THE SUN

OBSERVATION OF LIMB OF THE SUN

Fig. 32. Schematic presentation of energy incipient on primary mirror for extreme positions of solar observation

structures, ability to apply effective stress relieving treatments, and ability to be figured accurately using techniques or adaptations of techniques developed over many years for figuring glass mirrors. Final selection, therefore, will involve trade-offs of the various factors that must be considered.

a. Thermal distortion. A thermal analysis for the case representing viewing the center of the Sun has been conducted for quartz. A solid quartz mirror, 3 in. thick, provided with suitable means for holding the back surface temperature at 70°F during solar observation would be heated to a calculated temperature of 114°F at the surface. The peak temperature would occur at a distance of approximately 10 cm from the center of the primary (4 cm from the edge of the central hole). The model for quartz can be used to obtain a reasonable first approximation for the temperature distribution of metal mirrors by multiplying the maximum ΔT for quartz, i.e., 44°F, by the ratio of the thermal conductivity of quartz (k_s) to that of the metal in question (k_M), or:

$$\text{approximate } \Delta T = 44 k_s / k_M$$

For an aluminum mirror of identical dimensions, the maximum $\Delta T = 44 \times 0.91/80 = 1/2$°F. Thus it is evident that a metal, with its characteristically high thermal conductivity, will have drastically lower thermal gradients than will quartz.

The approximation used above seems particularly justified when the errors intrinsic in any calculation of thermal gradients are considered. The overwhelming error results from the measurement accuracy in the solar absorption of the mirror surface. The absorptance is computed from the measured reflectance according to the formula, $\alpha = 1 - R$. Since the measurement error in R is considered to be ± 0.03, the error in α is also necessarily ± 0.03. Thus, for example, for a wavelength where the reflectivity of aluminum is measured to be 0.88, the actual reflectivity lies between 0.85 and 0.91. The actual absorptance of aluminum, using the above relationship then lies between 0.09 and 0.15. This represents an error of $\pm 25\%$. Thus, it is evident that measuring techniques which are generally satisfactory for reflectivity ($\pm 3\%$ error) are entirely inadequate for measuring solar absorptance of highly reflective surfaces. Direct methods such as calorimetry would have to be used to obtain accurate absorptance data. to the writer's knowledge no such measurements have been made. Calorimetric methods have been used to determine directly the α to ε ratio, in which case the accuracy of α computed is dependent on the accuracy of ε.

In addition to thermal conductivity, a material property of major significance in influencing thermal distortion is the thermal expansion of the material in the vicinity of the ambient temperature for the system. Based on the thermal analysis discussed earlier, a computer program has been set up to analyze the thermal distortions occurring in quartz (Ref. 2). This program shows a peak distortion at the zone of maximum temperature of approximately 3700 Å, assuming the neutral axis at the back surface of the mirror. Simplified calculations, using thermal expansions in the thickness direction only, give a distortion of 2800 Å, assuming the neutral axis at the back surface of the mirror. Factoring the errors intrinsic in the solar absorptance values, the range of distortions for the simplified calculations is 1950 to 3250 Å. Thus, the simplified calculations are considered sufficiently close to the more sophisticated calculations to justify their use for comparative purposes in evaluating different materials.

Reference 3 makes use of a "Thermal Warpage Index" as a tool for comparing thermal distortions in mirrors of various materials. In the present study, the term "Thermal Distortion Index" (TDI) shall be used as more descriptive of the case for thick or ribbed mirrors, where a significant amount of distortion can occur because of expansion and contraction in the thickness direction. The TWI or TDI, as it is called here, it useful for comparing a wide range of materials from a thermal-distortion standpoint. The TDI is the ratio of the expansion coefficient to the thermal diffusivity,

$$TDI = \frac{\alpha}{k/\rho C_p} \quad \text{or} \quad \frac{\alpha \rho C_p}{k}$$

where

α = thermal expansion coefficient near 70°F

ρ = density

C_p = specific heat

k = thermal conductivity

The TDI is independent of the mirror configuration and is purely a function of the physical properties of the materials. For a given heat input, the thermal distortion obtained should be roughly proportional to the TDI. Pertinent physical properties and TDI's of a number of materials are given in order of decreasing index in Table 1.

Table 1. Comparative thermal distortions for various materials

Materials	α, 10^{-6}/°F	ρ, lbs/in.^{3}	C_p, $\left(\frac{\text{Btu}}{\text{lb °F}}\right)$	k, $\left(\frac{\text{Btu}}{\text{hr ft °F}}\right)$	[1]TDI, (10^{-10} hr ft/in.^{3})	[2]E, (10^6 psi)	E/ρ
Stainless steel (300 series)	9.6	0.29	0.12	9.4	225	28	96
Titanium (comm'l pure)	5.0	0.16	0.13	9.8	106	16.5	103
Nickel (pure)	7.4	0.32	0.11	45	58	30	94
Quartz (fused silica 7940)	0.28	0.079	0.17	0.77	49	10.6	135
Brass (70/30)	11.1	0.31	0.09	70,	44	16	52
Aluminum (5052)	13.2	0.097	0.23	80	37	10.1	104
Magnesium (ZK 60A)	14.5	0.066	0.24	69	33	6.5	98
Ni-Resist. Cast iron (type 5)	2.2	0.27	0.11*	23	28	10.5	39
Tantalum (pure)	3.6	0.60	0.036	31	25	27	45
Invar	0.5	0.29	0.12	7.8	22	21	72
Beryllium (QMV)	6.4 to 8	0.066	0.44	104	18–22	37–44	560–670
Cer-Vit (C 101)	0.08	0.090	0.21	0.97	16	13.4	149
Copper, cast (Cu-1Cr)	9.3*	0.32	0.09	182	15	16.5	52
Copper (pure)	9.3	0.32	0.092	225	12	17	53
Molybdenum (Mo-0.5 Ti)	3.1	0.37	0.061	67	10.5	46	124
Silver (pure)	10.6	0.38	0.056	242	9.3	10.5	28
ULE fused silica (7971)	0.04	0.079	0.17	0.77	6.9	10.6	135
Tungsten (pure)	2.4	0.70	0.034	116	4.9	53	76
Super invar	0.1**	0.29*	0.12*	8*	4.4	21*	72
Graphite (molded)	1.4	0.064	0.20	70	2.5	0.7	11

[1]Thermal Distortion Index $\left(TDI = \frac{\alpha\rho C_p}{k}\right)$

where: α = coefficient of thermal expansion near 70°F

ρ = density

C_p = specific heat

k = thermal conductivity

[2]E = Modulus of elasticity

Sources of data; Refs. 3 through 14.

*Estimated

**Possible to reduce through heat treatment, see text.

Also included is the modulus/density ratio for each material.

All things being equal, a high modulus/density ratio makes possible a stiffer structure for a given weight. A low ratio coupled with a low elastic limit and a low damping capacity would point toward distortion problems during launch.

It is possible to eliminate from further consideration a number of the materials in Table 1, as follows. Stainless steel and titanium both have very high TDI. Nickel and brass both have moderately high TDI and are not competitive with copper. Magnesium, with a fairly low TDI, is not competitive with aluminum with regard to coatings available, corrosion resistance, and general fabricability, especially brazing. Tantalum is expensive and has a low E/ρ ratio. Silver has a very low E/ρ and appears to have no particular advantages over copper. Tungsten, with its very low TDI, is expensive and very difficult to machine, especially in the very thin sections which its high density would require. Its availability in the sizes required, especially for the primary mirror, is highly questionable. Graphite has an attractively low TDI, but an extremely low E/ρ ratio. Obtaining a satisfactory figure appears almost impossible.

A more detailed discussion of the materials which survive the initial screening follows.

b. Aluminum. The age-hardening aluminum alloys, particularly the 356 casting alloy, have been used exclusively to date. Because of extreme difficulty in figuring bare aluminum, a hard coating, usually electroless nickel, is applied to a thickness of about 0.005 in. The favored process for applying the electroless nickel is the Kanigen process, a proprietary method of the General American Transportation Corporation. Electroless nickel coatings are alloys of nickel and 8–10% phosphorous with hardnesses comparable to those of quartz and CER-VIT. The coatings are also quite brittle. Because of the laminar structure of electroless nickel deposits and their reported

porosity (Ref. 22), there is some doubt that figures with sufficient accuracy (on the order of $\lambda/20$ to $\lambda/15$ at 5000 Å) can be obtained according to personnel at the ESSA National Environmental Satellite Center (Ref. 15).

Personnel at Kitt Peak National Observatory (Ref. 16) have noted that aluminum mirrors which have been lightened by removing more than about 50% of the material (compared with a solid structure) suffer warpage when cooled much below 32°F. Unfortunately, the warpage is permanent in nature and the figure is not recovered after reheating to higher temperatures. Possible explanations for this include mismatch of expansion coefficient of the Kanigen coating and the aluminum substrate (about 8 and 12×10^{-6}/°F, respectively). This explanation does not account for the irreversibility of the warpage, however, and does not account for similar behavior observed for light weight beryllium mirrors by the Kitt Peak Personnel. In the latter case, there is a very close match in expansion coefficients.

An explanation for the observed warpage favored by the writer involves the relieving of residual stresses in the mirror material. It is well known that the age-hardening aluminum alloys are very difficult, if not impossible, to stress relieve effectively. The usual elevated temperature treatments for stress relieving are particularly difficult to apply to the age-hardening aluminum alloys. The difficulty lies in the fact that, theoretically, effective stress relieving temperatures are higher than the aging temperature for the alloys. Thus, the metallurgist has the choice of selecting a stress-relieving temperature well below the aging temperature in order to prevent over-aging and softening, or he may select a higher stress-relieving temperature, accept the softening, and settle for a more effective stress relief. Unfortunately, the latter choice leaves the alloy in a metallurgically metastable condition where subsequent aging in service with attendant dimensional changes is likely to occur.

The apparent answer to the stress relieving dilemma posed above is to select a non-age-hardening aluminum alloy such as the aluminum-magnesium solid solution alloys (5000 series). Pure aluminum should be satisfactory from a stress relieving point of view, but it is very soft. The 5000 series aluminum alloys depend on solid solution hardening alone to achieve their strength in the annealed condition. In this regard they are similar to the brasses and the austenitic stainless steels. They are frequently chosen for applications where the ability to stress relieve thermally effectively is important. The alloy tentatively selected for further study is 5052, a moderately strong, readily available alloy of the solid solution hardening type, containing 2.5% Mg and 0.25% Cr. The 80-cm primary mirror could be fabricated by machining from a rolled plate or a pancake forging. Lightweight mirrors could be alternatively fabricated from thin sections, using dip brazing techniques.

In the event it should prove necessary to develop hard coatings for aluminum with expansion coefficients more closely matching that of aluminum, a major effort is foreseen. Most of the usual hard coating materials have expansion coefficients even lower than that of Kanigen. One possibility that needs further exploration is speculum (Cu-32Sn). Speculum is an intermetallic compound which can be applied by electroplating. Its use dates back to Roman times for mirrors.

A coefficient of expansion of approximately 10×10^{-6}/°F has been obtained for cast speculum. Indications are that such a material, as electrodeposited, would provide a better match with aluminum ($\alpha = 13 \times 10^{-6}$/°F) than does electroless nickel ($\alpha = 7.2 \times 10^{-6}$/°F).

c. Beryllium. Considerable work and publicity have been lavished on beryllium for light-weight mirror applications. Its principal attributes, compared with other materials, are low density and an extremely high ratio of modulus of elasticity to density. On the debit side, beryllium is very expensive, approaching $100 per pound for material for mirror blanks. Machining of the blanks is an expensive proposition because of special facilities required to be capable of coping with the toxicity problem.

The application of electroless nickel relieves the personnel doing the figuring of the toxicity problem and provides a hard surface which handles much like glass. The hard coating has an expansion coefficient closely matching that of beryllium. Despite this, the Kitt Peak people claim that lightweight beryllium mirrors are subject to similar warpage problems as those of aluminum. This observation tends to lend credence to the stress relief by the thermal cycling theory of warping. Much work has been done, largely by General Motors and General Precision, in an attempt to pin down the factors responsible for dimensional instability in beryllium for gyro and mirror applications. Perhaps some of this work will eventually prove helpful to the production of accurate, lightweight beryllium mirrors.

d. Quartz, CER-VIT, and Pyroceram. Quartz, CER-VIT, and Pyroceram are different forms of SiO_2. Quartz is a true glass, having an amorphous structure. CER-VIT

and Pyroceram are Owens-Illinois and Corning Glass Company trade names for specially formulated and processed "glasses" which have been converted through a special series of heat treatments to a crystalline or semi-crystalline state. They are known, generically, as "crystallized glasses" or "glass ceramics." All of these materials can be figured to great accuracies using techniques which have been developed over the years. They are all quite brittle and have a very low damping capacity, a combination which might require special provisions to prevent shattering if a resonant frequency is encountered during launch.

Fused quartz is SiO_2 in essentially pure form and is a true glass, i.e., it has an amorphous or non-crystalline structure. It is difficult to produce in a bubble-free version suitable for lenses because of its high softening temperature. Material sufficiently low in bubble count is available in sizes suitable for mirror blanks, however. The TDI for quartz at temperatures higher than 50°F is not outstanding, being slightly higher than aluminum. At temperatures below 0°F, quartz has an extremely low thermal expansion, the coefficient dropping to about 0.02×10^{-6}/°F. If it were possible to operate quartz below 0°F, its TDI of 3 would place it in a prime position among readily available materials. Its very low thermal conductivity precludes its use with the active temperature control that would appear to be required to maintain the nominal operating temperature below 0°F, however.

"CER-VIT" is the Owens-Illinois trade name for a group of semi-crystalline "glasses" whose composition and heat-treatment history have been designed to yield a structure consisting of both crystalline and amorphous phases, resulting in a material with a very low coefficient of thermal expansion. Because of low thermal conductivity, its thermal distortion index (TDI) is only slightly lower than beryllium and aluminum. For figuring purposes, it handles very much like quartz. Since it is a new material, little is known about its dimensional stability. Recently, techniques have been developed for lightening CER-VIT by a factor of about 50%, compared with a solid mirror. A rib-structured blank can be cast by the producer, or a rib structure can be grit-blasted into a solid blank. Cost is comparable to quartz (high). Even lower coefficients than that given in Table 1 can be provided at considerably higher cost on special order.

ULE (ultra low expansion) fused silica (7971) is a new material currently being developed by the Corning glass works. It is an "alloy" of high purity SiO_2 with another material, possibly TiO_2. Since the additive is in solution in the SiO_2, ULE silica is amorphous and retans most of the characteristics of fused quartz. Potentially, ULE quartz will be available in the same sizes as ordinary fused quartz. The cost will be about 10% higher.

e. Copper. Copper is of interest chiefly because of its very high thermal conductivity which gives it a low thermal distortion index. There is also some experience in figuring pure copper successfully (Ref. 17). Since copper may be fabricated by electroforming, there is a possibility of forming a rough figured blank using the spin-casting method developed by Caltech and the General Electric Co. Cast copper-1% Cr alloy has almost as high a thermal conductivity as copper with considerably higher strength.

f. Low expansion alloys. For a number of reasons, the low expansion iron-nickel base alloys are most interesting candidates for mirror materials for the solar telescope.

The low expansion characteristics of the iron-nickel alloys in the vicinity of the Fe-36% Ni composition were discovered in 1896 by Guillaume. The alloy containing 36% Ni was named Invar. It has a coefficient of expansion near room temperature of approximately 0.5×10^{-6}/°F in the fully annealed condition. The alloy is a solid solution type with a face-centered cubic (austenitic) structure. It is mildly ferromagnetic and owes its low expansion characteristics to magnetostrictive effects. The low expansion characteristics persist to the Curie temperature (about 350–500°F). Above the Curie temperature the alloy is paramagnetic and the expansion behavior is more characteristic of iron and nickel. The low temperature limit of the low expansion behavior occurs at the Ar_3 transformation temperature, where the austenitic structure begins to transform to the ferritic, body-centered-cubic structure. In the case of the Invar composition, the austenite is stable to well below −200°F.

Seven years after its discovery, Dr. G. E. Hale of the Mount Wilson Solar Observatory suggested the use of Invar for making stable solar telescope mirrors (Ref. 18) after experiencing stability problems, caused by solar heating, with the glass mirrors of the Snow telescope. Dr. Hale decided that in view of Invar's softness it would be subject to excessive scratching, a valid consideration for an Earth-bound telescope which is expected to function for from 25 to 50 years.

In the early 1930's Masumoto (Ref. 19) discovered that the thermal expansion properties of Invar could be further lowered by the addition of cobalt, the third ferromagnetic element. The optimum ternary alloy has been named Super Invar and contains about 31% nickel and 5% cobalt in addition to iron. It is currently available in the United States from the Simonds Saw and Steel Company of Lockport, New York, on special order.

Extremely low coefficients of expansion are achievable with Super Invar. The figure $0.1 \times 10^{-6}/°F$ in the fully annealed condition given in Table 1 is representative of high-purity, industrial grade material. Negative coefficients are obtained with Super Invar when it is cold worked. Values of minus 0.4 to $0.5 \times 10^{-6}/°F$ have been obtained by cold working about 50%, a method that is impractical for large mirror blanks. An alternate method of reducing expansion coefficient is to employ special heat treatments without resorting to cold working. One such treatment, known as the triple treatment, consists of heating at 1525°F for 30 min, and water quenching; heating to 600°F for 1 hr, and air cooling; and, finally, heating to 205°F for 48 hr, and air cooling. The coefficient obtained after such treatment is about minus $0.12 \times 10^{-6}/°F$ (Ref. 14). While such a negative coefficient does not in itself represent an improvement from thermal distortion considerations over the annealed value of plus $0.1 \times 10^{-6}/°F$, it does point to the potential for reducing the coefficient to extremely low values through proper heat treatment. It is not unreasonable to suggest that a further reduction of the annealed value by a factor of ten or more is possible. Special heat-treatment cycles compatible with effective stress-relieving cycles would have to be developed, possibly tailored to each heat of material or to each mirror blank. The limiting factor might well be the accuracy of the expansion measurement technique.***

Because of its low-expansion properties coupled with moderate thermal conductivity, Super Invar has a potentially very low thermal distortion index (See Table 1). Some advantages and disadvantages of the Invars as mirror materials are listed below.

Advantages:

(1) Low expansion characteristics.

(2) High thermal conductivity, compared with glass.

(3) Metallurgically simple (i.e., no phase changes in the service temperature region which, if present, could lead to dimensional instability).

(4) Easily welded or brazed using conventional techniques.

(5) Relatively easy to machine.

(6) Can be fully and, if necessary, repeatedly stress relieved during fabrication.

(7) Low cost.

(8) Compatible with reflective over-coatings.

Disadvantages:

(1) High density (roughly four times the densities of Be, Al, or CER-VIT).

(2) Figuring characteristics unknown.

(3) Low strength and modulus to density ratio.

(4) Subject to rusting (only slightly superior to iron).

(5) Weakly ferromagnetic (of concern only if a magnetometer is caried aboard the ATM).

Of fundamental importance to the ultimate selection of Invar or Super Invar as mirror materials is the question of figuring the material to the stringent optical tolerances required for the solar telescope. Experience in figuring soft materials is limited. One optical house (Ref. 17) claims to have developed techniques for accurately figuring soft materials such as pure copper, stainless steel, and Haynes Stellite, a cobalt alloy. These techniques may well be applicable to the Invars. A purchase order is being processed to have a 6-in.-diameter optical flat ($\lambda/20$ target flatness) processed in Invar. If this attempt is successful, the same supplier will attempt to process a parabolic mirror of f/4 aperture, with a 6-in. diameter. Success in this second step would give high confidence that an 80-cm mirror can be successfully figured in Invar or Super Invar.

In the event the problem of figuring bare Invar proves insurmountable, it will be necessary to develop a hard coating that can be applied and figured, a technique analogous to that employed for aluminum and beryllium. Unfortunately, the electroless nickel coatings do not appear suitable. This is illustrated in Fig. 33, where it can be seen that the Kanigen coating, which is applied at

***This paragraph applies to small (100–600 lb) induction melted heats of Super Invar. Larger heats will be required for the solar telescope primary mirror. Since the larger heats will be made in an arc furnace, under a slag, the chemistry control required to achieve optimum expansion characteristics remains an unknown.

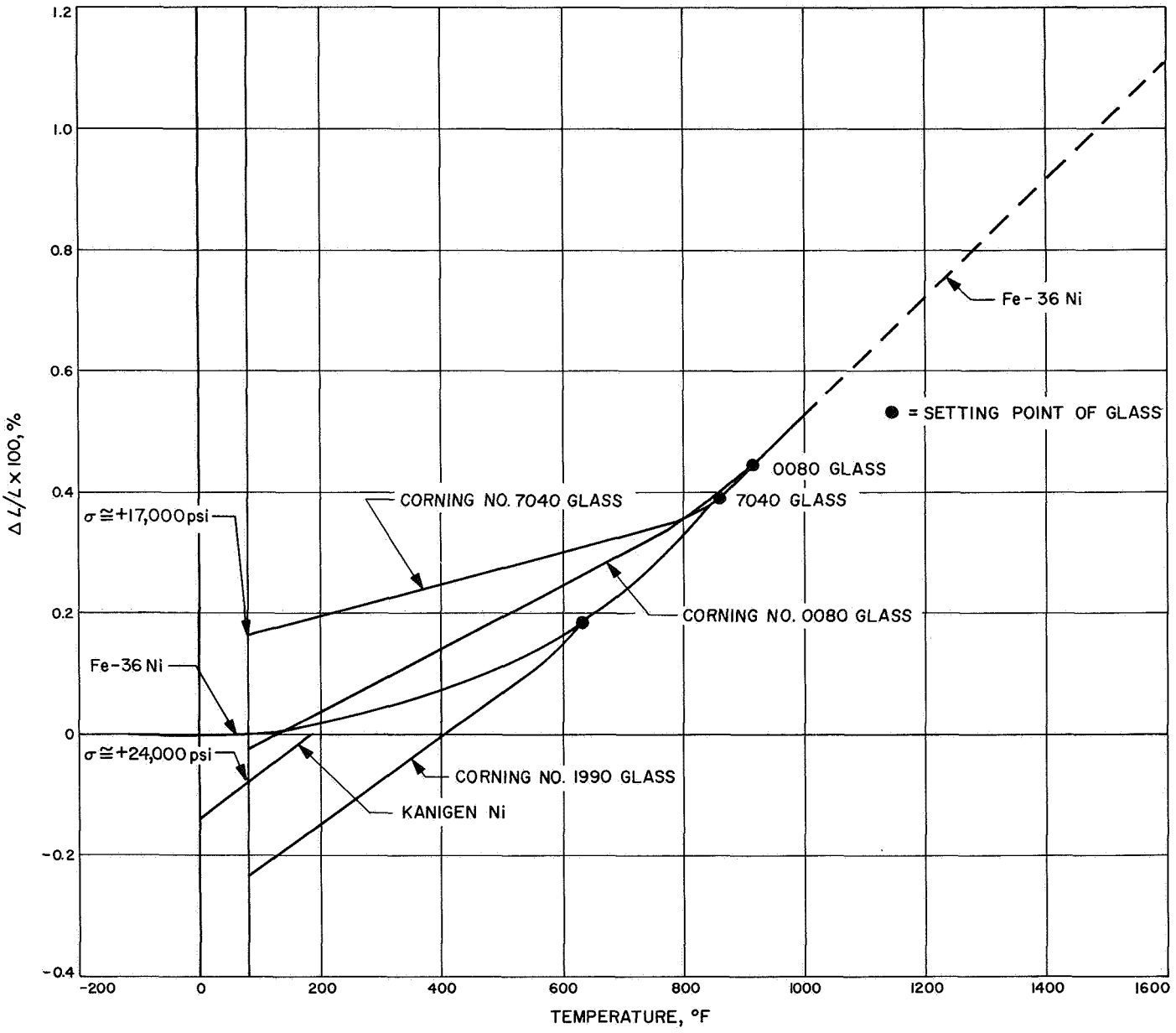

Fig. 33. Compatibility of hard-coating materials with Invar

about 200°F has a much higher expansion coefficient than does Invar. On subsequent cooling to room temperature, the Kanigen would be placed in tension at a calculated stress of about 24,000 psi. It is well-known that brittle coatings must be in a state of very low tensile stress or, preferably, in compression to avoid cracking and spalling.

Figure 33 also demonstrates that it is possible to apply a glass enamel to Invar in such a manner that a state of compression is maintained in the enamel over the service temperature range. The Corning #7040 glass, which fulfills these requirements, was developed for glass-to-metal seal applications. In the event the Invar cannot be figured bare, it appears feasible that a suitable glass could be selected and applied. Some development effort is indicated to obtain a glass coating that has the proper expansion properties, softening point, and firing temperature. It is also important to select a glass that is of a hardness similar to those used for optical elements and is sufficiently free from porosity to permit essentially scratch-free polishing.

Table 1 also lists Ni-Resist #5 cast iron. This is essentially a high carbon version of Invar with low expansion properties, as cast irons go. It was suggested to the writer by personnel at the ESSA National Environmental Research Satellite Center (Refs. 15, 20). The principal reason for interest is the very high damping capacity characteristic of cast irons. In the event resonant frequency problems are encountered in the launch environment, Ni-Resist #5 might provide a good compromise answer.

g. Molybdenum. Based on the information in Table 1, molybdenum appears attractive as a mirror material. Its low expansion coefficient (among metals) and its relatively high thermal conductivity give it a thermal distortion index about half that of beryllium. It also has an E/ρ ratio second only to beryllium among the metals. Problems with availability, machining, joining, and figuring could probably be solved. As with beryllium, the chief property of interest is the high E/ρ. Since the solar telescope will be in Earth orbit and will therefore be weightless during the photography portion of the mission, great stiffness does not appear to be a requirement. Stiffness might be desirable from a launch vibration standpoint, but this is not clear at this writing. Until such a requirement is clearly delineated, molybdenum will be considered inferior to the low expansion alloys and not sufficiently superior to copper from thermal distortion considerations to justify planning the not inconsiderable development effort that would be required.

h. Mirror weights. It is difficult, at this stage, to make realistic estimates of primary mirror weights, largely because of the unknowns in design. However, comparative figures can be calculated. The following table is an attempt to show some comparisons which, until further information is obtained, may be considered reasonably realistic. All calculations are based on a 31.5-in. (80 cm)-diameter, 3-in.-thick mirror with a 4.9-in.-diameter center hole. In the case where a ½-in.-thick bottom plate is added, the thickness is increased to 3½ in.

Material	Weight, lbs			
	Solid (1.85 ft)	50% Lightened	50% Lightened (+½-in. bot. pl.)	80% Lightened (no bot. pl.)
Super Invar	938	470	309	198
Aluminum	310	155	103	–
CER-VIT	288	144	–	–
Beryllium	214	107	71	–
Quartz	254	127	–	–

The *underlined figures* in the above table represent, in the writer's opinion, the lowest *practical* weight in each material, provided (a) that Super Invar can be accurately figured without resorting to a hard coating, and (b) a hard coating for aluminum with a matching expansion coefficient can be developed. In the event (a) and (b) cannot be accomplished, the weight will shift one or two columns to the left for Super Invar and one column to the left for aluminum. It is apparent that the high density of Super Invar may not result in as high a weight penalty as might be expected from considering the relative densities.

i. Conclusions. It is not possible at this stage of the study to make a final choice of mirror material or substrate-coating system. Practically every conceivable possibility has been considered, and many candidates have been eliminated. The following materials are the prime choices, in order of the writer's preference:

(1) *Super Invar*: There is a high probability that Super Invar will retain its figure under uneven heating conditions. A high degree of dimensional stability

(under aging conditions) should be achievable through careful processing–stress relieving cycles. Figuring to the high accuracies required for the solar telescope is an unknown. High density is the principal disadvantage, but does not preclude use.

(2) *Aluminum:* Considerably inferior to Super Invar with respect to thermal distortion. Further evaluation of the telescope system may prove aluminum good enough. Further evaluation of the 5000 series alloys and possibly of hard coatings with higher coefficients of expansion than those available probably will be required in order to reduce weight to a minimum.

(3) *CER-VIT*: While CER-VIT type materials are somewhat superior to aluminum from a thermal distortion standpoint, they are brittle and have low damping capacity–a combination which could lead to trouble during launch. Interest in CER-VIT could increase if problems with Super Invar and aluminum prove insurmountable.

(4) *Other Materials:*

(a) Beryllium would make the lightest, stiffest, and most expensive mirrors. Thermal distortions should be roughly equivalent to aluminum and CER-VIT. Dimensional stability appears to be the principal technical shortcoming of beryllium.

(b) Ni-Resist Type 5 Cast Iron is of interest chiefly because of its very high damping capacity. Thermal distortions should be low – inferior only to Super Invar. Dimensional stability is not well understood but should be satisfactory. As with other low expansion alloys, figuring may present serious problems.

3. Mirror reflective coatings. The proposed solar telescope will be expected to perform in the near ultra-violet region, down to 2000–2500 Å (Ref. 1). Since the design of the telescope utilizes a minimum of four mirror surfaces which must reflect the light before it strikes the film, it is necessary to use surfaces which are as reflective as possible, especially in the near-ultraviolet. For example, the losses which would occur at 4000 Å using a material with a reflectivity of 0.90 can be calculated for a four mirror system by multiplying the reflectivities of each surface by the others. Assuming all four surfaces are the same, the reflectivity of the system would be $(0.90)^4 = 0.67$. The table below gives the efficiencies of a four mirror system for various reflectivities.

Single Surface Reflectivity	Combined Reflectivity (R_s^4)
0.90	0.67
0.80	0.41
0.70	0.24
0.60	0.13
0.50	0.06

Reflectivity data are available for a large number of metals in Ref. 6. The most highly reflective material in the visible and near infra-red regions of the spectrum is vacuum evaporated silver, which has a measured reflectivity exceeding 0.98 in the wavelength region 6000 Å to the far infra-red. Unfortunately, the reflectivity of silver falls off rapidly in the near ultraviolet (UV) region. At 4000 Å, the reflectivity has fallen to 0.90, and at 2000 Å, the reflectivity is only 0.26.

This appears to leave vapor deposited aluminum as the only real choice of reflective coating for the solar telescope. The reflectivity of aluminum is lower than silver in the visible region as is shown in Fig. 34, varying from about 0.87 at 4000 Å to 0.92 at 10,000 Å. It is in the near ultra-violet that aluminum is superior to silver. Where silver starts losing reflectivity at 4000–6000 Å, aluminum maintains moderately high reflectivity down to 2500 Å. At 2000 Å the reflectivity of aluminum has dropped to 0.56. There is evidence to support the contention that the loss of reflectivity of aluminum in the far ultraviolet is caused by the naturally occurring oxide film, which acts much like a quarter-wave filter. This is supported by the improved reflectivity of aluminum when certain vapor deposited overcoatings, such as magnesium fluoride, are substituted for the aluminum oxide by depositing in the vacuum chamber before the aluminum oxide has time to form. This subject shall be discussed more fully in the next section of this report.

4. Mirror overcoatings. There are two principal reasons for applying an overcoating to telescope mirrors:

(1) To protect the delicate vapor deposited reflective coating from the effects of atmospheric corrosion and physical handling.

(2) To provide a controlled thickness substitute for the naturally occurring oxide films, thus increasing the reflectivity in the ultraviolet (Ref. 23).

A possible third reason may apply to the solar telescope. In the event the naturally occurring aluminum oxide film darkens as a result of the exposure to ultraviolet radiation

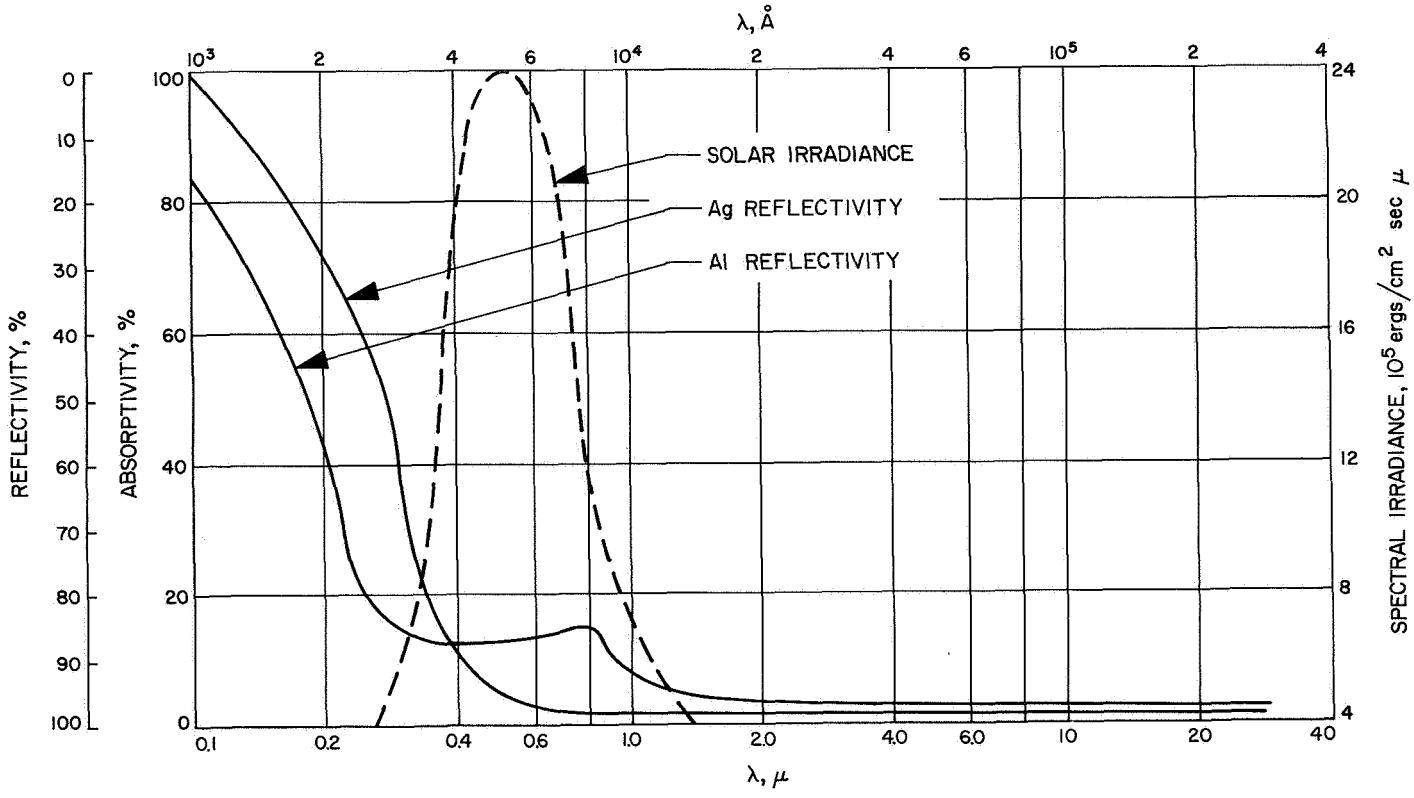

Fig. 34. Spectral reflectance of vapor-deposited aluminum and silver

in the space vacuum, a more stable film might be required in order to maintain reflectivity at acceptable levels. Work done under JPL contract at the Armour Research Foundation (currently IITRI) was summarized in Ref. 24. Evaluation of aluminum oxide as a *pigment* material for white paints indicated that the reflectivity of high-purity Al_2O_3 pigment material drops by 44% at 4000 Å after exposure to 50 hrs at 1.5 Suns in a vacuum of 10^{-6} torr. While these numbers are, of course, not directly applicable to the solar telescope, where a very thin film of aluminum may be present on the mirror surfaces, they do illustrate the fact that aluminum oxide is not stable under vacuum-ultraviolet exposure conditions.

Vapor deposited silicon monoxide has been evaluated in flight on the S-16 satellite (Ref. 25). The solar absorptance of an Al-SiO-Ge-SiO multi-layer coating increased by 10% after 130 days in Earth orbit. No further increase occurred after over 400 days. This would indicate that SiO may be a sufficiently ultraviolet-vacuum stable coating for use in the solar telescope. Further work needs to be done on:

(1) Evaluation of "uncoated" aluminum reflective coatings under vacuum-ultraviolet conditions, and if (1) shows that Al_2O_3 is not sufficiently stable, then

(2) Determine the effects of SiO on the reflectivity of aluminum near 2500 Å with and without vacuum-ultraviolet exposure.

Some of the work done at the Goddard Space Flight Center (Ref. 26) on evaluation of window and filter materials which are transparent in the 1050 to 3000 Å regions may provide some useful leads for a stable overcoating material in the event SiO is found to be unsatisfactory. The Goddard people evaluated LiF, MgF_2, CaF_2, BaF_2, Al_2O_3, SiO_2, ADP, Calcite, and several glasses for transmittance before and after exposure to 1-2 MeV electron radiation. The most promising materials were found to be BaF_2 and Al_2O_3. MgF_2, a popular overcoating material for mirrors and lenses, suffered nil loss in transparency in the very low ultraviolet, but did suffer a significant loss in the 2000–3000 Å region. The findings of the Goddard people that high purity Al_2O_3 was very stable after electron radiation illustrates the danger of extrapolating these data to the vacuum-ultraviolet case in view of the Armour findings.

It is, indeed, fortunate that photography down to the *near* ultraviolet only is satisfactory for the presently proposed experiment. The problems of extending the region

of interest to lower than 2000 Å in a broad spectrum telescope are formidable, indeed, and should properly be relegated to follow-on experiments.

5. Non-optical materials. Since this is a feasibility study, little detailed study has been given to date to materials for the telescope structural housing, the cameras, and related mechanical and electronic equipment. It is felt that suitable materials can be selected at the detail design stage. No problems that could jeopardize the success of the mission are foreseen.

Particular attention will have to be given to the choice of polymeric materials used, especially in locations that view the optical elements directly. Fortunately, a large amount of work has been done in this area. Stanford Research Institute (Ref. 27) under JPL sponsorship has tested many polymeric materials for behavior in a high-vacuum environment with particular emphasis on the evolution of outgassing products which can be harmful to optical elements. It appears that by and large either (1) intrinsically stable polymers can be utilized, or (2) polymers capable of being specially treated to reduce condensable products to extremely low levels can be utilized. A small amount of work to evaluate materials not covered by SRI is anticipated.

The film used will require special attention. Time has not permitted a significant effort to date.

It is expected that structural materials can be selected from within the state of the art. Particular attention will have to be given to materials that support the optical elements. Trade-offs among thermal conductivity, expansion characteristics, physical and mechanical properties will be examined leading to design of lightweight structures.

F. Telescope Alignment

In-flight alignment of the telescope is necessitated by several perturbing influences: thermal distortions in different parts of the system, mechanical and acoustical loads imposed on the system during launch, and possible in-flight mechanical jarring by docking procedures. It is assumed here that a guiding mechanism will point the telescope toward the Sun with the required degree of accuracy. What is being considered in this section is the relative alignment of the axes of the primary and secondary mirrors, telescope housing and the camera systems. In addition, jitter in the ATM may have to be cancelled out in the developed films. Techniques for doing this are presently in use.

Upper and lower limits to the precision of the position of the mirrors are set by the following considerations. Mirror surfaces are currently available with an accuracy of 0.02 wavelengths. At 6500 Å this is 1.3×10^{-6} cm. Computer ray tracing analysis shows that the longitudinal separation of the two mirrors must be accurate to within 7×10^{-4} cm, and that the transverse separation of their axes must be less than 2.5×10^{-2} cm to prevent serious image distortions. It will, therefore, be sufficient to align the telescope in each coordinate to an accuracy falling somewhere between the respective limits.

Preliminary investigations indicate that in a transversely unaligned system it may be possible to bring coma and aberration back to tolerable limits by rotation of the secondary mirror. At any rate, provisions for aligning the two mirrors in 5 deg of freedom (3 translational, 2 rotational) must be included in the alignment mechanism. It is assumed that the beam-splitter, diagonal flats and primary mirror will be one rigid unit.

Several methods for aligning the two mirror axes to within 2.5×10^{-2} cm transversely, 7×10^{-4} cm longitudinally, and 0.1 arc second rotationally are being considered. A first order correction mechanism will be needed to bring the mirrors into the range of application of a more sophisticated second-order alignment technique. Both corrections must be operable by the astronaut in a straightforward, objective way (such as turning a knob to position a meter needle) or the aligning mechanism may be partially servoed.

Different methods of alignment will be evaluated in the proposed scale model.

G. Power Conversion and Electrical Distribution

The total connected load is expected to be about 930 w at the ATM available 28 Vdc. The greatest demand appears to be about 600 w during the picture taking mode of the telescope operations. Power consumption will vary from about 270 to 600 w peaks during the experiment, as shown in the Table 2. A histogram is prepared for a typical sequence of operation, Fig. 35, showing the power demand as a function of the orbital time.

Beyond the mission, during the orbital storage period, it is anticipated that heat will be required to keep the electronics and optics relatively warm, i.e., to survive the thermal stresses of a space environment. Experiences from the *Surveyor* spacecraft have shown that electronic

Table 2. Solar telescope experiment power*

Power requirement	Connected power	Exp. set up	Stand By		Opers.	Orbiting storage	Duty cycle
			Light	Dark			
1. Optics alignment apparatus	50	50					C
2. TV subsystem	20	20	20		20		C
3. TV field monitor (LM console)	50	50	20		20		C
4. "A" scope-focus control (LM console)	50	50	50		50		C
5. TV remote controls	10	10	10	10	10		C
6. Camera focus motor	50		50		50		I
7. Telescope electronics survival heater	30			30		30	C
8. Film camera shutter and advance motor (6 @ 30)	180				180		I
9. Cassette transfer motor (3)	75				75		I
10. Filter wheel advance motor (2)	50				50		I
11. Primary mirror active thermal control	135	135	70	135		50	C
12. LM command module controls	20	20	20	20	20		C
13. Camera and vidicon heaters (3)	35	35		35		35	C
14. Primary and secondary coolant pumps	100	100	100	100	100		C
15. Lyon (H_α) filter heater and thermal control unit	40	40	40	40	40	20	C
16. Cover motor	50	50	50	50			I
17. Distribution and conversion losses	45	30	20	20	30	10	C
Sub-totals:	980	590	450	440	645	145	

*Power in watts
Duty Cycle: I = Intermittent
C = Continuous

equipment should be maintained at about −55°F. Two-watt carbon resistors were placed in compartments on that vehicle. The TV vidicon may need resistor heaters mounted on the face and base plates. If water is used as the coolant fluid, then water temperature must be maintained above freezing to avoid ruptures of piping.

The Lyot H_α monochromator is sensitive to minute temperature changes because the band pass of the optics elements will be shifted. Generally the operating temperature of the filter should be maintained at 68°F. It has not been determined at what temperature the filter should be maintained to preserve the quality of the optics during orbital storage.

1. Power conversion. Motors and resistance heaters will be used at 28 Vdc. Electronic voltage regulators will require bias supply voltages at 2 to 12 Vdc. The vidicon has small power requirements at 700–770 Vdc. Other vidicon power will require potentials as follows:

Target	10 to 2 Vdc
Grid 1	−50 to −100 Vdc
Filament	−6.3 Vdc
Cathode	ground to +10 Vdc

2. Electrical distribution. Suitable electrical harnesses will be prepared to mate the various electronic and electrical apparatus. MIL W 16878D, Type E TFE wire, will be used. In some applications where weight reduction may be necessary, wire with H Film Kapton insulation could be used. Generally, the available harness designs are compatible with the space environments and the critical pressure range for corona discharge. Interconnection with the equipment can use a variety of connectors

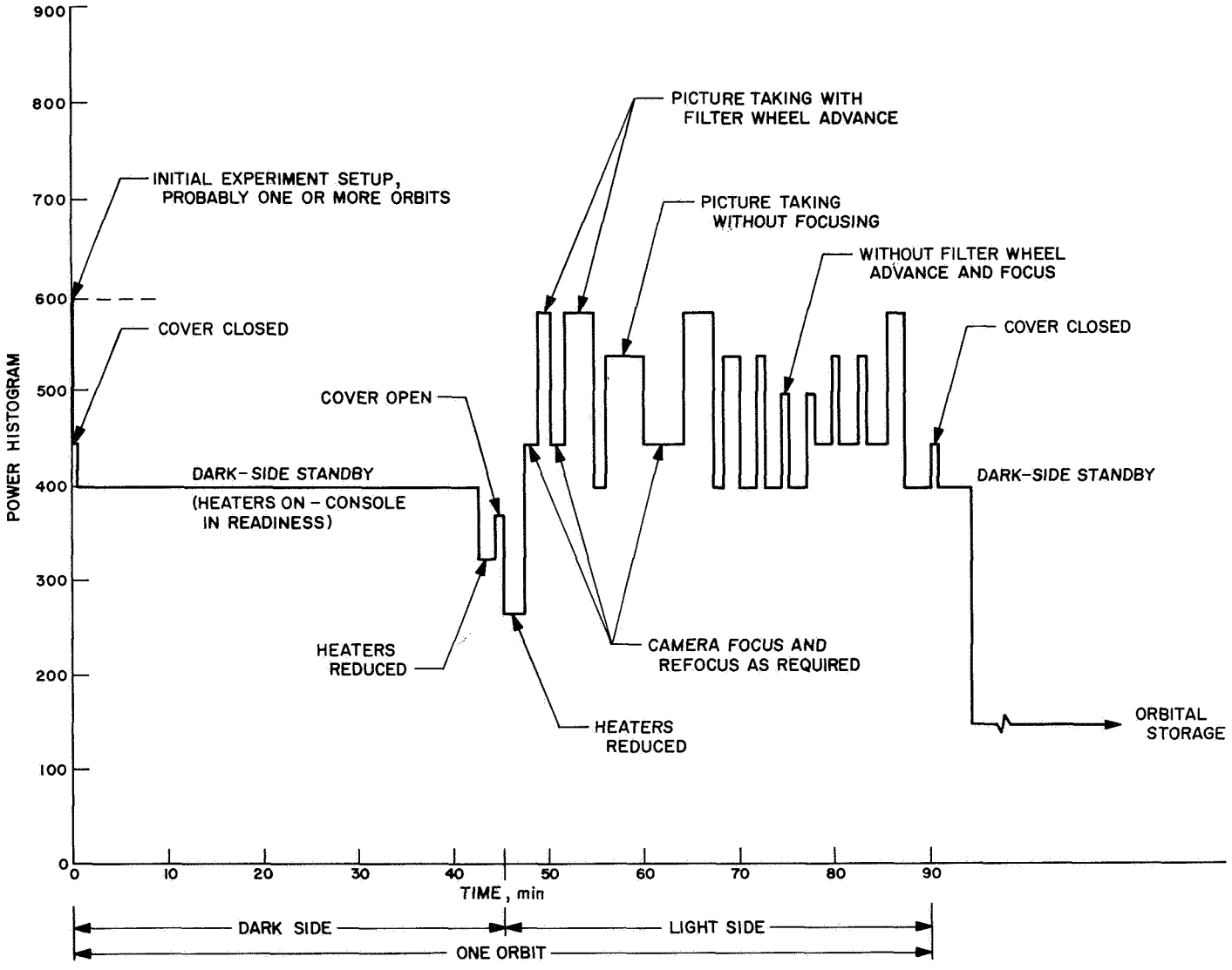

Fig. 35. Electrical power demands during orbiting

which have been flight qualified. A high-density connector MIL-C-38300 has been qualified on the *Gemini* program. A JPL qualified MIL-C-26482 circular miniature connector has been qualified as a high reliability part on *Mariner* and *Ranger* spacecrafts. Rectangular pattern connections to electronic panels can be installed with parts qualified to MIL-C-8384.

It is expected that connectors to the ATM 28 Vdc bus and the LM controls adapter will utilize connectors compatible with the LM design.

H. Reliability and the Telescope Testing Program

The probability of the telescope being operable during the lifetime of the mission is a matter of establishing confidence in the system through a reliability program of development and test evaluation.

From the designers' point of view, it is possible to design parts of the system to be failure-free and, in certain cases, to be fail-safe whereby the system is still operative but in some modified or restrictive mode. It is also possible that certain parts of the system can be repaired in space such that provision for access could be included in the design arrangement.

The thermal control apparatus is a system which should be designed to allow the telescope to be operative for a limited time under passive cooling conditions. Another example is the supporting structure for the optics which should be designed to maintain the exactness of the optics alignment during the experiment. Supplemental support during the launch and space maneuvers of the carrying vehicles could be designed to relieve the optics from being disturbed. The probabilities of the camera system failing completely are also minimized since the availability of the three cameras increases the chances of getting pictures. The film cassettes are removable so that faulty units can be removed and repaired within the orbiting workshop or the cassette can be replaced.

During the development, fabrication and functional operation of the telescope, confidence in the system can be established through a systematic program of test evaluation and reliability determinations, of which the major areas would be:

(1) The development of an analytical means of assessment through mathematical models and failure reporting.

(2) A reliability assurance test program for component and systems tests, where necessary. Such cases would be in areas of new technological developments.

(3) The establishment of standard parts, processes and materials qualified for the telescope mission requirements.

(4) A test program of the telescope to qualify the design function and integration with the ATM/LM systems.

Mathematical models of parts, components and subsystem elements can be derived to analyze worst-case conditions for failures in circuitry, mechanisms or any other moving parts. A procedure of failure reporting in designs which have been frozen can be used to assess a running account of confidence in the design and a need for revisions.

If new technology is being developed such as proper lubrication of moving parts in a space environment, reflective coatings of optics which are compatible to particle irradiation, and a reliable active thermal control means, then suitable individual tests to establish the reliabilities of such parts or sub-systems should be conducted.

As for item (4) of the Reliability Program, considerable experience is available from the utilization of parts in flight vehicles such as *Surveyor, Ranger* and *Mariner* which have been qualified through systematic tests and evaluations and are controlled by certification requirements by the JPL Preferred Parts List ZPP-2061-PPL. A list of many space compatible materials is also available.

A plan of Telescope Testing is presented in Tables 3 through 5. Three groups of tests are considered to establish confidence in the design during all the phases of evaluation of engineering development, fabrication and assembly, functional operations, systems integration and preflight evaluations.

The plan proposes that all parts, components, and subsystems will require type approval tests. That is, the designs will be subjected to levels of environment, numerous duty cycles and longer durations of tests than would be anticipated in the mission. Because these tests are destructive in nature, specimens which have survived the type approval tests would not be used as flight articles. All flight articles would be inspected and subjected to limited functional operations in order to ascertain conformance to the design which would have been previously affirmed by the type approval tests.

Table 3. Solar telescope testing program (parts and components)

Parts and components	Type of test	Method and procedure	Environment and applicable specs	Unusual equipment and facilities	Test location	Test unit	Facility availability and where	Costs
1. *Small Parts: electronic electrical, mechanical* wire, conn., fasteners, tape, resistors, etc.	Reliability (Engr.) Acceptance (Procure.)	Industrial and JPL Practice Visual inspection measurement	MIL and JPL Specs incl. ATM and Space Environment	UV/Vacuum VCM, radiation (wt less for certain parts)	Vendors and JPL	hi rel samples (per spec)		
2. *Approved Materials* metals, polymers, paints, adhesives, glass, etc.	Engineering Qualif. Acceptance (Procure.)	Industrial and JPL Practice Chem. Anal., Elect. and Mech. measurements	MIL and JPL Specs incl. ATM and Space Environment	UV/Vacuum VCM, radiation, wt. losses	Vendors and JPL	hi rel samples (per spec)		
3. *Films*	Spectral sensitivity, MTF. low press. stability, response to processing	Photometric measurements; processing procedures	Ambient, low pressure radiation abrasion	Complete dark room, photometer, spectrograph	Vendors and JPL	Dev. specimens, prototypes, flight film		
4. *Electronic and Electric Components:* heat sensors, relays, switches, etc.	Engr. Qualification Acceptance (Procure. and Flight)	Function Bench operations—measurements	MIL and JPL Specs incl. ATM and Space Environment	None	Vendors and JPL	hi rel samples 100% insp.		
5. *Optical Elements and Assemblies:* primary, secondary, flats, beam splitters, filters, optical windows	Dimensional, spectral transmission, reflectance thermal, structural and space environ. stability	Visual, spectrophotometric, thermal cycling, shock and vibration and acoustic cycling	JPL Specs all environment except UV and radiation	UV Spectrophotometer,* collimated light source, acoustic chamber, thermal/vac. simulator clean room	Vendors and JPL	1 set—dev spec 1 set—proto 2 sets—flight		

*New equipment and facilities, including modifications.

Table 4. Solar telescope testing program (subsystem)

Subsystems	Type of test	Method and procedure	Environment and applicable specs	Unusual equipment and facilities	Test location	Test units	Facility availability and where	Costs
1. *Mechanical Devices* mechanisms, motor drives, valves, shutters, covers, etc.	Engr. Qualification and Acceptance, Functional	Bench operations. Physical and electrical measurements	JPL Spec All ATM and Space Environment	RF screen room* Life testing of sliding surfaces*	Vendors and JPL	3 dev. & engr. 1 proto 3 accept for flight 3 TAT		
2. *Optics* a) Primary and secondary interaction b) (a) + flats and filters	Focal length, resolution, optical axes align., observations, distortions, MTF.	Foucault, Hartmann, Ronchi (others) Interferometry	JPL Specs ambient primary in zero (g) simult.	20 ft. Optical bench* 6328 Å lasers Scattering interfero.* Clean room*	Vendors and JPL	1 prototype 2 flight sets		
3. *Film Cameras*	Engr. Qualification and Acceptance, Functional	Bench operations physical and electrical measurements	JPL Specs thermal-vac, shock, vibration, acoustic radiation shielding	Acoustic chamber* radiation simulator bench vac equipment	Vendors and JPL	2 dev 4 proto (set and spare 9 flight (set of 3 and spare)		
4. *TV Cameras*	Engr. Qualification and Acceptance, Functional	Bench operations physical and electrical measurements, resolution	JPL Spec thermal-vac, shock vibration, acoustic radiation shielding	Acoustic chamber* radiation simulator bench vac equipment	Vendor and JPL	1 dev 2 proto (set and spare) 3 flight (set and spare)		
5. *Telescope Structural Housing*	Alignment, zero (g) stability, thermal stability	Mount telescope in alignment fixture Measure displacements	Ambient, mission thermal, zero (g) simulation	Alignment fixture* Heaters and zero (g) test fixtures*	Vendor	1 proto 2 flight		
6. *ATM Pointing*	Acceptance—compatibility with solar telescope	Bench operations, measure performance MSFC specs	Ambient	ATM Simulator (compatibility test)*	MSFC	2 ATM flight type units		
7. *Active Thermal Control*	Engr. Qualification and Acceptance, Functional	Bench development Functional-Accuracies thermal-vacuum	Ambient Thermal-vacuum	7 or 10 ft vacuum chamber 1 ft. solar simulator	Vendor, JPL	1 dev. 1 proto 2 flight		
8. *Telescope Lid Control*	Engr. Qualification and Acceptance, Functional	Bench development Functional-Accuracies and Life under thermal-vacuum	Ambient Thermal-vacuum	7 ft vacuum chamber heaters	Vendor, JPL	1 dev. 1 prototype 2 flight		
9. *Command Control Console (LM)*	Development Functional, Determine Flt Seq. and procedures	Breadboard design Bench operations—JPL specs	Ambient L M environment	ATM simulator* Video signal generator*	JPL	2 JPL Tests 2 flight units 1 proto		

*New equipment and facilities, includes modifications.

Table 4 (contd)

Subsystems	Type of test	Method and procedure	Environment and applicable specs.	Unusual equipment and facilities	Test location	Test unit	Facility availability and where	Costs
10. *Command* (Voice) *Link*	Acceptance for JPL operations	Bench operations	Ambient	None	JPL and MSFC	2 ATM Flt type		
11. *Data Communications Link*	Acceptance for JPL operations and evaluation	Bench operations JPL Specs	Ambient	None	JPL and MSFC	2 ATM Flt type		
12. *Data Process Equipment*	Acceptance Functional eval.	Bench operations JPL/CIT Specs	Ambient	Reregistration Camera* Photometers Plotters*	CIT	1 set		
13. Flight Tool Kit (EVA & IVA)	Acceptance Functional eval.	Eval. by Astronaut	Zero (g) environment	Solar telescope* mock-up Aircraft simulator or ground*	JPL and MSFC	1 Dev. 2 flt.		
14. Ground Support Equipment	Development Acceptance Evaluation	Combine with telescope Perform functional tests JPL Spec	Ambient for the equipment	(Telescope System and Subsystem)	JPL and MSFC	1 Dev. 1 System 1 field (MSFC)		
15. Electrical Distribution elect. harness, junctions, relays, etc.	Breadbord checkout Flight acceptance	Hook parts and comp. like flt. unit and conduct elect. test	Ambient and space environment	None	JPL	1 breadboard 3 flt type		
16. *Power Supplies* converters, inverters	Development and Qualif. Acceptance, Evaluation	Conduct bench oper., measure electrical *performance* JPL Specs	—ambient and space environ. —ATM mission	None	Vendor and JPL	1 dev. 2 ATM simulator 2 Flight		
17. *Personnel*	Functional Qualif. Astronaut Training, Crew Training	In person and reading manual, crew operations	JPL Oper. procedures ATM Oper. procedures	Prototype and ATM simulator* Prototype/ATM/LM*	JPL and MSFC	Train with prototype and flt units		

*New equipment and facilities, includes modifications.

Table 5. Solar telescope testing program (telescope system and ATM)

System telescope & ATM	Type of test	Method and procedures	Environment and applicable specs.	Unusual equipment and facilities	Test location	Test unit	Facility availability and where	Costs
1. Prototype Telescope Assembly	Checkout of telescope system Functional evaluation inc. photograph	Qualify align procedures Demonstrate rate operational capabilities	Ambient, shock, vibration and thermal-vacuum	Space Simulator ATM Simulator* Solar Telescope GSE*	JPL	Prototype		
2. Flight Telescope Assembly	Consent to ship-flight acceptance test	Operate telescope with OSE & ATM simulator Evaluate functions and operations	Ambient, shock, vibration and thermal-vacuum	Space Simulator ATM Simulator* Solar Telescope* OSE*	JPL	Flight Telescopes 1 and 2		
3. ATM/LM Integration	Compatibility with ATM LM interfaces	Install in ATM and operate with LM and ATM systems	Ambient	Solar Telescope* and ATM OSE* LM Simulator*	MSFC	Prototype and Flt. Telescopes 1 and 2		
4. Principal Investigator and Astronaut Training	Instruction in operation of solar telescope—evaluation of mission procedures	Practice abbreviated mission profile	Ambient	Solar Telescope* and ATM OSE* LM Simulator*	MSFC	Prototype		
5. Flight Acceptance	Operational Verification Calibrations	Install in ATM and operate with LM simulator and ATM systems	ATM mission profile @ ambient	Space Simulator ATM/LM flight type veh. and OSE*	MSFC	Flight Telescopes 1 and 2		
6. LM Integration and Launch Operations	Compatibility and interface with LM. Prelaunch validation, Verification of Calibration	Simulate abbreviated launch and mission profile	Ambient	All OSE and flight vehicles*	ETR	Flight Vehicles		
7. Final Evaluation Post Flight	Functional evaluation Failure analysis and eval non-std events	Operate telescope with G.S.E. and ATM Simulator	Ambient Vibration and thermal vacuum as required	Solar telescope GSE* ATM Simulator* Space Simulator	JPL	Prototype		

*New equipment and facilities, includes modifications.

As the subsystems are brought together to form the complete telescope, the compatibility of each could be evaluated as they interface with the composite elements of the telescope. At first, functional tests would be conducted under ambient conditions. These would be followed by tests in the thermal vacuum environment, and following procedures which would simulate parts of the mission.

An important subsystem test is the demonstration and evaluation of the optics alignment. An alignment fixture would be constructed for this purpose. Test of the alignment method and procedures would be verified before the final assembly of the telescope. Group C tests shown in Table 5 consider a plan of demonstrations to qualify and evaluate the complete telescope system as a separate entity and as it would be integrated with the ATM. A prototype telescope would be concerned as the first assembled unit to establish conformance of the design. Having gained an indication of the confidence level, the results of the prototype testing would be incorporated in the flight telescope.

Two flight telescopes could be fabricated to support a limited schedule of flight opportunities; one would be a spare. Both would be operated throughout a plan of functional tests which would simulate abbreviated launch and the mission profile.

It is anticipated that the mission can be supported by functional evaluation of events with the prototype telescope. In cases of failure and execution of non-standard procedures, the prototype telescope could be operated to simulate the condition in flight. Additional tests can be conducted to assist in the analysis of the experiment.

1. Scale model of the telescope. There are intrinsic errors in the data which has been provided for material properties; therefore, the analysis of thermal distortions may not agree with the actual conditions. A scale model telescope is needed to develop confidence in the material behavior and to evaluate the performance of optics made of the selected materials under conditions closely approximating the actual thermal conditions to be encountered during the mission. Tests to determine the figure of the mirrors and to determine the performance of the system are needed.

Interferometry will be the basic measuring technique supplemented by Hartmann tests, Ronchi tests, and Foucault tests. After the experimental results are obtained, mathematical analyses of these results are to be extrapolated by use of scaling factors to apply to the full-scale prototype.

The test model would also serve to give a method of evaluating the procedures of meeting alignment problems. The astronaut would need to be able to check the alignment of optics in space, and if launch stresses had changed the alignment, he would need to have procedures to re-establish alignment.

Three sets of model optics are considered. Primary and secondary mirrors are needed, made of CER-VIT, aluminum and Super-Invar.

In a procedure under consideration, shown in Fig. 36, one of these sets of optics could serve as optics for the collimator as another set is tested. The test would involve irradiating the optics, assembled in a Cassegrain system, to simulate the heating of the mirrors in space. The design currently considered would introduce the beam of heating radiation by means of a large diagonal mounted between co-axial collimator and test optics. After a period of heating, the diagonal is removed from the beam, and the optical tests carried out as rapidly as possible. The required positioning of the large diagonal is not extremely precise, and it is possible that polished plate glass may be good enough for the element.

Recommendation is made that a fractional-scale model of the telescope be constructed for test of thermal and optical performance in vacuum environment including solar simulator.

The scaling factors for reduced size models is that described in "Thermal and Structural Scale-Modeling of Optical Systems," by F. Gabron and A. A. Fowle. The applicable set of factors is that relating to reduced scale models made of the actual proposed materials. Constraints are that there are negligible body forces. Materials and radiative properties are identical in model and prototype. The ratio of temperatures is given by:

$$\frac{T_m}{T_p} = \left(\frac{L_p}{L_m}\right)^{1/3}$$

L_p/L_m is the ratio of characteristic lengths on the prototype to those of the model.

The ratio of strains is

$$\frac{\Delta L_m/L_m}{\Delta L_p/L_p} = \left(\frac{L_p}{L_m}\right)^{1/3}$$

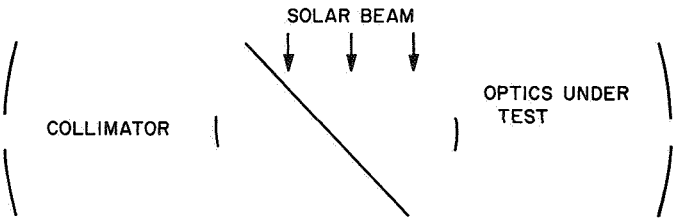

Fig. 36. Optics for the collimator

and displacements are

$$\frac{\Delta L_m}{\Delta L_p} = \left(\frac{L_m}{L_p}\right)^{2/3}$$

The ratio of heat flow per unit area is

$$\frac{q''_m}{q''_p} = \left(\frac{L_p}{L_m}\right)^{4/3}$$

This is related to the decision to be made regarding the scale factor for the model. If the model is half-scale and of identical materials, the heat flow from an area of the mirror surface would need to be $(2L_m/L_m)^{4/3} = 2.52$ solar constants. A third-scale model would require 4.32 solar constants.

The question of the scale of model to be recommended will be related to trade-offs involving available sources of flux, available test chambers, and techniques of optical testing and fabrication.

Since the heating of the primary is anticipated to be due to a spot of light from the beam converging to form an image behind the primary, the collimation angle is a most important parameter, as it would determine the size of the spot and heat per unit area on the primary. One procedure would be to use the Sun's rays, directed into the chamber by a heliostat, to heat the mirrors.

Appendix A

Proposal for Photographic Exploration of the Sun: High-Resolution Solar Telescope for the Apollo Telescope Mount

I. Management Section

A. Work Plan

Seven phases of activity can be identified for the program as follows:

(1) Preliminary design.

(2) Detail design and breadboarding.

(3) Development, fabrication and testing of subsystems.

(4) Integration and system testing at JPL.

(5) Integration with the ATM.

(6) Launch and flight.

(7) Post-flight data analysis and reporting.

The conceptual design as described in the technical section is about completed, and preliminary design of the entire system can begin immediately. The design and development of the telescope is believed to be the pacing item. This would be undertaken under subcontract. At the same time, a breadboard of the entire system would be built in-house to allow project personnel to become familiar with each subsystem and allow an early definition of interfaces.

Major subcontracts are anticipated for the following subsystems:

(1) Telescope

(2) Film camera

(3) Television camera and display

(4) Astronaut console

(5) Power

(6) Ground support equipment

An integration and testing support contract will also be let to support the JPL staff. The experiment system integration and testing will be performed at JPL under the direction of the JPL staff. When the systems have completed acceptance testing, they will be delivered to the ATM for integration and testing. A small JPL staff would reside with the spacecraft contractor to assist with this phase.

Post-flight data analysis will be the prime responsibility of the principal investigator and his staff.

B. Personnel

The key personnel are: (1) Professor Harold Zirin, Caltech, Principal Investigator; and (2) Dr. Robert F. Howard, Mount Wilson and Palomar Observatories. Professor Zirin and Dr. Howard will provide overall direction for the project. They shall be responsible for the following items:

(1) Assure adequacy of engineering implementation to meet experimental objectives.

(2) Approval of test, operations, and calibration procedures.

(3) Participate in and direct operations.

(4) Astronaut training.

(5) Analysis of test and flight data.

(6) Write the final report.

Supporting investigations such as the following will be carried out:

(1) Collateral high resolution ground-based observations of the Sun to specify important areas to photograph.

(2) Development of data analysis techniques and specification of instrumentation necessary for timely flight data analysis.

Key JPL support personnel will be the following:

(1) Project management: J. Denton Allen, Member of the Technical Staff

(2) JPL management support: R. K. Sloan, Assistant Manager, Space Instruments Section

Table A-1 shows the peak JPL manpower allocation by task. Table A-2 shows JPL manpower by quarters.

Table A-1. JPL peak manpower

Number of People	Task
1	Task Leader/Technical Manager
1	Assistant Task Leader (1) Liaison with MSFC and MSC (2) Responsible for budgets, schedules and documentation
1	Administrative Assistant (1) Schedule and budget assistance (2) Contract administration (3) Facilities
2	Secretarial Staff
1	Science Coordinator (1) Liaison with the investigators (2) Data analysis (3) Experiment planning and astronaut training
1	Optical System Engineer
5	Optics Personnel (1) Telescope design and breadboard (2) Filters (3) Optical system testing
1	Mechanical Systems Engineer
4	Mechanical Systems Personnel (1) Structure (2) Mechanisms (3) Film camera (4) Focus and alignment mechanism (5) Materials
1	Electronic Systems Engineer
10	Electronics Personnel (1) TV Subsystem (2) Power (3) Astronaut Console (4) Sequencer (5) Ground Support Equipment
1	Engineering Support and Test Engineer
14	Personnel (1) Operations and launch support (2) System testing (3) Configuration Control (4) Cabling (5) Documentation (6) Data analysis (7) Parts acquisition (8) Design and drafting (9) Thermal design (10) Environmental requirements (11) Environmental testing (12) Quality assurance and reliability
Total: 43	

C. Schedule

Instrument development should proceed at a pace to allow the results of STM, TCM and prototype testing to be incorporated before flight equipment is completed. The attached performance schedule is based on this type of operation. The telescope has been scheduled separately as it represents the pacing development.

The following telescope systems will be constructed:

(1) Breadboard

(2) Prototype

(3) Flight systems (2)

(4) Temperature Control Model (TCM)

(5) Structural Test Model (STM)

The prototype and two flight systems will be delivered to the spacecraft system. Three sets of ground support equipment will be constructed and one set shipped with the flight instruments.

Table A-2 shows the proposed performance schedule according to the seven phases outlined above.

D. Cost Proposal

Table A-3 shows an accumulative cost-flow summary by quarters and the subcontract procurement milestones. It shows accumulated spending on an obligation basis. Table A-4 shows a summary of costs for both labor and procurement. Figure A-1 shows a curve of projected accumulated JPL costs as a function of time.

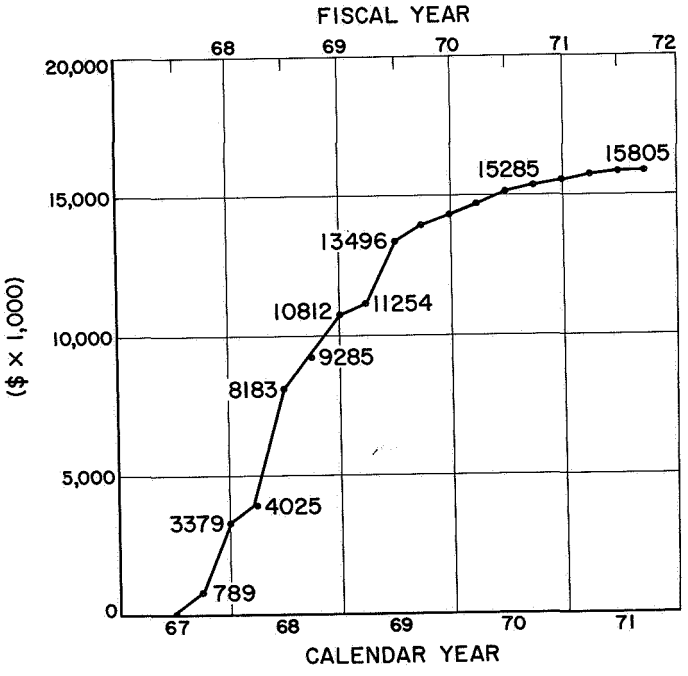

Fig. A-1. Projected accumulated JPL cost ($ × 1000)

ITEM		FY 68 / CY 67 J	F	M	A	M	J	J	A	S	O	N	D	FY 68 / CY 68 J	F	M	A	M	J	FY 69 J	A	S	O	N	D	J	F
SCHEDULE OF EVENTS																											
1. Telescope Statement of Work									▲																		
2. Tel. Contractor Start													▲														
3. Other Contracts Start																	▲										
4. Ship to ATM																											
5. Launch																											
1. Preliminary Design		▨	▨	▨	▨	▨	▨																				
2. Detail Design and Breadboarding								▨	▨	▨	▨	▨	▨	▨	▨	▨											
3. Development Fab. & Testing																											
a. Telescope																											
Design													D	▨	▨	▨	▨	▨									
Fab. & Test TCM & STM																		F	▨	▨	▨	▨					
Fab. & Test Prototype																						F	▨	▨	▨	▨	▨
Design Modification																							P	▨	▨	▨	▨
Fab. & Test Flight Units																											
Deliver to JPL																											
b. TV, Film Cameras, Power, Console & GSE																▨	▨	▨	▨	▨	▨	▨	▨	▨	▨	▨	▨
Deliver to JPL													OSE ▲											OSE	1 ▲	2 ▲		
4. Assembly & Test at JPL																											
a. STM, TCM																			TCM	STM ▨	▨	▨	▨	▨	▨		
b. Prototype																											
c. Flight Units																											
5. Integration with ATM																											
6. Launch & Flight Operations																											
7. Data Analysis																											
a. Final Report																											
MANPOWER (No. of People)	DIRECT LABOR	6			15			26			33			36			36			36			36			36	
	JPL SUPPORT PERSONNEL	0			2			5			7			7			7			7			7			7	
	TOTALS	6			17			31			40			43			43			43			43			43	

D—Design F—Fabrication FU—Flight Unit STM—Structural Test Model P—Prototype TCM—Thermal Control Model OSE—Operation Support Equipment

Table A-2. Performance schedule and JPL manpower

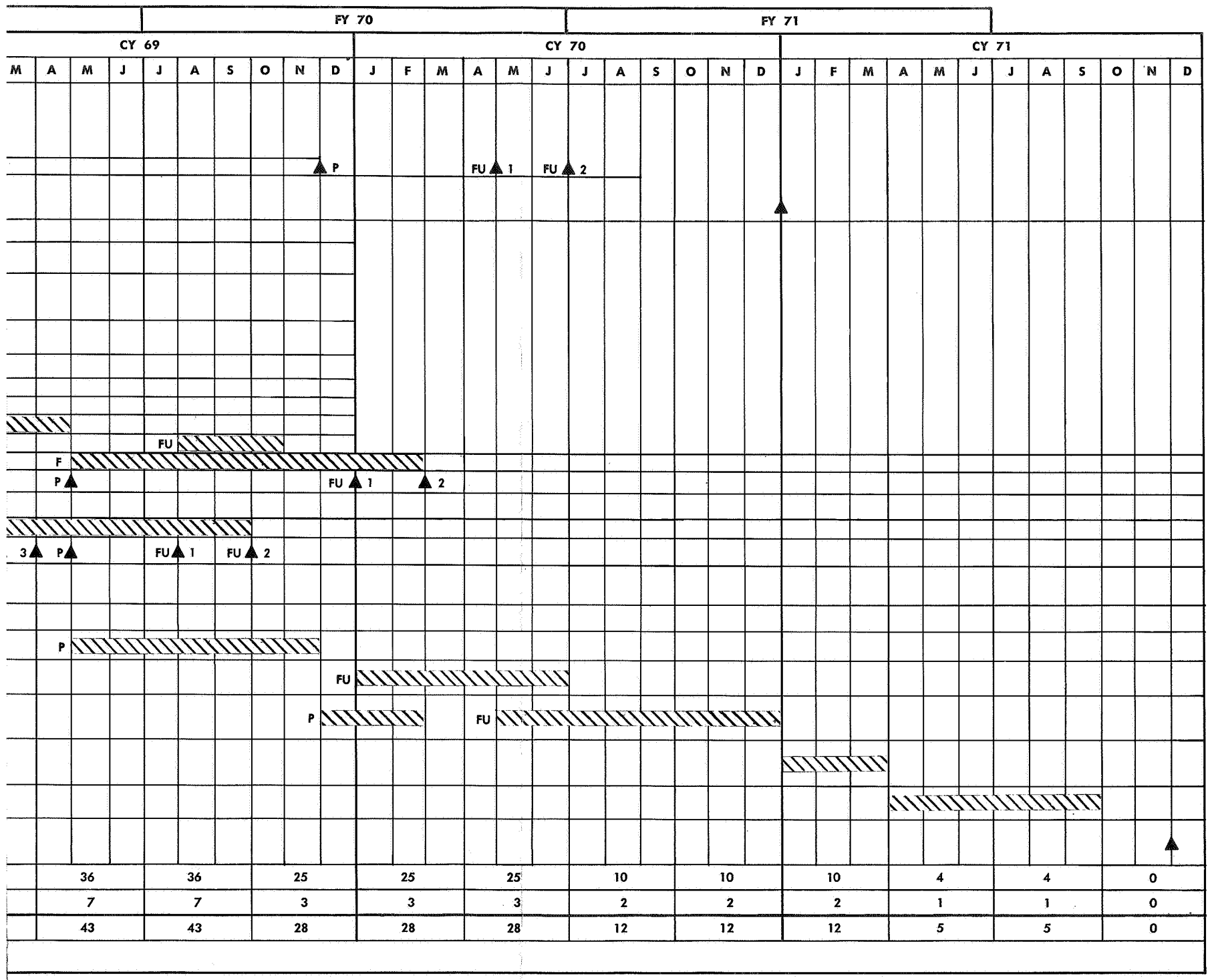

#2

Table A-3. JPL procurement and manpower accumulated costs

ITEM		FY 68 CY 67 J	F	M	A	M	J	J	A	S	O	N	D	FY 68 CY 68 J	F	M	A	M	J	J	A	S	O	N	D	FY 69 J
SCHEDULE OF EVENTS																										
PROCUREMENTS	OBLIGATION DATE $ × 1000																									
1. Telescope Phase I Design, TCM, STM, Proto. $1800													1800													
Phase II Flight Units $800																										
2. Film Cameras	Phase 1 Design & Proto. $400																400									
	Phase 2 FU $200																						200			
3. TV Subsystem	Phase 1 Design & Proto.																1000									
	Phase 2 Flight Units																						500			
4. Astronaut Console	Phase 1 Design & Proto.																300						200			
	Phase 2 Flight Units																					120				
5. Power								200					300			100					300					
6. GSE	DSE																2000					10				
	OSE 1 set 2 sets																					20				
	CSE							15																		
7. Test & Cal. Instrumentation								30			30			20												
8. Optical Filters								5	5	5	5	5	5	5	5	5	5	5	5	5	5	5				
9. Consultant											20			50							105					
10. Breadboard Comp.								100			100															
11. Material								30			30			100			100				130			130		
12. Cabling								390			2295			285			3815				790			1030		
13. TCM STM Test Instrumentation																										
14. Integration & Testing Support																										
TOTAL PER QUARTER																										
JPL DIRECT LABOR & SUPPORT		48		168				399			694			1055			1398				1710			2207		
ACCUMULATED PROCUREMENTS		0		0				390			2685			2970			6785				7575			8605		
ACCUMULATED END OF QUARTER TOTALS		48		168				789			3379			4025			8183				9285			10812		

#1

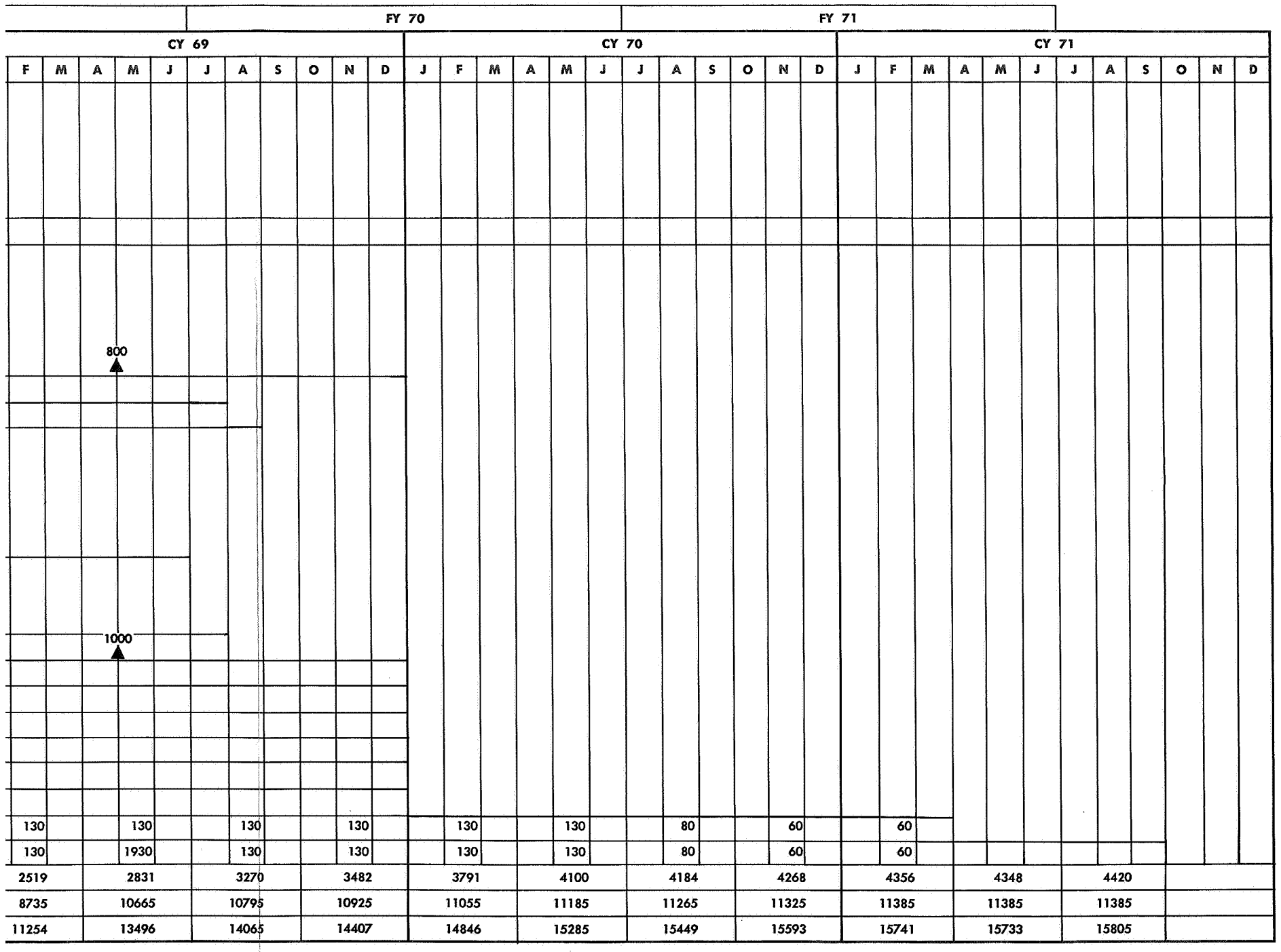
FY 70
FY 71
CY 69
CY 70
CY 71
F M A M J J A S O N D J F M A M J J A S O N D J F M A M J J A S O N D
800
1000
130 130 130 130 130 130 80 60 60
130 1930 130 130 130 130 80 60 60
2519 2831 3270 3482 3791 4100 4184 4268 4356 4348 4420
8735 10665 10795 10925 11055 11185 11265 11325 11385 11385 11385
11254 13496 14065 14407 14846 15285 15449 15593 15741 15733 15805

#2

66B

66C

Table A-4. Cost summary ($ × 1000)

		($ × 1000)
CALTECH		
Labor & Support		300
Data Analysis		100
Data Analysis Equipment		240
Travel		40
	Subtotal	680
JPL		
Labor and Support (112 man years @ $32K per man year including burden)		3584
Design Services (4 man years @ $11/hour)		85
Quality Assurance and Reliability (2 man years)		64
Environmental Testing		
10-ft Space Simulator (54 days @ $8K/day)		432
Vibration, acoustics, etc.		100
Inside Fabrication		100
Travel		60
	Subtotal	4425
SUBCONTRACTS		
Telescope (STM, TCM, prototype and 2 flight systems)		2600
Film Cameras		600
TV Subsystem		1500
Astronaut Console (man rated)		500
Power		120
GSE and Handling Fixtures		1000
Integration and Testing Support (40 man years)		1500
	Subtotal	7820
MISCELLANEOUS PROCUREMENTS		
Test and Calibration Instrumentation		3000
Optical Filters		20
Consultant (optics)		15
Breadboard Components		80
Material		75
Cabling		175
STM, TCM Test Instrumentation		200
	Subtotal	3565
	JPL Subtotal	15810
	Caltech Subtotal	680
	Total Estimated Cost	16490
	Contingency	2000
	Total Estimated Cost and Contingency	18490

II. Technical Section

The scientific objectives of the Technical Section are to:

(1) Obtain high-resolution motion pictures in white light, near ultraviolet and narrow band H_α.

(2) Study the structure and lifetime of solar granulation.

(3) Study the sunspot structure: umbral granulation and penumbral fibrils.

(4) Study the fine structure in the chromosphere.

(5) Study the brightness oscillations in the wing of H_α in higher resolution.

The instrumentation will comprise the following:

(1) An 80-cm aperture solar telescope with three film cameras.

(2) A TV system to provide display for the astronaut and the investigators on the ground.

(3) An instrument performance evaluation and operation via the TV link.

Significant parameters are as follows:

(1) Weight: 1500 lbs.

(2) Power: 500-w total connected load with a 50% demand on the average.

(3) Dimension: 4 ft × 4 ft × 10 ft.

(4) Special Requirements:
  (a) Boresighted pointing by the ATM.
  (b) Voice and TV telemetry to Earth by the ATM.
  (c) Contamination-free environment during data acquisition.

A. Preliminary Statement

The California Institute of Technology (Caltech) proposes to participate in the development and flight of an orbiting solar telescope to obtain high-resolution motion pictures of the sun in white light, narrow band H_α and near ultraviolet. The Mount Wilson and Palomar Observatories will participate through the investigators. The Jet Propulsion Laboratory (JPL) will be responsible for the instrumentation, bringing together experience in both ground-based observations and space photography. With JPL providing the instrumentation, a close working relationship will be established with the investigator team, thus allowing the investigators to become intimately familiar with the design and performance of the instruments. It is believed that this familiarity is necessary to adequately evaluate and interpret the data. The instrumentation has been configured to be compatible with the planned and proposed flights of the *Apollo* Telescope Mount (ATM). This will offer one of the first opportunities to gain experience with a large telescope in space.

B. Scientific Objectives

In the study of any astronomical body, simple spatial resolution of the morphology of the body has always played an extremely important role. In recent years this has been graphically illustrated by the great improvement in our knowledge of the moon and Mars resulting from vehicles such as *Mariner* and *Ranger* which have enabled us to obtain photographs from close range. In the case of the Sun, which may be said to be the most important astronomical body, the same improvement in our knowledge has come from the use of higher resolution. The improvement over the past has not come in such dramatic steps as were produced by the *Ranger* and *Mariner* spacecraft. We can safely say that many of the features we are studying today were discerned by careful observers one hundred years ago. This is because the terrestrial atmosphere limits daytime seeing to ½ sec of arc at best for a few brief moments at a few selected places. The seeing at most established solar observatories is in fact horrible most of the time, and even at best is not better than a second of arc under typical "good conditions." Still, careful analysis of direct photography and cinematography of the Sun through various filters has provided a wealth of information about the structure of the surface, and about the physical conditions which obtain there. In the one attempt so far to carry out photography of the Sun from above the terrestrial atmosphere (Schwarzschild's Stratoscope I program), a great advance was made in our knowledge of solar granulation through a relatively short white light movie. Although present techniques enable us to almost duplicate this movie from ground based observations, there is no doubt that it provided us with important new information on both the structure of sunspots and solar granulation.

Our present situation in solar physics is that we see a great many surface phenomena with scales greater than 700 km (1 second of arc). We have some idea of the physical conditions in these phenomena from spectroscopy, although we are never sure because of the difficulty of interpretation and because of producing spectra of a given small element of the surface. The explanation of the behavior of these structures is to be sought in further application of spectroscopy, and in the pursuit of higher resolution down to the mean free path of particles in the solar atmosphere. A few examples of this possibility are worth presenting. The Sun's surface is covered with a rice grain pattern called the granulation, with a typical scale of about 1000 km per granule. The dark lanes which separate the granules are much narrower than the granules themselves, measuring about 300 km. In fact these lanes were just barely on the limit of resolution of the Stratoscope, and it is possible there are many dark lanes only 100 to 200 km across. If these exist, then the mean granulation size will be decreased by the presence of the many new lanes separating the granules. Higher resolution will tell us what the true granule size is. Although some sequences of granulation were obtained by Schwarzschild with the Stratoscope, they were not very complete, primarily because of image motion, and only suffice to give the mean lifetime of each granule, about 8 min. We do not have extended films of given areas on the Sun with high resolution. It is not known whether the life of a granule is a recurrent phenomena, with a single granule appearing over and over at the same point, whether granules appear in groups or just what they do. When we know more about the granulation, we will know more about the energy transport at the solar surface.

The same kind of problems beset us in the study of sunspots. Sunspots have been observed in white light for some time; indeed, some extremely good photographs have been made, with resolution as good as ½ second of arc. These show that there may in fact be granulation in sunspots. They show other intriguing features, such as the fibrils in the penumbra, and they reveal the wonderful complexity of the large sunspot groups, particularly those that produce great flares. But what we see is only a fleeting glance of what may be happening in the sunspot groups. High-resolution photographs over long periods or even moderate periods would certainly give us a far better chance to observe magnetic field changes before and after great flares, and perhaps to observe some of the photospheric phenomena that accompany the flares. In the study of the chromosphere, the same problems of spatial resolution exist. Spicules have been recognized for many years; however, they are extremely difficult to observe, and the picture we have of them rests at best on a few relatively fuzzy images occupying 10, 20 or 50 film grains on exceptional frames. Most of the studies of spicules have been devoted to the larger features which are more easily seen and whose lifetime may be more easily traced. The other features of the upper chromosphere are just barely visible with present systems. Achievement of a resolution of a tenth second of arc would enable us to see these features clearly. Motion pictures of them over periods of time would resolve their structure and their sources in the low chromosphere. Motion pictures in the wing of H_α show a remarkable brightness oscillation like that in the weaker Fraunhofer lines. The presence of the oscillation is determined by a general review of the number of frames which just barely show it. If the motion pictures

are stopped, we see in a single frame a few blurred features whose nature is quite uncertain. The relation to the velocity oscillation seen in weaker lines is not clear. In every case the problem calls for more resolution and longer periods of observation. There is no doubt that we must also carry out extensive spectroscopic observations of the features we have already identified. We can look forward to a period when this shall have been carried out, and we shall need the next step in resolving power.

1. Proposed experiment. We therefore propose to design and build a telescope with nominal resolving power of about 0.15 seconds of arc, to fly in the ATM program. The choice of the 80-cm aperture is viewed as a compromise. The largest telescope that has flown so far has been the ultraviolet telescope on the OSO of a few inches aperture. It is important to have a large enough aperture to give important scientific results. Obviously, it would be of great value to fly a very large telescope with spectrographs, magnetographs, and various auxiliary instruments. We do not see this as a possibility at the present time, but only as a result of an orderly development of telescopes in the visible region. We feel it is important to fly a telescope which would give substantial new scientific results; but we also feel it is important to fly an instrument which has a reasonable prospect of success. With appropriate filters and versatility, a telescope with 0.15 sec of arc resolving power has many possibilities. Such a telescope will make possible (1) white light pictures in the visible region with resolution of 0.15 arc seconds, (2) pictures in the near ultraviolet, between 2000 and 3000 Å, to study upper photospheric structures, and (3) narrow band H_α pictures of the chromosphere. By use of appropriate filters isolating that region, we are able to take photographs which will show structure similar to that shown in the Ca-K spectroheliograms. It is well known that pictures in the near ultraviolet look something like K-line spectroheliograms, and as we go further into the ultraviolet, the structure of the higher atmosphere should be revealed. Modern developments in thin filters make it possible to fly either multilayer or mica filters with a bandpass of 1 Å, or perhaps narrower. Although these do not present the ultimate in versatility which one obtains with the Lyot type filter, their simplicity will make them useful for the present purpose. It should be borne in mind that with high spatial resolution, we will not be as dependent on the high spectral purity of the filter as we are now with poor spatial resolution. With the use of sophisticated filters, a telescope for direct cinematography has great versatility. It avoids the difficulties of a telescope spectrograph combination, which requires a great deal of space, alignment and so forth. Presumably such a telescope would be in the second generation. We feel that the first step should be made by an instrument with expansion capability, with various types of film and limited to simple type filters of multilayer or Fabry–Perot type. Such an optical system is well within the present state of the art. We can then deal with the problems of thermal control, alignment and focus control, and operation. A series of motion pictures in white light, near ultra-violet and H_α with high spatial resolution will provide important new answers to solar physics which are required today.

The principal investigator (Prof. H. Zirin) and co-investigator (Dr. R. Howard) have carried out programs of high-resolution ground-based studies of the Sun for some years and intend to continue. We believe that the proposed experiment is a natural extension of our present work. We shall continue our normal observational program, using it as a strong basis for identification of problems for study with the proposed instrument.

C. Experimental Approach

Images will be recorded on photographic film utilizing a moderate size telescope of 80-cm effective aperture and 6000-cm focal length. A folded system will be used to reduce the instrument length to about ten feet. The film is to be recovered from orbit and processed under the direction of the principal investigator and his staff. Extravehicular Activity (EVA) by the astronaut will be required to recover and replace the film. Solar images will be available to the astronaut by means of a television link to facilitate focusing, alignment, and pointing of the instrument. A low rate channel will be required to telemeter an image to the ground for evaluation by the investigators. A voice link between the astronaut conducting the experiment and the investigators must also be provided. Image re-registration will be done after the film is processed to account for low rate drifts occurring during the data acquisition time. The effects of high rate drifts or jitter will be reduced by the camera shutter. Secondary guiding could be provided if necessary to further reduce the effects of jitter, although such provision is not a part of this proposal.

A complete telescope using the breadboard system will be in operation in Pasadena throughout the program. The system will first be used to verify adequacy of the design and later as a training instrument. Pasadena provides very favorable conditions for solar observations so

it is expected that typical and useful data will be obtained with the ground-based system.

1. Data reduction and analysis. Data reduction will be carried out by established techniques. Successive frames will be re-registered by an autocorrelating optical printer. Time variations will be studied by motion picture projection of the registered films. Detailed time variations will be examined by superposition of a positive "T_0" print on successive negatives. The correlation of the films in different wavelengths will be studied by blink comparators. Microdensitometer and isodensitometer analysis will be carried out. Photographs of the solar limb will be used to evaluate the instrument modulation transfer function. If necessary, image rectification will be performed on selected frames using this function.

D. Instrument System Description

The proposed experiment will be conducted with the following instrumentation (see functional block diagram, Fig. A-2):

(1) Optical Group (001)

(2) Film Cameras (3) (002)

(3) TV Camera (1) (003)

(4) Focus and Alignment Control (004)

(5) Astronaut Display and Control Console (005)

(6) Operations Sequencer (006)

(7) Power Conversion (007)

(8) Structure (008)

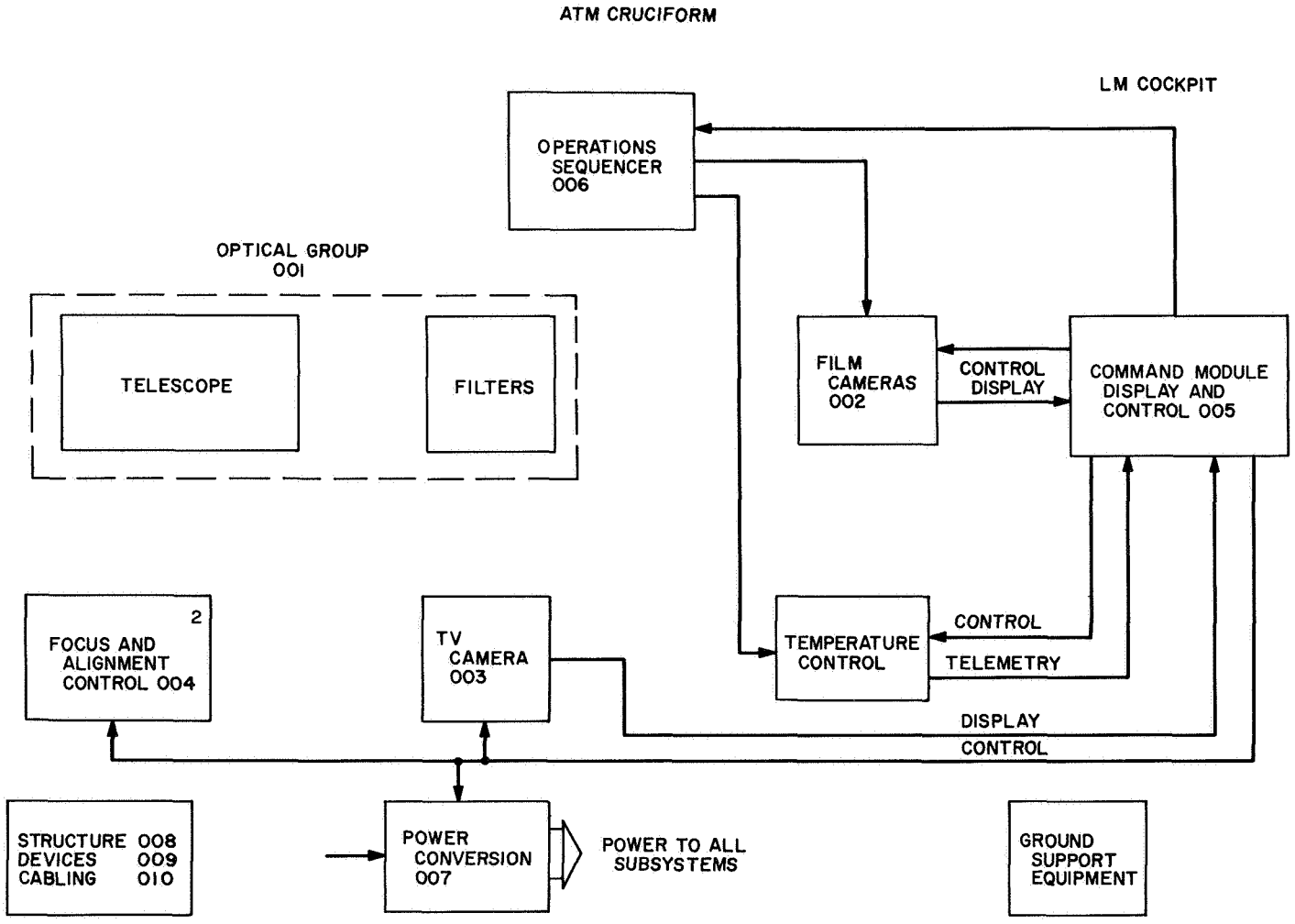

Fig. A-2. High-resolution solar telescope; functional block diagram

(9) Devices (009)

(10) Cabling (010)

(11) Temperature Control (011)

(12) Ground Support Equipment

1. Functional description. The flight system (reference artist sketch, Fig. A-3) will consist of a Cassegrainian telescope, three film cameras, one TV camera and the display and control console for the astronaut. One film camera will be used for each of three spectral bands, namely white light, UV and H_α. Simultaneous recording of images will thus be possible. An active thermal control system will be used to stabilize system performance during data acquisition and minimize stabilization time at the beginning of the solar observation period.

The TV camera will be used primarily to provide the astronaut with optical performance information. By observing the signal characteristics on an "A" scope displaying a single TV line, he will be able to adjust the position

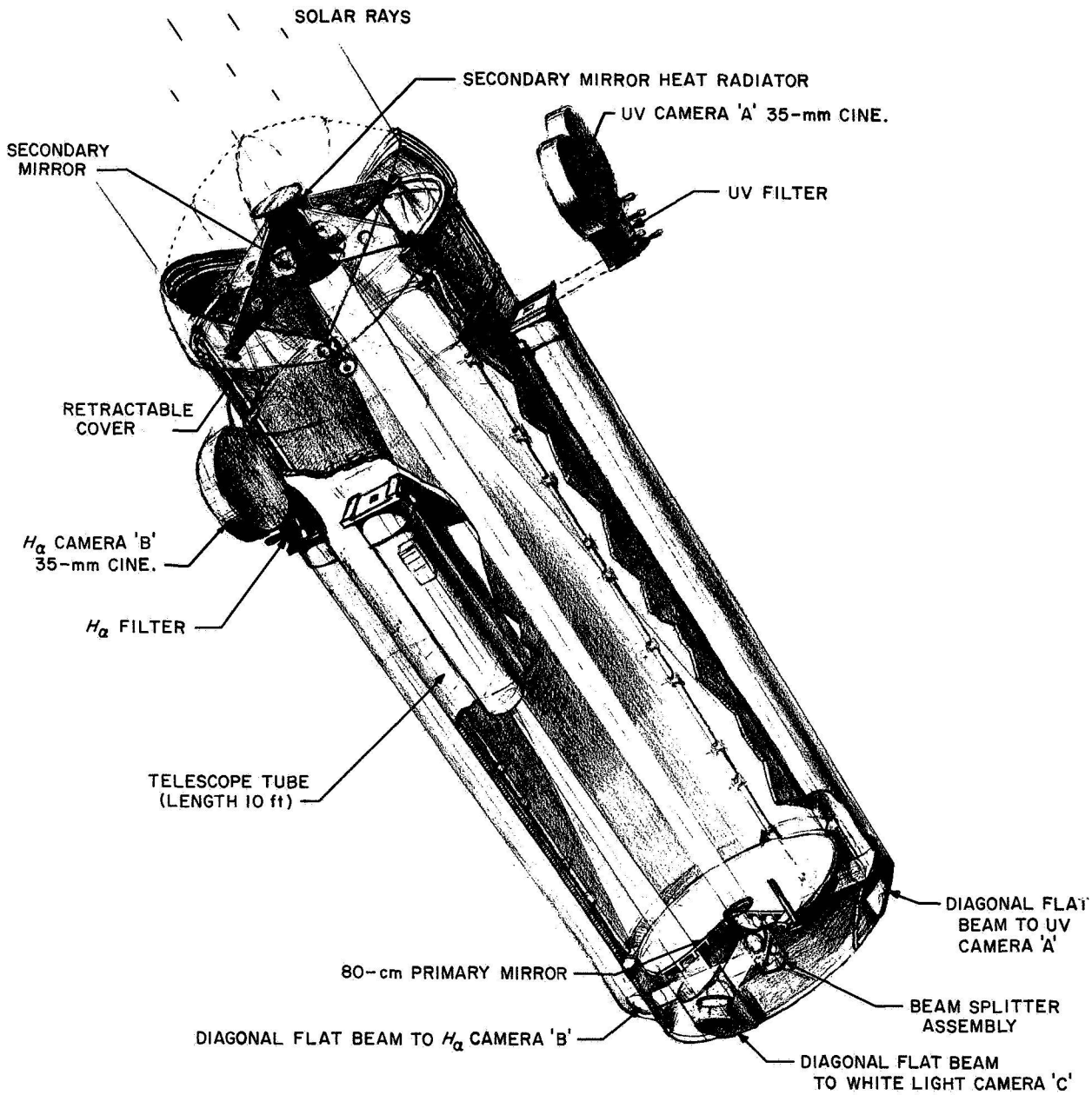

Fig. A-3. Solar telescope

of the primary mirror to affect optimum focus at the film plane. A field monitor will also be provided which will show him which TV line is being viewed on the "A" scope. Optical focus will be accomplished by operating drive motors on the primary mirror assembly. A slow scan TV mode will be provided to allow a selected TV frame to be telemetered to Earth and displayed to the investigators. It is assumed that the transmitter for such purposes is provided by the ATM.

2. Mode of operation. Upon entering the bright side of the orbit, it is assumed that the astronaut will point the ATM instrument complex at the Sun. During this acquisition period, the TV camera will be on and in the normal scan mode. The optics cover will be released and the TV system will then be adjusted and optical performance evaluated. The telescope will then be aligned and focused and the film cameras turned on. At the end of the pass, the film cameras will be turned off and the TV camera placed in standby mode. Periodically during the bright pass the TV image will be telemetered to Earth by switching to the slow scan mode and placing the TV telemetry switch in the *on* position. The majority of the time the TV system will be in the normal mode with the astronaut observing optical quality and making necessary adjustments. Optical "tick" marks will be placed on the film when the focus motors are operating to call attention to this fact. It will therefore not be necessary to turn off the film cameras during focusing.

The temperature control cycle will be as follows:

(1) Upon acquiring the Sun, the mirror heaters will be turned off, the telescope heater turned off, and the cooling system turned on.

(2) Upon entering the dark side, the cooling system will be turned off, and the telescope and mirror heaters turned on.

Other than this, the temperature control system will operate automatically.

A multi-orbit standby mode will be used in the event that photography is suspended for a number of orbits. This will consist of application of a small amount of power to certain critical components to facilitate rapid return to normal operation.

3. Optical group (see schematic diagram, Fig. A-4). An on-axis optics arrangement has been selected, based on computer ray tracing analysis, which will provide a 55.7-cm image of the full Sun. The telescope system is a

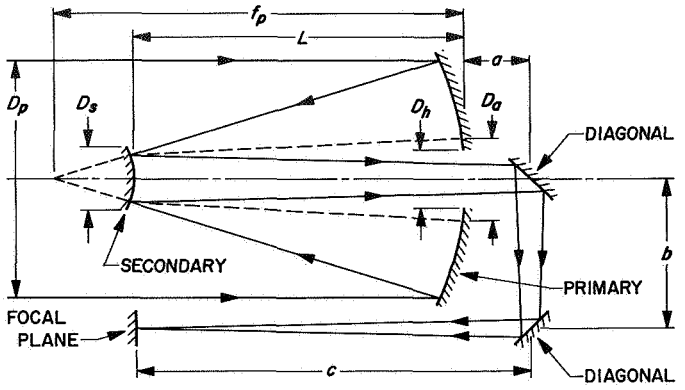

SCHEMATIC DIAGRAM OF OPTICAL SYSTEM :
D_p = 80 cm, D_s = 12.1 cm, D_h = 12.5 cm, D_a = 31.2 cm,
f_p = 320 cm, L = 285.7 cm, $a+b+c$ = 360 cm

Fig. A-4. Schematic diagram of optical system of solar telescope

Cassegrainian design containing an 80-cm parabolic primary and a 12.1-cm hyperbolic secondary. Both mirrors will be supported independent of the telescope housing in order to maintain alignment and focus.

The exit rays of the solar beam are divided by a system of beam splitters allowing simultaneous recording of white light, UV and H_α images. This design provides for future modifications to do far ultraviolet, and narrow band H_α by adding additional cameras, beam splitters, rotating flats and a Lyot type filter.

4. Film camera and filters. A number of cameras are being studied for this application. They can accommodate easily attachable magazines containing up to 1200 ft of film. It is desired to have a film format of 35 mm and at least 2000 ft of white light film for the mission. Multiple magazines which can be positioned remotely from the cockpit are being investigated for use on the white light camera to reduce the EVA requirements.

An ultraviolet and H_α camera each using up to 1200 ft of film will be provided. By using multiple magazines for white light and single 1200-ft magazines for UV and H_α, the mission could be accomplished with a single EVA to retrieve the exposed film. Footage indicators for each camera will be provided in the cockpit.

The white light camera will be equipped with a reflex mirror to provide an image for the vidicon camera. The beam splitters and diagonal mirror assembly will be mounted on a rigid structure which will be adjusted for focus and alignment under ambient conditions. The primary will be positioned for focus and alignment during

flight. Contrast filters will be used for white light photography. Interference and other Fabry–Perot type filters are being developed for UV and H_α under an existing program.

5. TV camera (see functional block diagram, Fig. A-5). An all-magnetic 1-in. vidicon camera will be attached to the white-light camera reflex mirror. The camera will have two modes of operation: a normal mode for closed circuit viewing by the astronaut, and a slow scan mode for telemetry to Earth. The camera head will be attached to the white-light camera reflex optics with the remaining electronics in the cockpit. The camera head will contain the tube, deflection components, preamplifier and voltage distribution. A typical TV camera will have the following characteristics:

(1) Tube: 1-in. all magnetic vidicon
(2) Scanned area: 0.5-in. by 0.5-in.
(3) Number of scan lines: 1400
(4) TV resolution based on a 0.7 kell factor: 1000 TV lines corresponding to 0.05 arc seconds per TV line
(5) Frame time: 1 second normal mode; 60 seconds slow scan mode
(6) Analog video bandwidth (10% blanking and retrace): 1 Khz to 1.1 Mhz normal mode; 20 Hz to 18 Khz slow scan mode

Six bit per picture element A to D conversion will be included if PCM telemetry to Earth is required. The data rate would be 216,000 bits per second. This proposal assumes, however, that an analog telemetry channel capable of an 18-Khz bandwidth will be provided by the ATM.

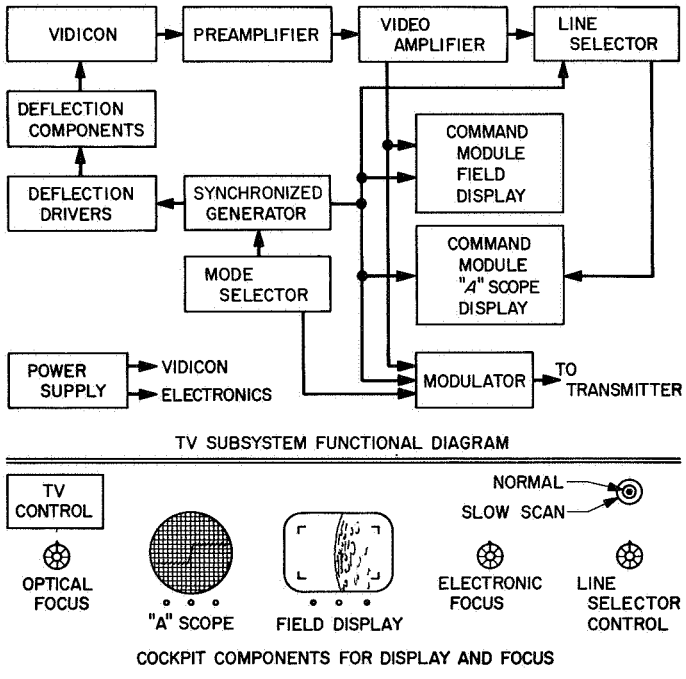

Fig. A-5. TV subsystem functional block diagram

An "A" scope and a field monitor will be provided in the cockpit to display the TV data. Controls for adjustment of the TV system will also be provided.

6. Focus and alignment control. The astronaut will focus and align the telescope by operating the drive mechanism on the primary mirror from the cockpit. By observing the signal characteristics on the "A" scope, he will be able to position the mirrors for optimum focus. Manual adjustment capability will be provided which could be used during an EVA, although this would not be the normal procedure. For further discussion on focus and alignment see Section F.

7. Operations sequencer. Certain functions performed by the astronaut can be incorporated in an automatic sequencer. Once the orbit is established for instance, the sequencer can be used to cycle power on and off for subsequent orbits. This would allow the astronaut to concentrate on pointing and instrument adjustment. The film camera sequencer will be a part of the camera control system. Detail requirements for the sequencer will be established when the level of participation by the astronaut is better understood.

8. Power conversion (see Fig. A-6). The total connected load is expected to be about 500 w at 28 Vdc. The demand is expected to be 250 w on the average. Attached is a histogram showing the anticipated demand as a function of orbital time. The power subsystem will convert the 28 Vdc to provide operating potentials for the TV camera, astronaut console and film camera controls. The connected power load has been estimated as follows:

(1)	TV subsystem	18 w
(2)	TV field monitor	50
(3)	"A" scope	50
(4)	TV controls and panel lights	10
(5)	Optics focus and alignment motors	50
(6)	Film camera shutter and advance motor (3 @ 30)	90 w
(7)	Film magazine transfer motor	15
(8)	Filter wheel advance motor	5
(9)	Cockpit controls	20
(10)	Mirror active thermal control	65
(11)	Telescope heater	100
(12)	Distribution and conversion losses	30
	Total	503 w

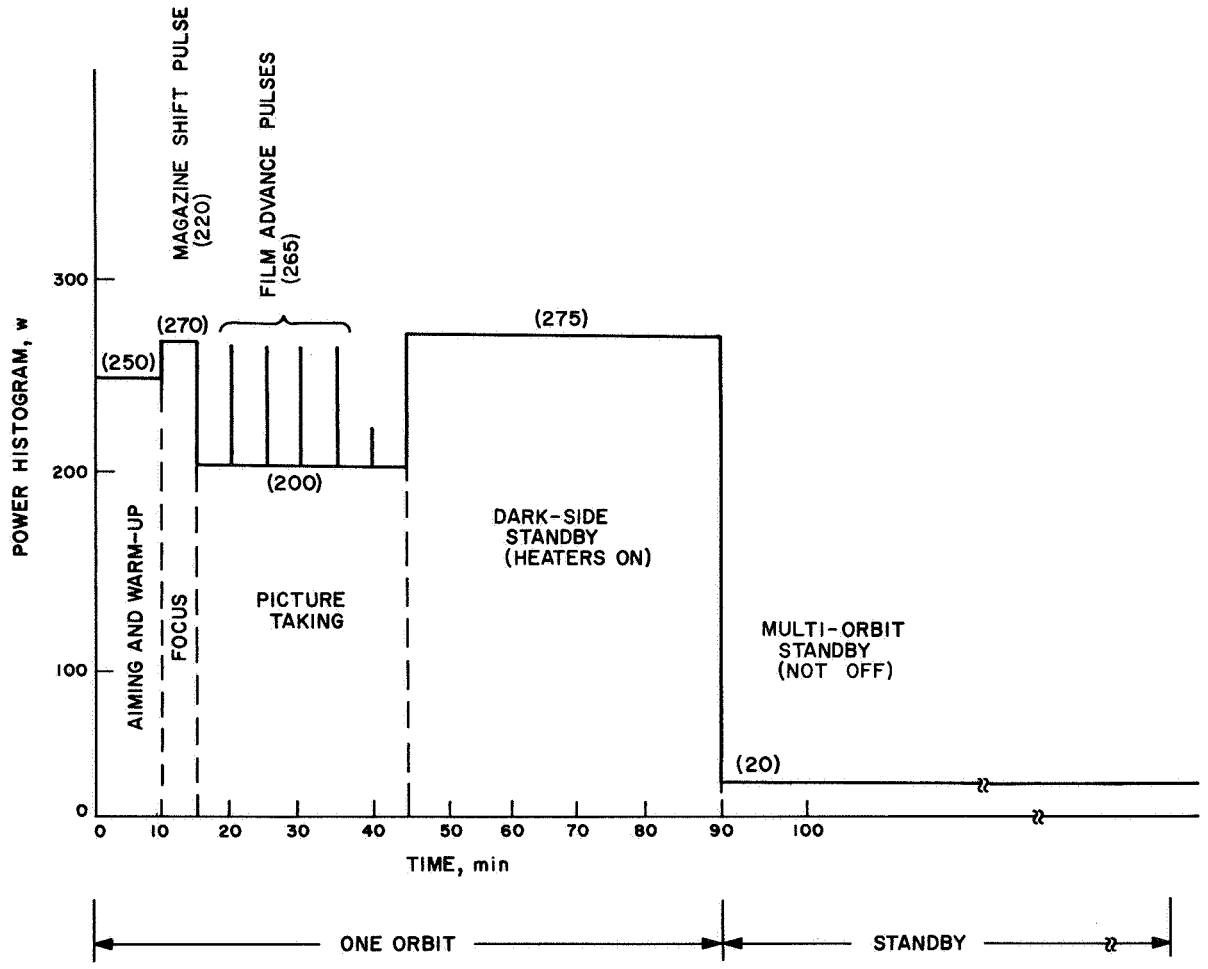

Fig. A-6. Electrical power consumed during hypothetical orbit (total connected load = 503 w)

9. Weight. The telescope system weight has been estimated on the basis of using a quartz primary mirror and a beryllium secondary mirror as follows:

Primary Mirror Assembly	*lbs*
Primary Mirror (Quartz)	220
Mirror Cell	20
Support structure to housing	50
Focus and Alignment mechanism and motors	25
Secondary Mirror Assembly	
Mirror (Be)	1
Heat radiator (Be)	4
Spider and Standoff structure assembly	118
Beam Splitter and Diagonal Assembly	
Diagonal Flats	12
Assembly support (Be)	15

Telescope	*lbs*
Housing (main tube)	190
Insulation	25
Telescope aperture cover	25
Lid motor drive and mechanism	15
Thermal control (heaters, sensors and control)	5
Diagonal camera housings (3 tubes)	60
Launch cage and release mechanism	25
Mount to ATM structure	(ATM furnished)
Truss structure, telescope mounting	50
Diagonal assembly support	20
Control electronics housings	10
Camera (3 Cine and 1 TV)	
Magazines and transport system (mech. and motor)	200

Film 35 mm 4800 ft	24
Airtight housing and access ports	80
Turrets for filters	20
Twin magazine shifting mechanism (1)	20
Camera mounting brackets (3 @ 10)	30
Vidicon (1-in. incl. yoke)	10
Interference filters, stepping motor and mechanism	10
Electrical Harness and Distribution	*lbs*
Telescope, internal distribution and cable assembly	25
LM monitor and control cable assembly	10
Relays, junctions, switches, electronics	30
ATM/Telescope 28 Vdc bus	20
Inverters, converters, regulators (high dc voltage)	50
Controls	
Temperature sensors and indicators	5
Command display (TV), LM	15
Camera sequencer and shutter controls, switches, logic and electronics	20
Meters, indicators, relays, sensors, LM	10
Total	1469 lbs

10. Temperature control. Temperature control is considered to be one of the most serious design problems. The thermal design will therefore be as independent of the ATM environment as possible. We propose to use an active system maintaining temperatures in a range where analysis is possible using available structure and material information. A further discussion on temperature control is contained in Section E-5, below.

11. Ground support equipment (GSE). The GSE will consist of operations support equipment (OSE), breadboard development support equipment (DSE), calibration support equipment (CSE) and handling fixtures.

Three sets of OSE will be constructed and one set with selected spares shipped with the flight instruments to support integration with the ATM and launch. The OSE will be transportable and consist of the following elements:

(1) ATM electrical simulator
(2) LM simulator
(3) General test equipment
(4) Test data recorder
(5) ATM test fixture

The DSE will be set up in the development lab to operate the breadboard system. This equipment in general will not be transportable and will remain with the breadboard system. The CSE consists of those items specifically used for calibration, alignment and focus testing. Such items as light sources, temperature instrumentation and equipment to measure optical performance will be included.

E. State of Development

1. Optical group. A number of telescope designs, including both on-axis and off-axis configurations have been studied using computer ray tracing. An f/75 on-axis configuration which fulfills the performance requirements of the experiment has been selected for detail analysis. (See schematic diagram, Fig. A-4.)

An 80-cm parabolic primary and a 12.1-cm hyperbolic secondary will be used in conjunction with two diagonal flats, allowing the cameras to be located at the open end of the telescope for easy access. The telescope will have an overall focal length of 60 meters. It will be diffraction limited at an angular resolution of 0.157 arc seconds at a wavelength of 5000 Å. At f/75, the field of view is 0.766 deg. The full solar image after a magnification of 18.8 will be 55.7 cm at the focal plane. No transmission elements are required other than beam splitters allowing for eventual modification to do far ultraviolet photography. The optical design is straightforward and well within the state of the art. The difficult problems are those of thermal control, structure and materials, and testing. These are discussed in Sections E-4, E-5, and F, respectively.

2. Television subsystem and astronaut console. The TV camera is essentially a closed circuit system with a slow scan mode for image telemetry to earth. The TV camera will present no new design problems and will utilize the same vidicon and circuit designs being used for the *Mariner Mars '69* camera system, which is in an advanced state of development at JPL.

The astronaut console consists principally of display and controls. The high-resolution field monitor may present a problem in obtaining 1000 TV lines at a 1-second frame rate in a reasonable size. Two alternatives are possible if this problem becomes prohibitive:

(1) A higher frame rate can be used in the normal mode, allowing the use of a faster phosphor, thus improving resolution.
(2) An expanded sweep can be used to view 500 lines at a time rather than the full 1000.

3. Film cameras and film emulsions. A number of pulse type film cameras have been studied and are suitable for this application. Some development work will have to be performed to provide ease of magazine removal and replacement. Material problems associated with lubrication of moving parts and evaporation of film materials will have to be solved. These problems may best be approached by hermetically sealing the cameras. We understand that film cameras are being designed for current ATM applications, and we will investigate these for application with this instrument.

Resolution of 14 microns is possible with 649 GH film for the white-light camera. H_α images will be recorded on SO 375 film with comparable capability. A film for the ultraviolet (2000 to 3000 Å) has yet to be chosen; but it appears that 649-0 will be suitable.

4. Materials and structural considerations.

a. Telescope optics. Although a quartz primary and beryllium secondary are proposed, a number of materials are being investigated for the primary and secondary mirrors. The ideal material should have low density, high thermal conductivity, high modulus of elasticity, and very low coefficient of expansion. Ideally, it should be capable of being polished to mirror configuration using existing techniques developed over the years for glass mirrors. Among the materials being considered are:

(1) *Fused quartz* (99+% SiO_2). This material has a very low coefficient of expansion, and can be fashioned into a mirror using familiar techniques. Like most ceramics, it has very low thermal conductivity, which renders its use questionable for the solar telescope.

(2) *"Recrystallized" glasses.* This family of materials which includes the Pyrocerams* and CER-VITS* are of interest largely because of the extremely low thermal expansion coefficient, approaching zero for limited temperature ranges, of some of them. The "recrystallized" glasses, like quartz, have low thermal conductivity. Conventional techniques are usable for producing mirrors.

(3) *Light metals.* Of principal interest are beryllium, aluminum, and titanium. All have thermal conductivities much higher than the glasses. In the case of titanium the conductivity is higher by a factor of 10. Aluminum and beryllium are higher by a factor near 100 as compared with glass. Tending to offset the advantage of higher thermal conductivity is their higher expansion coefficients as compared with quartz. Titanium has a coefficient approaching 20 times that of quartz, while the coefficients for beryllium and aluminum are 30 and 40 times that of quartz, respectively. Beryllium has an extremely high modulus of elasticity coupled with a low density. Its high cost and toxicity are disadvantages.

(4) *Low expansion alloys.* Alloys of iron and nickel centering around the Fe-36 Ni composition are extensively used because of their low coefficients of expansion over a limited but useful temperature range. Coefficients approaching that of quartz are achievable in the zero to 100°C temperature range. Coefficients approaching zero for a similar temperature range have been achieved in the laboratory by substituting 4 to 6% cobalt for 5% nickel. Like most metals, thermal conductivity is relatively high, about half that of aluminum. Mirror polishing and surfacing should present no insurmountable problems. Because of nil porosity and low surface activity, conventional plating methods, such as vapor deposition, electroplating, and electroless nickel plating should be usable. The chief disadvantages of these alloys are high density, about 4 times that of beryllium or glass, and lack of experience in making mirrors.

b. Telescope structure. The basic structural housing, being mechanically isolated from the mirrors, may be fabricated from aluminum alloys using conventional aircraft techniques. Beryllium and beryllium-aluminum (Lockalloy) structures will be evaluated to determine whether the very high material and fabrication costs are warranted for this application. A lightweight series of quartz rods or Invar-type tubes may be used to connect the mirrors and hold them in alignment. Low coefficient of expansion to protect against temperature variation appears to be a prime requirement.

5. Temperature control. The telescope system will be made as independent as possible of the temperature excursions of the ATM as it moves from sunlight to shade. Thermal isolation will be provided by means of low conductance bolted joints at the interface. There will, however, exist requirements from the ATM for electrical power for temperature control, and it may also be necessary to use fluids from certain of the ATM fluid loops to provide active temperature control of the mirrors.

*Trade names of Corning Glass Company and Owens-Illinois, respectively.

The primary and secondary mirrors pose two major temperature control problems:

(1) Variable heat input to the primary mirror due to variation in illumination from full, when viewing the solar disc, to zero, when the spacecraft is in Earth shadow, gives rise to temperature variations in both time and physical location within the mirror. In addition, for the on-axis design, there exists a region of high heat input due to the reflection of the secondary in the primary, and this reflection will vary in position as the aiming point of the telescope is changed.

While the total excursion in temperature for the primary mirror is not likely to be very large during an orbit, the gradients in degrees centigrade per centimeter, both radially and axially, give rise to anxiety, and their effects on the mirror figure are being investigated.

While a steady-state temperature distribution is desirable during the picture taking sequence, this will not be attainable, particularly with a non-metal primary mirror. By a suitable combination of passive and active control, it seems that a suitable mirror figure can be maintained.

(2) The ray convergence from the primary mirror gives rise to a large total heat input at the secondary, and a very high heat flux. This is considerably greater than the amount of energy that can be removed by the normal passive radiative surface and conduction paths provided by the secondary mirror back and the supporting spider, respectively. Additional radiating surfaces, shaded from direct sunlight under normal viewing conditions, must be provided in order to maintain reasonable secondary mirror temperatures. In addition, the low thermal mass of the secondary mirror, wC_p, means that there would be rapid excursions of temperature when entering or leaving direct sunlight. This will necessitate active thermal control with an electrical heater during the period when the telescope is eclipsed by the Earth. With these problems in mind, it was decided that a metal secondary mirror will be used.

Passive thermal control in vacuum relies on radiation as the final point of heat rejection. Heat transfer is thus dependent on the properties of the radiating surface and their degradation with time. Most temperature control surface materials which have been developed for spacecraft to date are used in the vicinity of room temperature (between 0° and 200°F) and, in this range, their properties and degradation under ultra-violet are well known. For this reason, any thermal control system for the secondary mirror should be designed to operate within this range. If the spider is used as a conduction path for large quantities of heat, small variations in the legs of the spider will give rise to differences in temperature drop along each leg which may tilt the secondary mirror. For this reason it is proposed to control the secondary mirror at an equilibrium temperature of about 150°F in sunlight, by using suitable radiating surfaces, and to supply sufficient electrical power during the eclipsed part of the orbit to maintain this temperature. This will avoid losses in observation time when it is first possible to observe the sun in an orbit.

The primary mirror, if it is to be of a non-metal, due to the low thermal conductivity of these materials, will have to be provided with heat sinks at the periphery, around the center hole, and at the back. Preliminary calculations indicate that a non-metallic mirror, 3 in. thick, will rise in surface temperature by roughly 45°F in the region of high illumination during the sunlit portion of the orbit, and that the thermal gradients within the mirror will be extremely steep, both radially and axially. Other calculations using a metal for the mirror, with the same heat sinks, indicate a temperature rise in the region of high illumination of less than 1°F. Thermal stress analysis will determine whether this is likely to affect the mirror figure to a sufficient extent to degrade the optics of the telescope. The degree of sophistication involved will be determined by the effect of the gradients within the body of the mirror on the surface figure.

Other methods of temperature control, such as fluids circulating through the spider support arms to cool the secondary mirror, the use of a solid/liquid mixture in a cavity behind the mirror to provide fixed temperatures, or some combination of these, may have to be considered for both mirrors in the final configuration. Quantitative analyses and model experiments will readily demonstrate the feasibility of these and other proposed solutions.

Other temperature control problems exist in the telescope tube, the cameras and focus mechanism; however, these are not new problems. Access through insulating covers for changing film will provide some difficulty, but this does not appear insuperable. In general, the major problems are predicted to lie in the temperature control of the primary and secondary mirrors, since none of the previously developed orbiting telescopes have been for direct observation of the Sun, and they are therefore designed for much lower thermal loads.

F. Test and Calibration

In order to obtain the required system performance, techniques must be established to verify focus and alignment. It is necessary to check these under ambient, launch, and in-flight operational conditions. The telescope manufacturer will be responsible for performing necessary tests to ensure that the system meets the optical performance requirements under ambient conditions. Focus and optical alignment can be adjusted in flight.

The primary mirror will be equipped with three drive mechanisms which, when operated simultaneously, will position the mirror axially, and when operated separately, will change the tilt. These will be used to adjust focus and alignment, respectively. Once the telescope is pointed at the Sun, alignment will be checked by first observing the signals from four photodiodes which will be located on the spider. These diodes will be illuminated by the second reflected image from the primary, and tilt adjustments made until an equal output is obtained from each diode. The focus will then be adjusted, as described previously.

A further check on alignment will be made by observing the position of a small source of light which will originate at the film camera and be returned by small mirrors on the outer end of the telescope. A small solid state matrix detector will be used, and alignment adjusted to position the returned spot. The position of the spot corresponding to optimum alignment will be established under ambient conditions. It is expected that this procedure will be performed by the astronaut.

These procedures will be verified under flight conditions by using the JPL 10-ft simulator. A resolution test target can be used as shown in Fig. A-7.

Computer analysis is currently being performed to determine the effects of misalignment on the system performance. The design details will depend on the results of this analysis.

G. Astronaut and Spacecraft Considerations

The astronaut can play a very important role in this experiment by optimizing system performance during the picture-taking sequences. By use of the boresighted pointing telescope provided by the ATM, he can choose the region to be observed upon instruction from the investigators on the ground. A suitable program will be set up for him to follow in the event of loss of ground observation or telemetry. The astronaut will be trained in solar observation of this type by several weeks' work at observatories in Pasadena.

The proposed instrument has been designed to be accommodated in a portion of the 82-in. ATM instrument cruciform. Access to the camera film magazines will be provided at the outer end of the telescope. All mechanisms will be power-actuated by the astronaut. Access doors will be provided for simple and hazard-free handling in the event that EVA is required for corrective action. Pyrotechnics will not be used.

1. Environmental constraints. The only constraint dictated by the solar telescope is cleanliness. The instrument must not be subjected to condensible outgassing products from other assemblies. The optics cover must be in place during waste dumps and control jet excitation. The immediate environment must also be free from optical scattering to assure optimum results.

2. Interface summary.

a. Pointing and guiding. The telescope system will be rigidly attached to the ATM cruciform. It is required that the telescope be pointed at the center of the Sun for in-flight alignment and that pointing capability from limb to limb be provided by the ATM. The jitter rate must be less than 2 arc seconds per second for 30 min with a maximum excursion not to exceed 3 arc seconds. The roll rate must not exceed 100 arc seconds per second, with a maximum excursion not to exceed ¼ deg.

b. Power. The power is as follows:

Total power: 500 w

Average power: 250 w

Power profile: Section D-8

c. Weight. Total system weight, including the astronaut console, is estimated to be 1500 lbs. The weight in the LM will be 35 lbs.

d. Dimensions. The dimensions are:
Telescope system: 4 ft x 4 ft x 10 ft
Astronaut console: 18 in. x 10 in. x 18 in.

e. Telemetry. Two-way voice communication is required to be provided by the ATM. A slow-scan TV image will be available for telemetry to Earth. It is assumed that the transmitter will be provided by the ATM. An analog system is proposed with an 18-KHz bandwidth required.

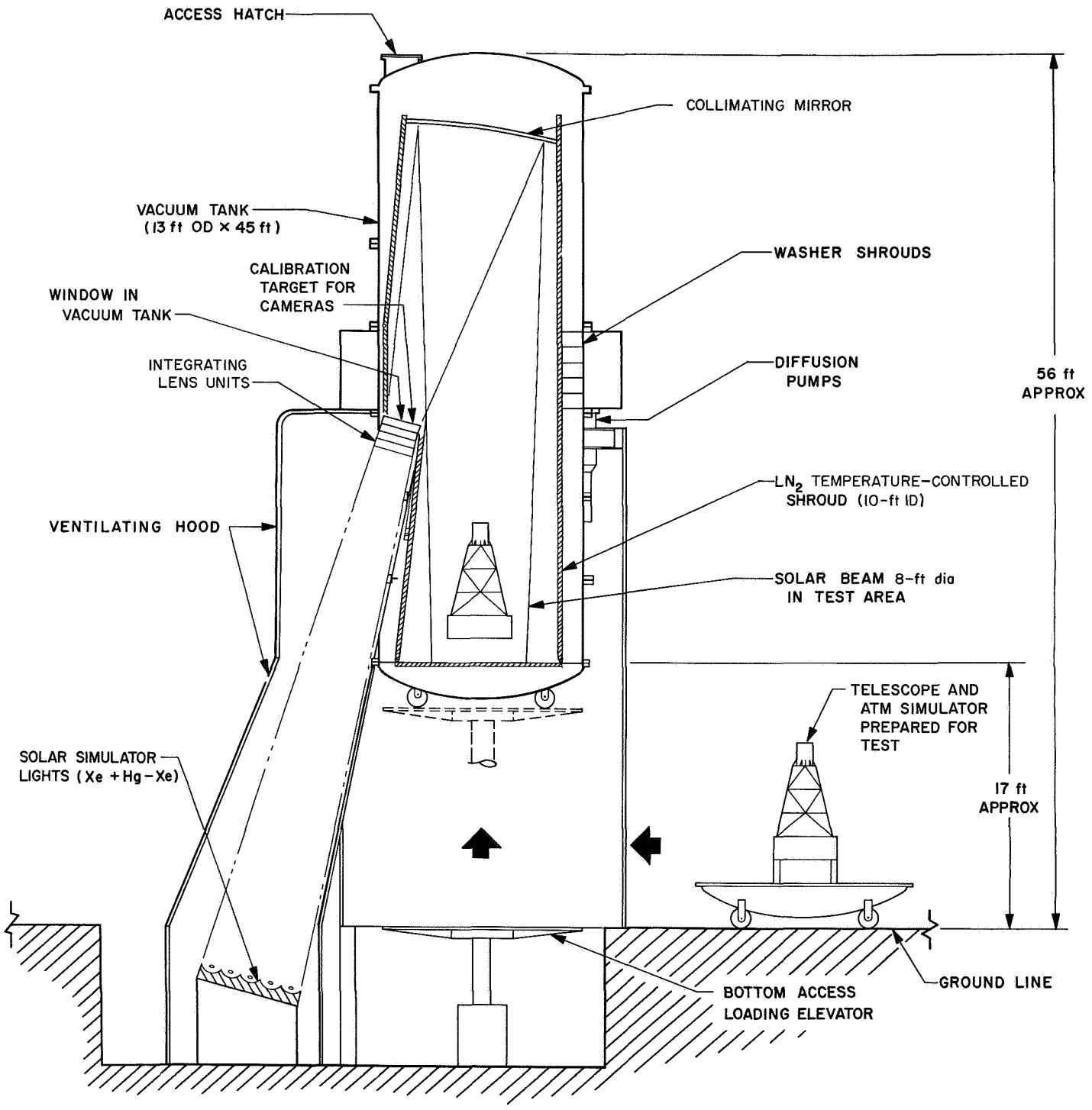

Fig. A-7. Solar telescope TCM in 10-ft solar and space simulator

f. Control console. This includes:

Optics cover on/off

Heaters on/off

Coolant system on/off

Multi-orbit standby on/off

Optical focus and alignment drive control

Film Cameras:

- On/off (UV, H_α and white light)
- Magazine transfer
- Mode selector
- Footage indicator

TV Camera:

- On/off/standby
- Normal/slow-scan mode
- Picture telemetry on/off
- Camera adjustments
- Line selector

Controls will be provided for adjustment of the TV "A" scope and field displays in the LM.

g. Recording. Recording of engineering measurements will be required, but specific requirements have not yet been established.

Appendix B

Basic Optics and Imaging

I. Introduction

The optical design of a near diffraction limited telescope for solar observations is described in the following sections of this report. Basic objectives for the system include UV photography of the Sun in the 1500 Å–2500 Å wavelength region, white light movies centered at 5000 Å, and narrow band photography of the H_α spectrum. A spatial resolution of around 0.1 arc sec for observing fine structures of the Sun is desired. Constraints imposed on the system by the ATM limit the available aperture to a diameter of 80 cm and telescope tube length to 350 cm.

An F/75 Cassegrainian system is analyzed in detail and a model telescope is defined as a candidate for potential flight application. Because of spacecraft size limitations, only the on-axis system is considered for actual use in the experiment. Although the model telescope described is not, at this time, intended to be the ultimate system, it does delineate the general properties of the device and defines major areas where detailed thermal, mechanical, and metallurgical analysis is required.

II. Background Summary

A. Sign Convention

It is necessary at the onset of the optical design to adopt a convention of signs for distances and angles. Many such conventions are in use and all have some points in their favor. In this report we shall use the following set of conventions (Ref. 28):

(1) Draw all figures with light incident on reflecting or refracting surfaces from left.

(2) Consider object distances positive when object lies at left of vertex of reflecting (refracting) surface.

(3) Consider image distances positive when image lies at the right of the vertex.

(4) Consider radii of curvature positive when center of curvature lies at the right of the vertex.

(5) Consider angles positive when the slope of the ray with respect to the axis (or with respect to radius of curvature) is positive.

(6) Consider transverse dimensions positive when measured upward from axis.

B. Spherical Mirrors

The relation between object distance p and image distance q for a spherical mirror whose focal length is f is given by

$$\frac{1}{p}-\frac{1}{q}=-\frac{1}{f}=-\frac{2}{R_c}$$

Adoption of the sign rules stated in Section II-A results in a negative focal length for a concave mirror and a positive focal length for a convex mirror (see Fig. B-1). A negative value of q corresponds to a real image and a positive value to a virtual image.

The expression for lateral magnification of a spherical mirror is

$$m=\frac{q}{p}$$

or the ratio of object distance to image distance.

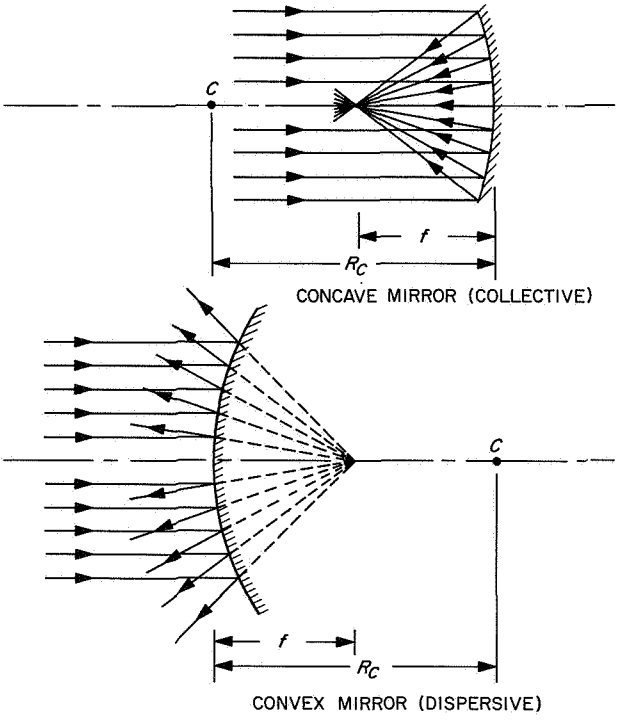

Fig. B-1. Spherical mirrors

C. Cassegrainian Optics

Consider a folded optical system utilizing two spherical mirrors as shown in Fig. B-2. The real image formed by the concave primary mirror at f_p is magnified by the convex secondary mirror to form a final image. The final image is brought outside the optical system through a hole in the center of the primary. For this familiar system the following equations apply:

$$F_p = \frac{f_p}{D_0}$$

$$F = \frac{f}{D_0}$$

$$FOV = \tan^{-1} 1/F$$

$$p = D'_s F_p$$

$$q = D'_s F$$

$$m = \frac{q}{p}$$

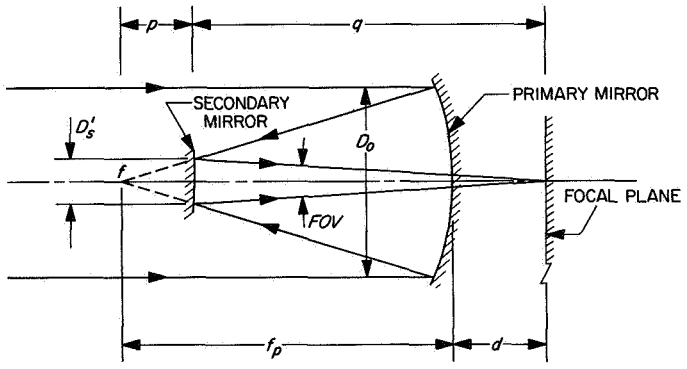

Fig. B-2. Cassegrainian optical system

D. Aberrations

Rays incident from an axial point source on the outer portion of a spherical mirror will be imaged closer to the optical surface than will rays incident on the inner portion. A simple but useful approximation to the image size produced on axis by a spherical mirror is (Ref. 29):

$$\delta_s = \frac{7.8 \times 10^{-3}}{N^3} \text{ (radians)}$$

At F/1 this approximation gives a value too small by several percent. In slower systems the agreement is much closer.

The aberration known as *coma* affects rays from points not on the axis of the mirror. It is similar to spherical aberration (which relates to points on the mirror axis), in that both arise from the failure of the optics to image central rays and rays through outer zones of the aperture at the same point. *Coma* differs from spherical aberration in that a point object is imaged not as a circle but as a comet-shaped figure.

E. Conic Mirrors

In a particular system even the most advantageous choice of radii for the primary and secondary mirrors may not produce images small enough to be satisfactory. While more complex systems could be designed with additional elements the normal practice is to utilize nonspherical surfaces. In this case, the primary becomes ideally a paraboloid and the secondary a hyperboloid.

Analysis of a Cassegrainian telescope employing conic mirrors follows the construction in Fig. B-3. Consider a hyperbola with focii at $\pm c$ and vertices at $\pm a$. It is easily seen that (using undirected segments)

$$q = a + c$$

and

$$p = c - a$$

The simultaneous equations may be solved for a and c. Hence,

$$a = \frac{q - p}{2}$$

$$c = \frac{q + p}{2}$$

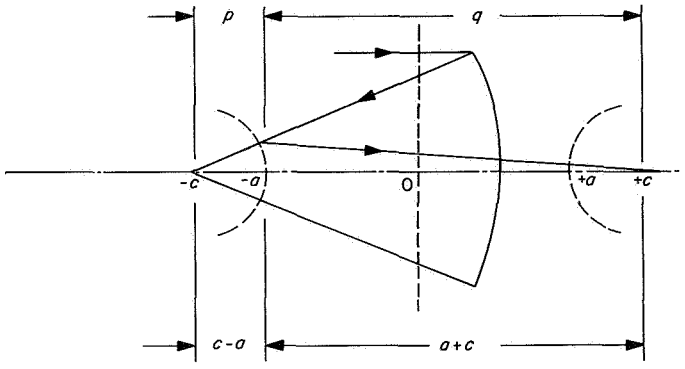

Fig. B-3. Construction for conic mirrors

And, since the eccentricity is equal to

$$e = \frac{c}{a}$$

we select a hyperboloid for a particular system whose eccentricity is equal to

$$e = \frac{q+p}{q-p}$$

The eccentricity of the paraboloid is, of course, unity. It is only necessary that its focal point coincide with hyperboloid focus at $-c$.

F. Tolerances

The effect on the performance of the optical system due to small changes in p and q is analyzed in this section. Given (Fig. B-4a)

$$\frac{1}{p} - \frac{1}{q} = -\frac{1}{f}$$

we have, for incremental changes Δp and Δq

$$\frac{1}{p+\Delta p} - \frac{1}{q+\Delta q} = -\frac{1}{f}$$

Solving for Δp we obtain, after some algebraic manipulation,

$$\Delta p = \frac{\Delta q\,[f+p] + q\,[f+p] - f_p}{f-q-\Delta q}$$

But, since

$$q = \frac{pf}{f+p}$$

then

$$\Delta p = \frac{\Delta q\,[f+p]}{f-q-\Delta q}$$

or

$$\Delta p = \Delta q\left(\frac{f+p}{f-q}\right)\frac{1}{1-\dfrac{\Delta q}{f-q}}$$

$$= \Delta q\left(\frac{f+p}{f-p}\right)\left[1 + \frac{\Delta q}{f-q} + \left(\frac{\Delta q}{f-q}\right)^2 \cdots\right]$$

Hence,

$$\Delta p = \Delta q\left(\frac{f+p}{f-q}\right)$$

to a first order approximation.

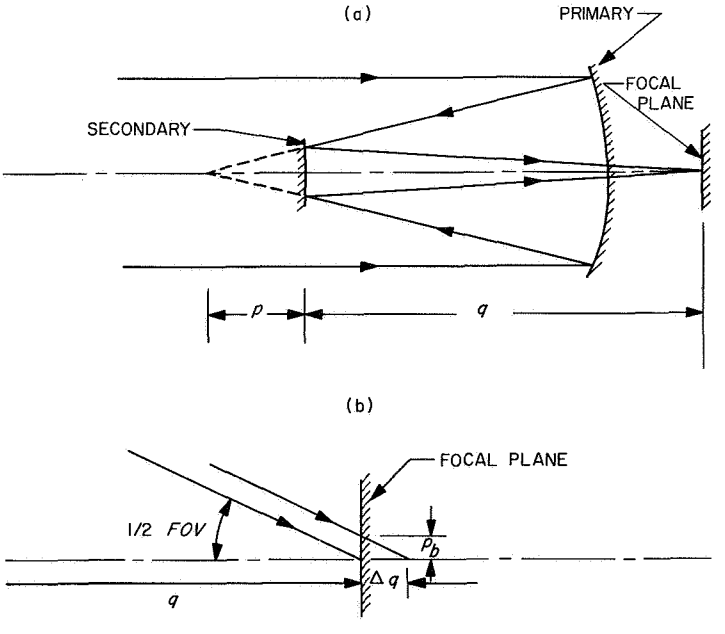

Fig. B-4. Construction for tolerance determination

With reference to Fig. A-4b, it is seen that the blur diameter $2\rho_b$ corresponding to a small change Δq in the image distance is very nearly

$$2\rho_b = \Delta q \tan FOV$$
$$= \frac{\Delta q}{F}$$

The maximum value of Δq that is permissible in a diffraction-limited system is found by substituting the Rayleigh limit $\overrightarrow{RL}$ for $2\rho_b$. Thus,

$$\Delta q_{max} = F\overrightarrow{RL}$$

and

$$\Delta p_{max} = \left[\frac{f+p}{f-q}\right] F\overrightarrow{RL}$$

G. Vignetting

The falling off of light intensity at increasing distances from the optical axis (at the focal plane) is analyzed in this section.

The vignetting curve by the secondary mirror may be calculated in the following manner. If, as shown in Fig. B-5, we place our eye at various points on the focal plane (suppose the primary is transparent), we will see differing areas of illumination on the secondary mirror. This situation is depicted in Fig. B-6. Here, the secondary mirror is drawn with center at c, and a section across the light cone is drawn with center at c'. The portion common to both constructions is shaded and represents the illuminated part of the secondary mirror. This portion has an area equal to

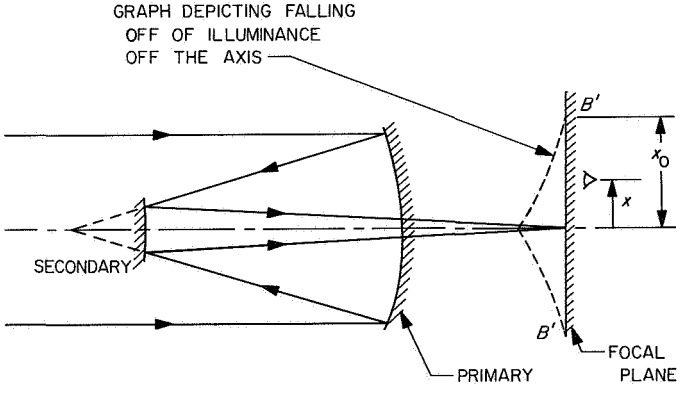

Fig. B-5. Construction (1) for vignetting by secondary mirror

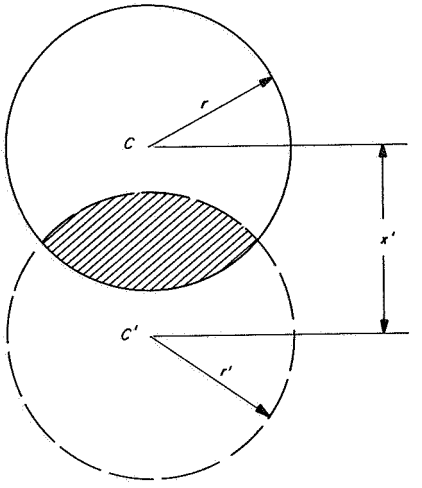

Fig. B-6. Construction (2) for vignetting by secondary mirror

$$A_{(y)} \doteq 2r^2 \left[\cos^{-1} y - y\,(1-y^2)^{1/2}\right]$$

where

$$y = \frac{x'}{2r}$$

and x' is the distance between centers.

The illuminance at any point on the focal plane whose distance from the center line is x may be found by noting a linear correspondence between x and x'. Two points may be used to determine the linear relationship for a particular system. One point is conveniently chosen at maximum illumination ($x = x' = 0$) and the other at the point where total vignetting occurs.

The second point is found as follows:

Let B in Fig. B-7 be the point on the focal plane where total vignetting occurs. Since distance $A'B'$ at the prime focus corresponds to AB at the focal plane we have, using similar triangles,

$$\frac{A'B' - D_s/2}{p} = \frac{D_p + D_s}{2L}$$

or

$$A'B' = \frac{1}{2}\left[\frac{p}{L}(D_p + D_s) + D_s\right]$$

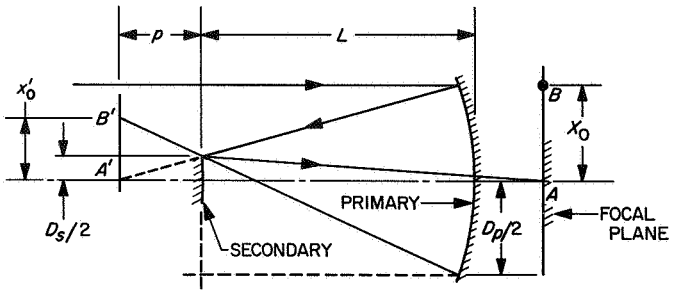

Fig. B-7. Construction (3) for vignetting by secondary mirror

Now, since

$$AB = mA'B'$$

the equation becomes

$$AB = x_0 = \frac{m}{2}\left[\frac{p}{L}(D_p + D_s) + D_s\right]$$

When

$$A_y = 0$$

we have

$$x_0' = 2r_s$$

and since

$$x = \frac{x_0}{x_0'}x'$$

there results

$$x = \frac{m}{4r_s}\left[\frac{p}{L}(D_p + D_s) + D_s\right]x'$$

It should be observed that using circles of equal radii in Fig. B-6 is a fair assumption since the diameter of the light cone is very nearly equal to the diameter of the secondary mirror. Vignetting by the primary mirror in the on-axis system is discussed in Section III.

H. Resolving Power

The light from a point source, diffracted by a circular opening, is focused by an optical system not as a geometric point but as a disc of finite radius surrounded by dark and bright rings. The separation of two just-resolved points is given by

$$\widehat{RL} = \frac{1.22\lambda}{D}\text{(radians)}$$

The larger the wavefront admitted (i.e., the larger the aperture in the optical system) the smaller the diffraction pattern of a point source—and the closer together may two point sources be before their diffraction discs overlap and become indistinguishable.

According to the Rayleigh criterion, two point sources are just resolvable if the central maximum of the diffraction pattern of one source just coincides with the first minimum of the other. Thus, the separation of the centers of the patterns equals the radius of the central bright disc. This distance, the minimum separation of two points that can just be resolved, is called the limit of resolution of the instrument. The smaller the distance the greater the resolving power.

The intensity distribution may be calculated for the case of the circular aperture of radius R by summing up the light waves which start from the aperture plane in the same phase and are diffracted by a diffraction angle θ. The intensity distribution is (Ref. 30):

$$I = A_R^2$$

where

$$A_R = \int_0^{2\pi}\int_0^R \rho\cos 2\pi\frac{\rho\cos\phi\sin\theta}{\lambda}\,d\phi\,d\rho$$

$$= \pi R^2\sum_{n=0}^{\infty}(-1)^n\frac{1}{n+1}\left[\frac{m^n}{n!}\right]^2$$

The integration has polar coordinates (ρ, ϕ) at the aperture plane and $m = (\pi R/\lambda)\sin\phi$.

A graph of intensity vs radial distance at the focal plane is presented in Fig. B-8. A second pattern has been superimposed to illustrate the minimum resolution of two points.

I. Modulation Transfer Function

In imaging devices, contrast may be defined by (Ref. 31)

$$C = \frac{I_{min}}{I_{max}}$$

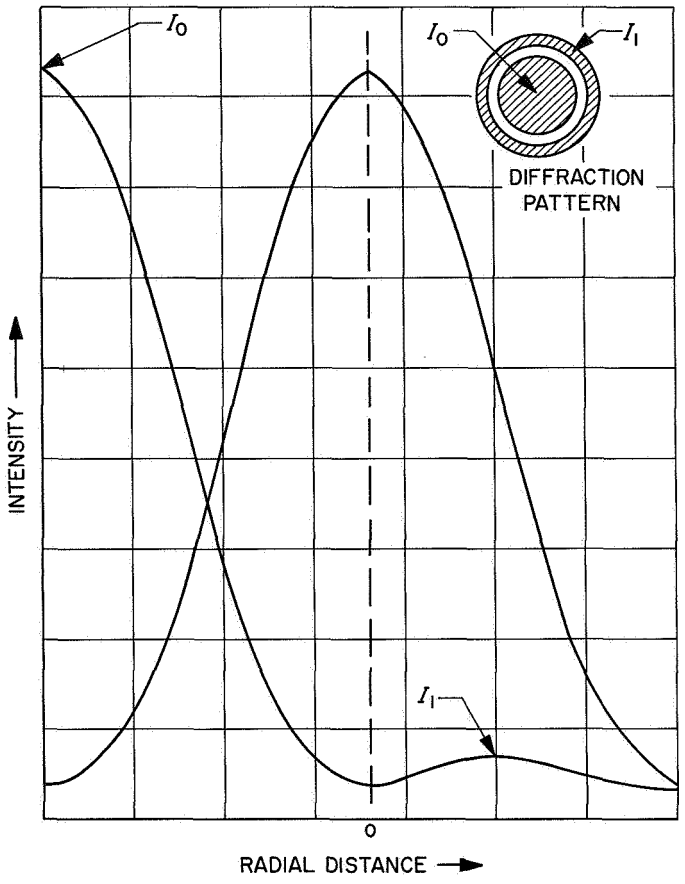

Fig. B-8. Intensity distribution of diffraction pattern for circular aperture

where I is the intensity. $C = 0$ implies maximum contrast and $C = 1$ implies minimum contrast. Modulation is defined by

$$M = \frac{I_{max} - I_{min}}{I_{max} + I_{min}} = \frac{I_v}{I_a}$$

It is clear that $M = 1$ denotes maximum contrast and $M = 0$ denotes minimum contrast. The relation between M and C is

$$M = \frac{1 - C}{1 + C}$$

An optical component may be considered as one or more elements in the information transmission link from scene to presentation. The optics have a transmission characteristic equivalent to a low pass filter network. Hence, the contrast in the image varies according to spatial frequency.

Consider a sinusoidal variation of intensity I with distance x as shown in Fig. B-9. The intensity variation of the object I_0 is

$$I_0 = I_{a0} + I_{v0} \sin 2\pi \frac{x}{x_r}$$

and the intensity variation of the image I_i is

$$I_i = I_{ai} + I_{vi} \sin 2\pi \frac{x'}{x'_r}$$

The relations between the factors of these two equations are

$$\frac{x'}{x_r} = \frac{x'}{x} = m$$

where m is the magnification of the optical system. Also

$$I_{ai} = (\tau) I_{a0}$$

where τ is a constant for the system. Finally

$$I_{vi} = T_{(x'_r)} I_{v0}$$

where $T(x'_r)$ is the modulation transfer function (MTF) for the system. The MTF, a function of space frequency, is a measure of ability of the system to transfer contrast.

If we consider all elements in the transmission link such as atmosphere, lens, and film, then

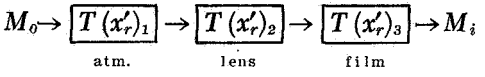

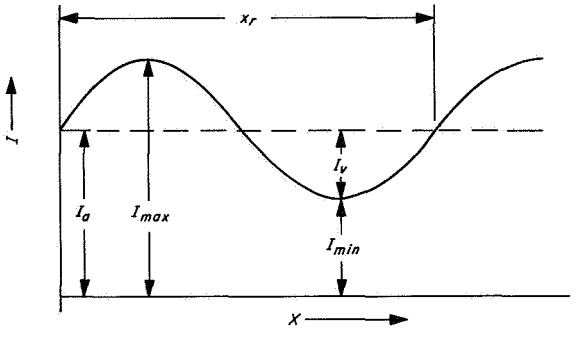

Fig. B-9. Sinusoidal variation of intensity

In general

$$M_i = M_0 \prod_{j=1}^{n} T_j(x'_r)$$

As an example, consider a system of normalized spatial frequency $\bar{\nu}$ which is defined by

$$\bar{\nu} = \delta\nu$$

where ν = sinusoidal spatial frequency in cycles/mm, and $\delta = \lambda f/D_p$ in mm. A plot of the modulation transfer function for the system is given in Fig. B-10. If, in this example, the spot diameter $\delta = 2 \times 10^{-2}$ mm, we have 70% modulation of energy at a spatial frequency of 10 cycles/mm. The modulation at the image falls to 10% at approximately 37 cycles/mm.

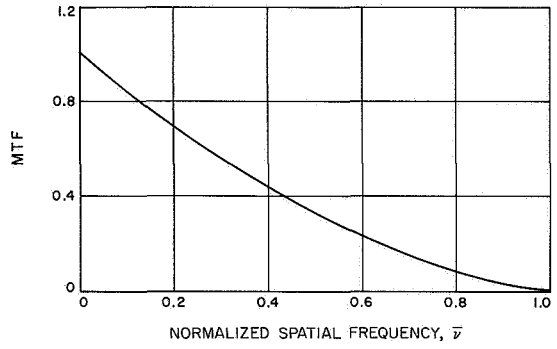

Fig. B-10. Example of modulation transfer function

III. Analysis of Telescope Configurations

A. On-Axis System

The ring aperture, due to central obscuration of the primary mirror, which characterizes the on-axis Cassegrain system, requires special attention. The intensity distribution for a full circular aperture (Section II-H) is

$$I = [A_R]^2$$

where

$$A_R = \int_0^{2\pi}\int_0^{R} \rho \cos 2\pi \frac{\rho \cos\phi \sin\theta}{\lambda} d\phi\, d\rho$$

This equation is modified for the case of a ring aperture as follows (Ref. 30):

$$I = \left[\int_0^{2\pi}\int_r^{R} \rho \cos 2\pi \frac{\rho \cos\phi \sin\theta}{\lambda} d\phi\, d\rho\right]^2$$

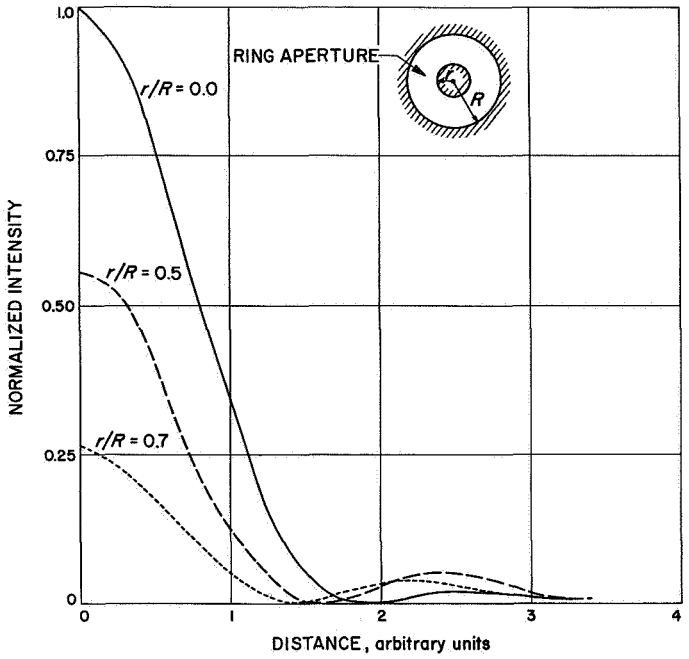

Fig. B-11. Intensity distribution of diffraction pattern for ring aperture

where r is the radius of the central obscuration. Rewriting,

$$I = \left[\int_0^{2\pi}\int_0^{R} \rho \cos 2\pi \frac{\rho \cos\phi \sin\theta}{\lambda} d\phi\, d\rho - \int_0^{2\pi}\int_0^{r} \rho \cos 2\pi \frac{\rho \cos\phi \sin\theta}{\lambda} d\phi\, d\rho\right]^2$$

$$= [A_R - A_r]^2$$

The intensity distribution is plotted in Fig. B-11 for various values of r/R. It is interesting to observe from this graph that the diameter of the central maximum decreases with increasing size of obscuration. The intensity of the central maximum, however, decreases as the radius of the obscuration is increased. This effect is emphasized in Fig. B-12 where I_1/I_0 vs r/R is plotted. I_0 is the intensity of the central maximum and I_1 is the intensity of the first bright ring.

1. Fundamental formulas for telescope design and basic construction parameters. A diagrammatic sketch of the on-axis system is shown in Fig. B-13. By analysis of similar triangles, we obtain the equation

$$\frac{D_p}{D'_s} = \frac{f_p}{p}$$

$$= \frac{f_p}{f_p - L}$$

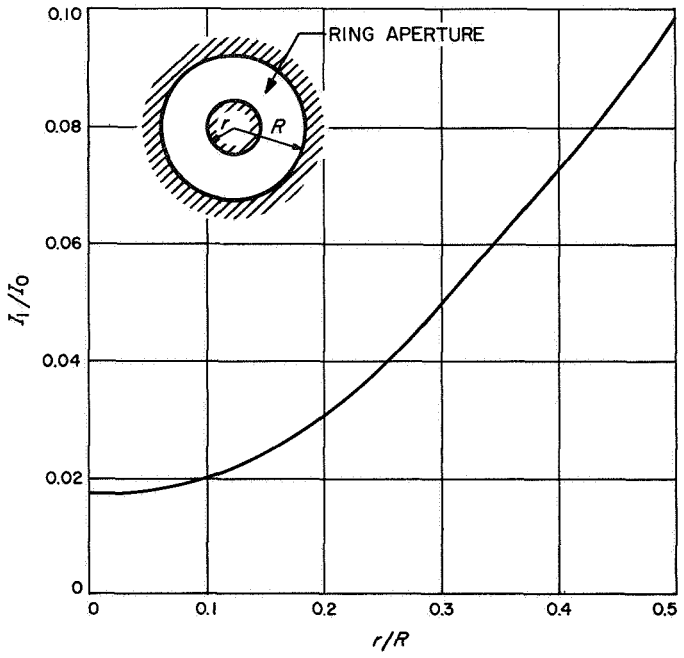

Fig. B-12. Contrast curve for ring aperture

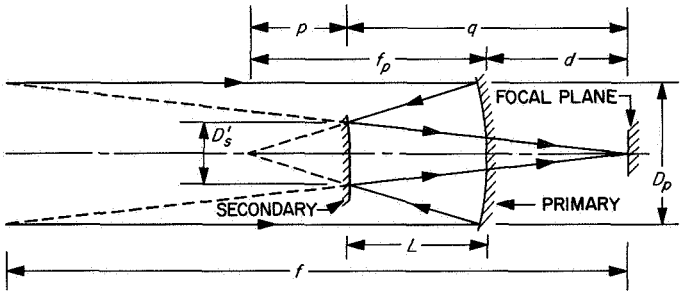

Fig. B-13. Construction for heating factor determination, on-axis system

The heating factor H is conveniently introduced at this point. It is defined by the relation

$$H = \frac{D_p}{D'_s}$$

Heat concentration by the primary on the secondary is proportional to H^2, hence its name. Combining the last two equations

$$H = \frac{f_p}{f_p - L}$$

This equation may be solved for the tube length with the result

$$L = f_p(1 - 1/H)$$

or

$$L = D_p F_p (1 - 1/H)$$

The last expression is deemed a fundamental formula for the design of an on-axis telescope. A graph of this equation is given in Fig. B-14.

Other important formulas are obtained by consideration of the image magnification m. (Image size at the Cassegrain focus is m times the size at the prime focus.) It is recalled that

$$m = \frac{f}{f_p}$$

or, with reference to Fig. B-13,

$$m = \frac{L + d}{p}$$

Rewriting,

$$\frac{f}{L + d} = \frac{f_p}{p}$$

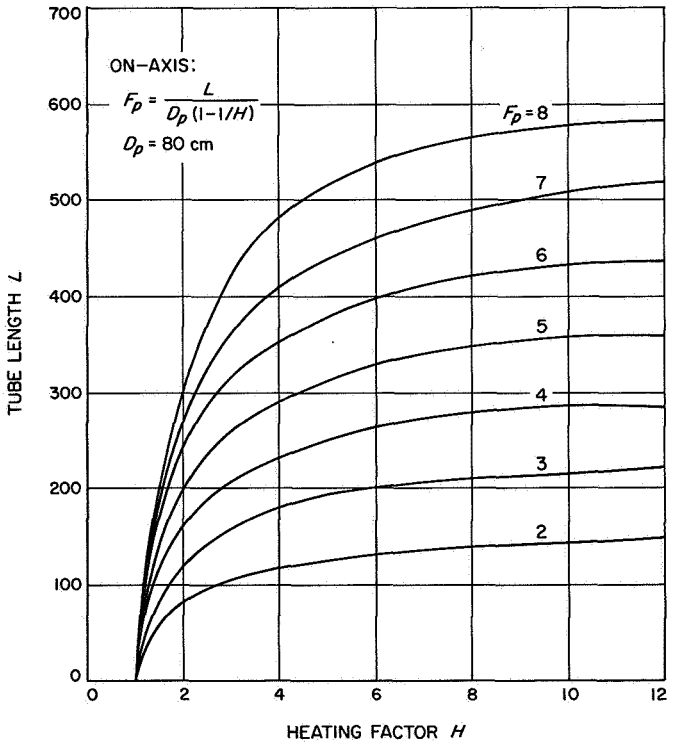

Fig. B-14. Tube length vs heating factor, on-axis system

and noting that the right hand member is equal to the heating factor H, we obtain

$$f = H(L + d)$$

as the second fundamental formula for the design of the on-axis telescope. A graph of the parametric equation is given in Fig. B-15. It is noted that the formulas

$$L = D_p F_p (1 - 1/H)$$

and

$$f = H(L + d)$$

are independent from each other and contain six important construction parameters. They are (1) the tube length L which is limited by the capacity of the spacecraft, (2) the primary diameter D_p which is determined by the desired angular resolution of the optical system, (3) the primary focal ratio F_p which determines the field width at the focal plane and is limited by mirror fabrication techniques, (4) the heating factor H which is of utmost importance in the design of a solar telescope, (5) the equivalent focal length f which determines the final image size and is constrained by the resolution of the emulsion used, and (6) the back focal length d which is vital to the planning of camera location.

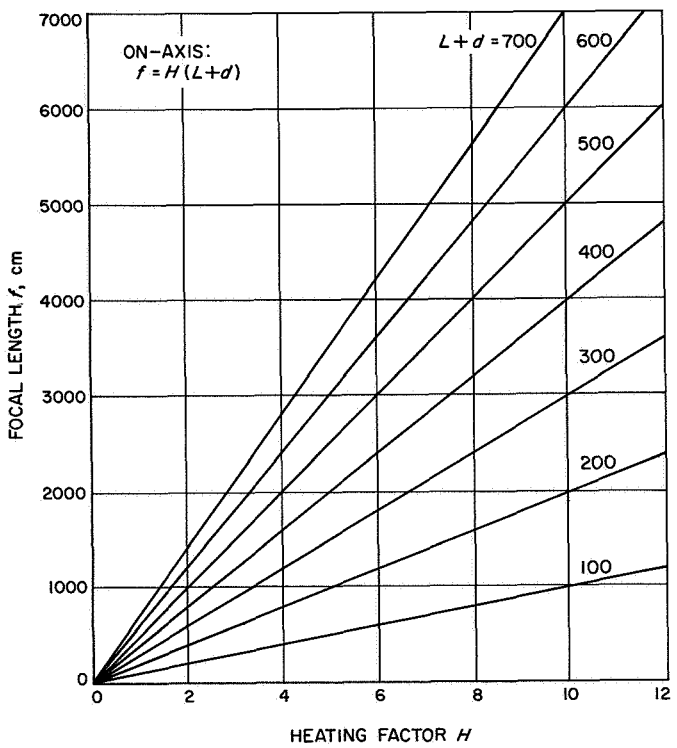

Fig. B-15. Focal length vs heating factor, on-axis system

2. Mask diameter (D_m). An important consideration is depicted in Fig. B-16. It is necessary that the inspection point at the focal plane be masked from direct rays of the Sun. The figure depicts the solar disc in a centered as well as limb viewing position. The minimum diameter of the mask necessary to prevent direct rays of the Sun from reaching the picture frame in focal plane is equal to

$$D_m\,(min) = (L + d)\,2 \tan s + FS$$

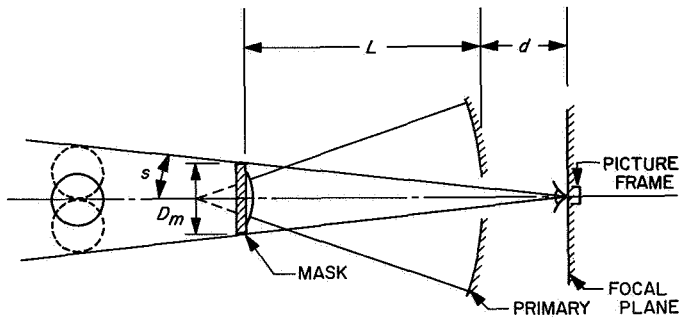

Fig. B-16. Construction for mask diameter determination, on-axis system

3. Diameter of secondary mirror (D_s). The total diameter of the secondary mirror is determined from vignetting considerations. In Fig. B-17 we let $AA' = D'_s$ and $BB' = D_s$. It may be seen from this drawing that D'_s is the illuminated portion of the secondary mirror for an axial port source. It has diameter

$$D'_s = q \tan FOV$$

$$= q \frac{1}{F}$$

Let distance FS' at the prime focus correspond to distance FS on the focal plane. That is, $FS' = FS/m$. If we want to see FS' without vignetting, it is necessary to extend D'_s by an amount larger than $2A'B'$. From Fig. B-17 we see that, very nearly

$$\frac{A'B'}{L} = \frac{FS'/2}{f_p}$$

$$2A'B' = L \frac{FS'}{f_p}$$

$$= L \frac{FS'}{F_p D_p}$$

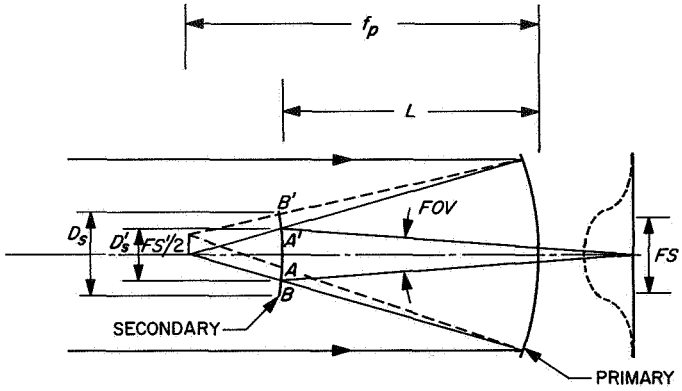

Fig. B-17. Construction for secondary diameter determination, on-axis system

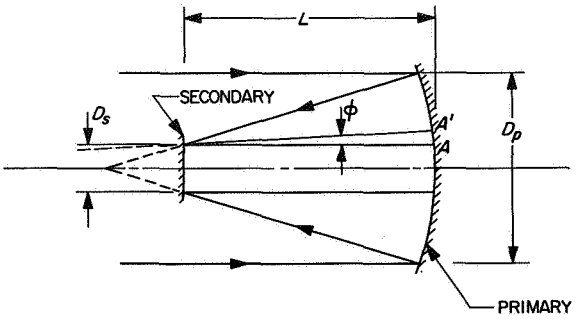

Fig. B-18. Construction for primary hole diameter determination, on-axis system

But, since

$$FS' = \frac{FS}{m}$$

$$= \frac{FS}{F/F_p}$$

we have

$$2A'B' = L\frac{FS}{FD_p}$$

and

$$D_s \geqq D'_s + 2A'B'$$

$$\geqq \frac{q}{F} + L\frac{FS}{FD_p}$$

$$\geqq \frac{1}{F}\left[q + L\frac{FS}{D_p}\right]$$

4. Diameter of primary hole (D_h). The diameter of the mask D_m, dictates very nearly the maximum diameter of the hole in the primary mirror. This is true since the r/R ratio of the ring aperture must be preserved through the tube length of the telescope. However, unless further precaution is taken it is possible that reflected light from the secondary on the primary will be re-reflected to the secondary and go through the hole to the focal plane. To prevent these multiple reflections from reaching the picture frame it is necessary to have a primary hole that is slightly larger than D_s. With reference to Fig. B-18 the necessary extension AA' is found in the following manner.

The angular size α of the field for a particular frame size FS is easily found by noting that

$$\frac{FS}{I} = \frac{\alpha}{s}$$

or

$$\alpha = s\frac{FS}{I}$$

$$= s\frac{FS}{fs}$$

$$= s\frac{FS}{FD_{ps}}$$

$$= \frac{FS}{FD_p}$$

Now, since any ray leaving the secondary with angle $\alpha/2$ (or smaller) about the optical axis is equivalent to one leaving the Sun with the same angle, we have

$$AA' = L\tan\phi$$

$$= L\tan\alpha/2$$

$$= \frac{L}{2}\frac{FS}{FD_p}$$

Thus, the central obscuration of the primary is

$$D_h \geqq D_s + \frac{L \times FS}{FD_p}$$

5. Diameter of re-reflected radiation on primary (D_a). The diameter of re-reflected radiation on the primary mirror is an important consideration in the analysis of a Cassegrainian optical system. This is especially critical to the design of a solar telescope where reflected radiation, that does not pass through the primary, forms a bright ring around the hole that may cause severe thermal gradients in the mirror.

A sketch of the optical system pertinent to this discussion is shown in Fig. B-19. It is noted, with reference to this sketch, that

$$D_a = D_s + 2y$$

Also, by similar triangles

$$\frac{y}{L} = \frac{\frac{I}{2} - \frac{D_s}{2}}{q}$$

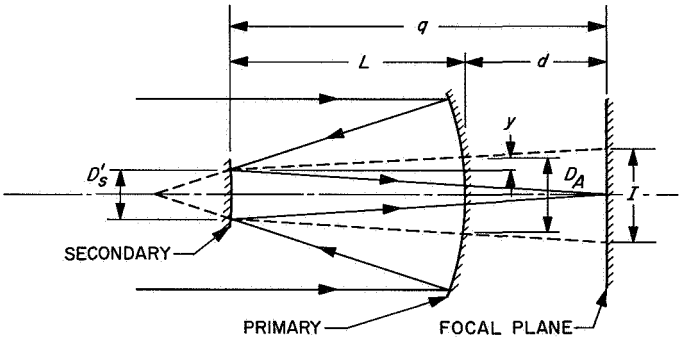

Fig. B-19. Construction for determination of diameter of re-reflected radiation on primary mirror

or

$$2y = \frac{L}{q}(I - D_s)$$

so that

$$D_a = D_s + \frac{L}{q}(I - D_s)$$

when the telescope is pointed at the center of the solar disc.

6. Vignetting by primary mirror. In Section II-G the effect of vignetting by the secondary mirror for a hypothetical transparent primary was discussed and an appropriate equation derived. It is now necessary to examine the effect on this result by an on-axis primary mirror with hole diameter D_h. The pertinent construction is given in Fig. B-19A. It is apparent from this diagram that no vignetting by the primary occurs within a focal plane circle, centered on the optical axis, of radius x_1. Total vignetting, it is also observed, occurs on the focal plane at a radial distance x_2 from the optical axis.

The radius x_1 is easily obtained from Fig. B-19A by analysis of similar triangles. Thus

$$\frac{x_1 - D'_s/2}{L + d} = \frac{D_h - D'_s}{2L}$$

or

$$D_{v1} = 2x_1 = \frac{1}{2}\left[D'_s + (D_h - D'_s)\left(\frac{L + d}{L}\right)\right]$$

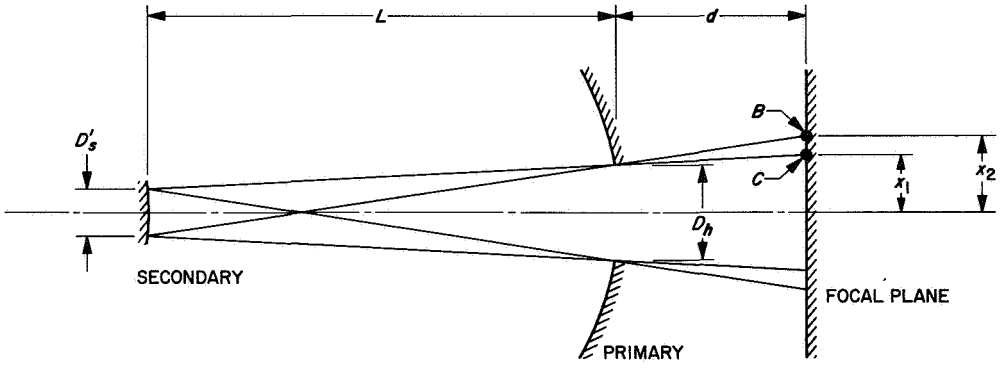

Fig. B-19A. Construction for determination of vignetting by primary mirror, on-axis system

The radius of the circle of maximum vignetting, x_2 is calculated in a similar way. The result is

$$D_{v2} = 2x_2 = (D_h + D_s)\left(\frac{L + D}{L}\right) - D'_s$$

The effect of the primary mirror, then, is truncation of the hypothetical vignetting curve (Section II-G) by a line defined by the points B and C in Fig. B-19A. An application of this effect is illustrated later in Section V-D.

B. Off-Axis System

The off-axis Cassegrainian telescope is obtained by truncating an on-axis system. Advantages of an off-axis system include elimination of the central obscuration by the secondary. This improves image quality and eases the problem of secondary thermal control. Major disadvantages are the expense of a large aperture and very fast primary mirror.

The front view of the off-axis telescope is sketched in Fig. B-20. Since the entrance pupil is not obscured, the intensity distribution of the diffraction pattern for a circular aperture developed in Section II-H applies.

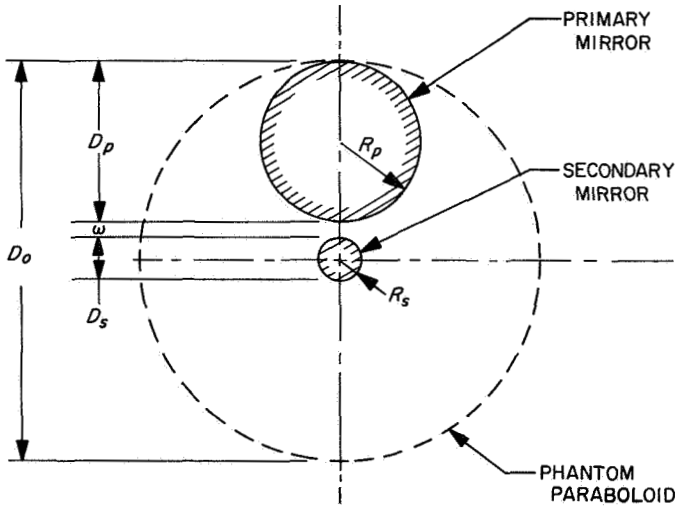

Fig. B-20. Front view, off-axis system

1. Fundamental formulas for telescope design and basic construction parameters. The fundamental formulas for the off-axis system are derived from the construction depicted in Fig. B-21. By making use of similar triangle considerations, we obtain for the primary focal ratio

$$F_p = \frac{L}{2(D_p + \omega)}$$

or

$$L = 2F_p(D_p + \omega)$$

as the first fundamental equation. It is graphed in Fig. B-22. The second fundamental equation, as in the on-axis case, is derived from magnification considerations. That is, since

$$m = \frac{f}{f_p} = \frac{L + d}{p}$$

we have

$$\frac{f}{L + d} = \frac{f_p}{p}$$

But, since

$$H = \frac{D_p}{D'_s} = \frac{f_p}{p}$$

then

$$H = \frac{f}{L + d}$$

or

$$f = H(L + d)$$

As in the on-axis situation this, the second fundamental equation, is independent from the first. It is depicted in graphical form in Fig. B-23.

Summarizing, the fundamental formulas for the off-axis case are

$$L = 2F_p(D_p + \omega)$$

and

$$f = H(L + d)$$

These equations contain seven important construction parameters. The first six are identical to those for the on-axis system (Section III-A-1). The seventh, ω, is the lateral distance between the primary and secondary mirrors.

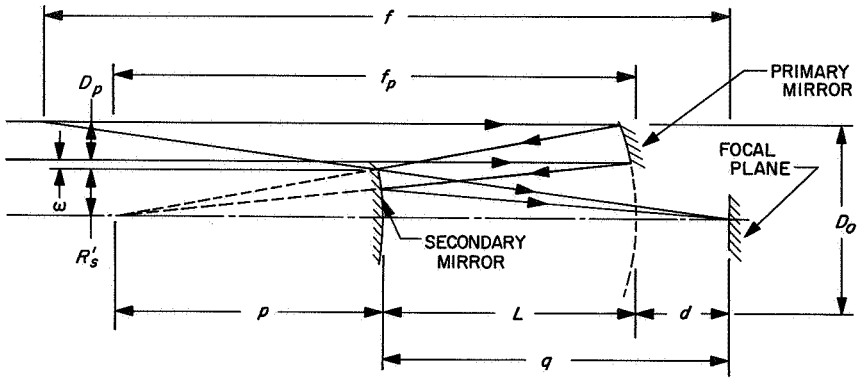

Fig. B-21. Construction for heating factor determination, off-axis system

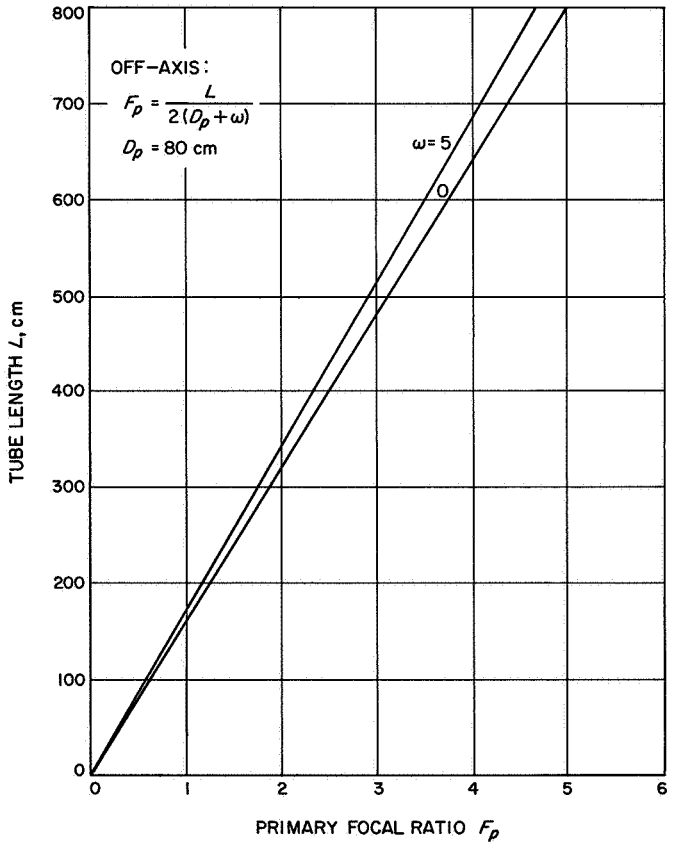

Fig. B-22. Tube length vs primary focal ratio, off-axis system

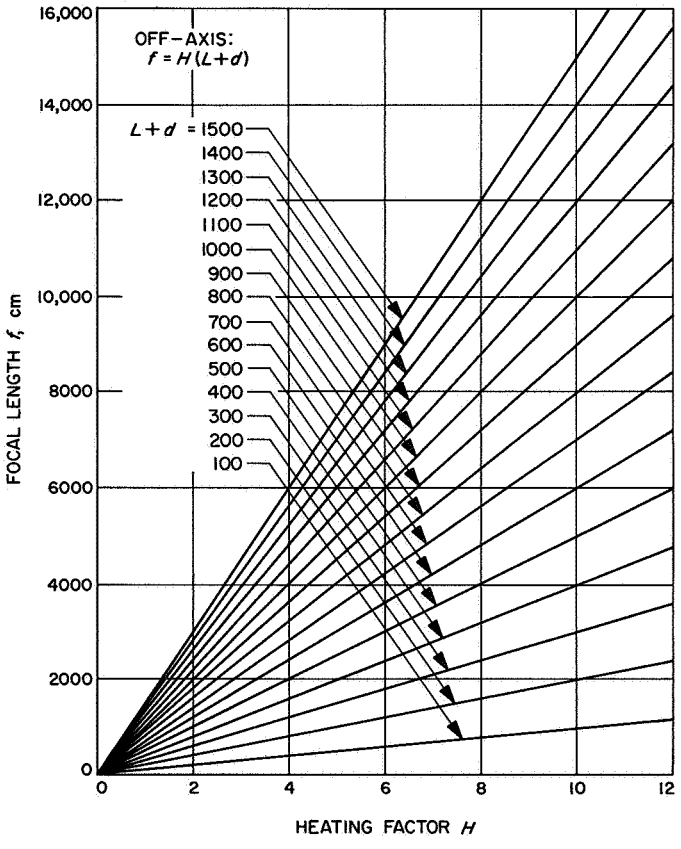

Fig. B-23. Focal length vs heating factor, off-axis system

2. Telescope focal ratio (F). The focal length for the off-axis system is defined by the relation

$$F = \frac{f}{D_0}$$

But, since

$$f = H(L + d)$$

$$F = \frac{H(L + d)}{D_0}$$

A precautionary note is worth mentioning here. In the on-axis configuration we have

$$F = \frac{f}{D_p}$$

whereas in the off-axis situation

$$F = \frac{f}{D_0}$$

Hence the Rayleigh limit

$$\overrightarrow{RL} = \frac{1.22\lambda f}{D_p}$$

equals $1.22\lambda F$ only for the on-axis configuration. Experience has shown that focal length, not focal ratio, is the more desirable parameter for describing a Cassegrain telescope.

3. Radius of secondary mirror (R_s). The radius of the secondary mirror is determined from vignetting considerations. In Fig. B-24 we let $OA = R'_s$ and $OB = R_s$. It is easily seen that R'_s is the illuminated portion of the secondary mirror for an axial point source. It has a radius (Section III-B-2)

$$R'_s = \frac{q}{2}\frac{D_0}{f}$$

where

$$D_0 = 2(D_p + \omega + R'_s)$$

Thus,

$$R'_s = \frac{q(D_p + \omega)}{f - q}$$

Consider a frame size FS. Let distance FS' at the prime focus correspond to FS at the focal plane. That is $FS' = FS/m$. If we want to see FS' without vignetting it is necessary to extend R'_s by an amount larger than AB. From Fig. B-24 we see that, very nearly

$$\frac{AB}{L} = \frac{FS'/2}{f_p}$$

$$2AB = L\frac{FS'}{f_p}$$

But, since

$$FS' = \frac{FS}{m}$$

$$= \frac{FS}{f/f_p}$$

we have

$$AB = \frac{LFS}{2f}$$

and

$$R_s \geqq R'_s + AB$$

$$R_s \geqq \frac{q}{f - q}(D_p + \omega) + \frac{L}{2f}(FS)$$

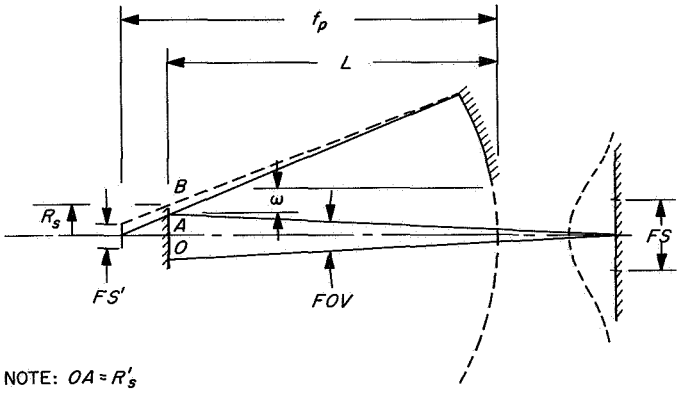

Fig. B-24. Construction for determination of radius of secondary mirror, off-axis system

4. Radius of mask (R_m). It is important, under all viewing conditions, that the picture frame in focal plane be masked from direct rays of the Sun. Figure B-25 depicts the solar disc in a centered as well as limb viewing position. As in the case of the on-axis configuration, the diameter of the mask at the mouth of the telescope is

$$R_m \geqq (L + d)\tan s + FS/2$$

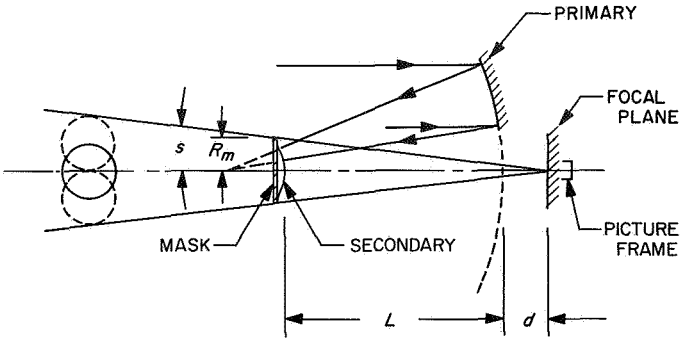

Fig. B-25. Construction for determination of radius of mask, off-axis system

5. Off-distance of primary from optical axis ($R_h = \omega + R'_s$). As with the on-axis configuration the possibility of multiple reflections must be investigated. That is, unless sufficient precaution is taken it is possible that reflected light from the secondary on the primary will be re-reflected to the secondary and pass on to the focal plane. It is necessary to prevent these multiple reflections from reaching the picture frame. Thus, with reference to Fig. B-26, it is important that R_h be slightly larger than R_s. The required extension AA' places a lower limit on an acceptable value for ω. It is found in a manner very similar to that outlined in Section III-A-4.

The angular size α of the field for a particular frame size was found in Section III-A-5 to be

$$\alpha = \frac{FS}{f}$$

and, since any ray leaving the secondary with angle $\alpha/2$ (or smaller) about the optical axis is equivalent to one leaving the Sun with the same angle, we have

$$\begin{aligned} AA' &= L \tan\phi \\ &= L \tan \alpha/2 \\ &= L\frac{FS}{2f} \end{aligned}$$

Thus,

$$R_h \geqq R_s + \frac{L(FS)}{2f}$$

or

$$\omega \geqq (R_s - R'_s) + \frac{L(FS)}{2f}$$

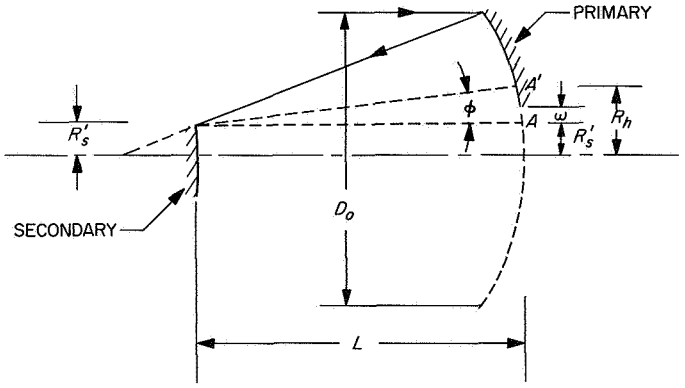

Fig. B-26. Construction for determination of $R_h = (R'_s + \omega)$, off-axis system

6. Radius of re-reflected radiation (R_a). Re-reflected radiation is of extreme interest in the design of an off-axis system. With reference to Fig. B-27 it is observed that a portion of the radiation reflected from the secondary is intercepted by the primary mirror. The radius of the light cone at this position is R_a, and its value is determined as follows.

Using the constructions depicted in Fig. B-24 we have

$$\frac{y}{L} = \frac{\frac{I}{2} - R'_s}{q}$$

or

$$y = \frac{L}{2q}(I - 2R'_s)$$

Since

$$R_a = R'_s + y$$

we obtain

$$R_a = R'_s + \frac{L}{2q}(I - 2R'_s)$$

for the

$$= R'_s\left(1 - \frac{L}{q}\right) + \frac{L}{2q}I$$

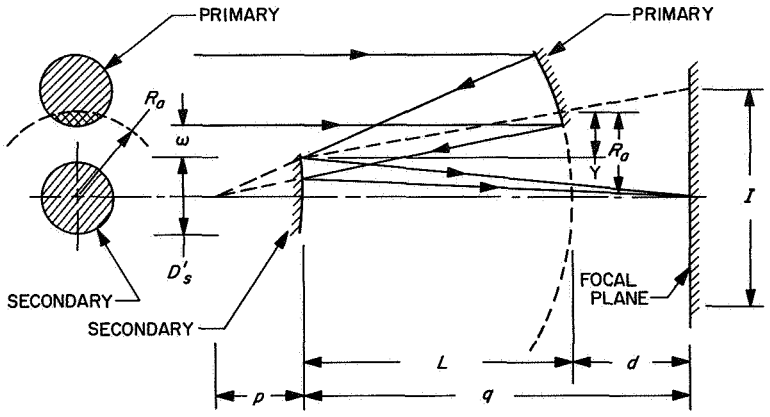

Fig. B-27. Construction for determination of radius of re-reflected radiation, off-axis system

IV. Design of Solar Telescope

A. Telescope Objectives

The proposed telescope is intended for flight aboard the *Apollo* Telescope Mount (ATM). Specific objectives include UV photography of the Sun in the 1500 Å–2500 Å wavelength region, white light motion pictures centered at 5000 Å, and narrow-band photography of the H_α spectrum. It is desired to have a spatial resolution of around 0.1 arc sec for observing the fine structures of the Sun. Spacecraft size and weight capability along with the experimental objectives form rather rigid constraints on the optical design which are discussed in the following paragraphs.

B. On-Axis System

1. Design constraints.

a. Diameter of primary mirror (D_p). A graph depicting resolution of a diffraction-limited telescope as a function of aperture size for various wavelengths is presented in Fig. B-28. Spatial resolution increases as the diameter increases, hence, the largest mirror compatible with the ATM is chosen. It has a diameter of 80 cm. This results in a Rayleigh limit of 0.15 arc sec at $\lambda = 5000$ Å, 0.07 arc sec at $\lambda = 2000$ Å and approximately 0.2 arc sec at $\lambda = 6563$ Å (H_α).

b. Maximum value of the central obscuration. Two components of the telescope are included within the central obscuration. They are the mask (D_m), and primary hole (D_h). In Section III-A the degradation of contrast in the diffraction pattern due to obscuration of the primary is discussed. Data developed in that section are presented in Fig. B-12. Here, the intensity contrast ratio I_1/I_0 is plotted

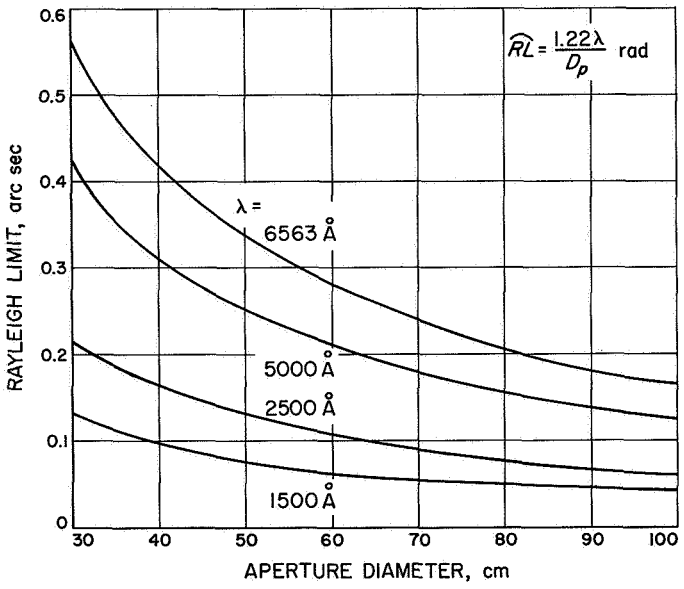

Fig. B-28. Rayleigh criterion vs telescope aperture

as a function of the ring aperture ratio r/R. For high contrast photography, a maximum value of $r/R = 0.20$ corresponding to a cutoff value of $I_1/I_0 = 0.03$ is appropriate.

Hence

$$[D_m, D_H] \leqq 0.2D_p = 16\,\text{cm}$$

for an 80-cm primary.

c. Limiting values of heating factor (H). The heating factor H was defined by the relation

$$H = \frac{D_p}{D'_s}$$

Since D'_s is the illuminated portion of the secondary it follows that

$$D'_s < D_s < D_h$$

According to the discussion of the diffraction pattern in the previous section

$$D'_s < 16$$

Consequently

$$H = \frac{D_p}{D'_s} > \frac{80}{16} = 5$$

Other treatments involving thermal considerations have resulted in a preferred maximum value of H equal to 10. Thus,

$$5 < H \leq 10$$

d. Maximum value for tube length (L). The maximum tube length for the telescope is dictated by the size of the ATM and is

$$L_{max} = 350\,\text{cm}$$

e. Minimum value of primary focal ratio (F_p). A minimum value for F_p has been set at 3 due to manufacturing difficulties involved in faster systems. Also, the off-axis aberrations for $F_p < 3$ are significant.

f. Maximum value of back focus distance (L + d). In Section III-A-2, it was shown that for the on-axis case the minimum value for the mask diameter is given by the equation

$$D_m \geq (L + d)\,2\tan s + FS$$

When this result is combined with the restriction on D_m in Section V-E, we have

$$(L + d)\,2\tan s + FS < 16\,\text{cm}$$

$$(L + d) < \frac{12.5}{0.0186} = 675\,\text{cm}$$

for a frame size $FS = 3.5$ cm.

g. Minimum value of focal length (f). The minimum value of f is determined in the following manner. It is desired to have an angular resolution of 0.07 arc sec at $\lambda = 2000$ Å. Let this angular measurement correspond to a linear interval Δy at the focal plane. Then, since the Sun subtends s sec of arc

$$\frac{\Delta y}{0.07} = \frac{I}{s}$$

where I is the image diameter of the solar disc at the focal plane. Rewriting this equation

$$I = \frac{s}{0.07}\Delta y$$

or

$$f \tan s = \frac{s\Delta y}{0.07}$$

At this point we insist

$$\Delta y \geq g$$

where g is the grain size of the emulsion. Then

$$f \tan s \geq \frac{s}{0.07} g$$

or

$$f \geq \frac{gs}{0.07 \tan s}$$

Now

$$s = 1920\,\text{sec}$$

and for

$$g = 14\mu$$

we have

$$f \geq \frac{14 \times 10^{-4} \times 1920}{0.07 \times 9.3 \times 10^{-3}}$$

or

$$f \geq 4086\,\text{cm}$$

h. Summary, on-axis system. The design constraints developed in the preceding sections are shown as limiting values on the graphs in Figs. B-29 and B-30. Any point lying within the bounded areas of the graphs denotes a system which satisfies the important constraints described

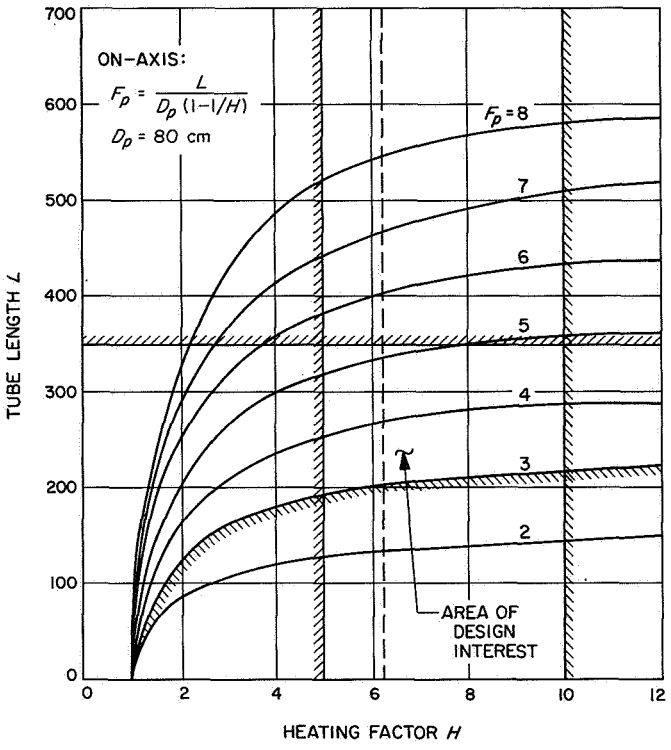

B-29. Design constraint (1), on-axis system

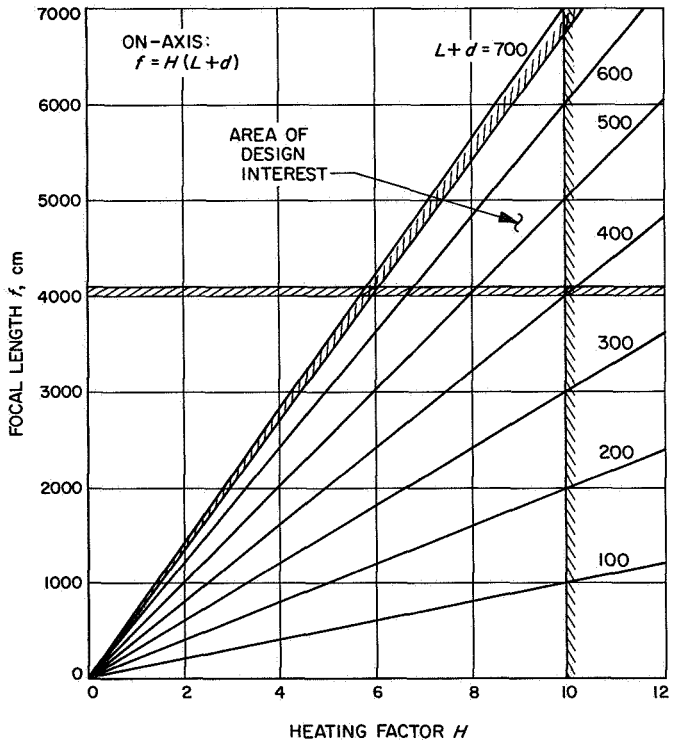

Fig. B-30. Design constraint (2), on-axis system

in Section IV-B-1. A revised value of $H_{min} = 6.1$ from Fig. B-30 has been superimposed on Fig. B-29.

2. Preliminary design of the on-axis solar telescope. Enough information has been presented in the preceding sections to complete a preliminary design of the optical system for the solar telescope.

As discussed in Section IV-B-1-a, a diameter of 80 cm is selected for the primary mirror. The selection of the other basic parameters has some freedom as shown by the areas of design interest in Figs. B-29 and B-30. A primary focal ratio $F_p = 4$ was chosen on the basis of data shown in Fig. B-29. For a value of $H = 9.3$ this choice resulted in a tube length of 286 cm. Adoption of the value $f = 6000$ cm results in a back focus distance $(L + d) = 646$ cm.

A schematic diagram of the optical system is given in Fig. B-31. Key values, which have been described, are

$$D_p = 80\,\text{cm}$$
$$F_p = 4$$
$$H = 9.3$$
$$L = 286\,\text{cm}$$
$$f = 6000\,\text{cm}$$
$$L + d = 646\,\text{cm}$$

Then, using formulas developed in Sections II and III we calculate:

$$F = f/D_p = 75$$
$$m = F/F_p = 18.8x$$
$$I = f \tan s = 55.5\,\text{cm}$$
$$FOV = \tan^{-1}(1/F) = 0.766\,\text{deg}$$
$$f_p = F_p D_p = 320\,\text{cm}$$
$$p = f_p/H = -34.4\,\text{cm}$$
$$D_s' = q/F = 8.6\,\text{cm}$$
$$f_s = \frac{pq}{p-q} = 36.6\,\text{cm}$$
$$D_s \geqq D_s' + \frac{L(FS)}{f} = 8.8\,\text{cm}$$
$$D_m \geqq 2q \tan\Delta + FS = 15.7\,\text{cm}$$
$$D_h \geqq D_s + \frac{L(FS)}{f} = D_s + 0.2$$

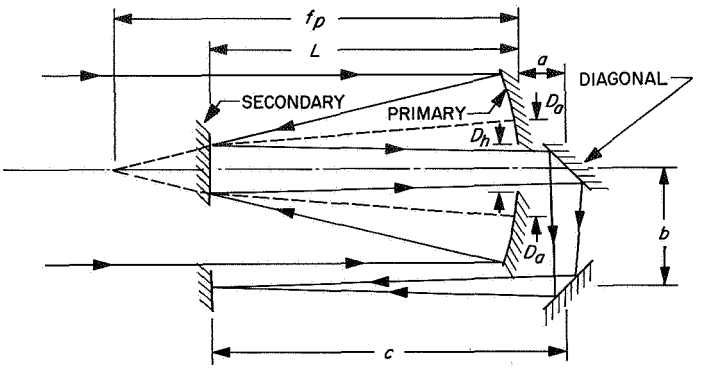

Fig. B-31. Preliminary design, on-axis telescope

The last three relations show that the central obscuration is given by D_m. Since 16 cm is the maximum obscuration permissible (see Section IV-B-1-b) it is possible to adopt the values $D_s = 9.0$ cm and $D_m = D_h = 16$ cm.

An analysis of this design, which includes tolerances, multiple reflections, vignetting and aberrations is presented in Section V.

C. Off-Axis System

1. Design constraints.

a. Diameter of primary mirror (D_p). The selection of D_p, for both the on-axis and off-axis configurations is based on resolution requirements for a diffraction-limited system. A graph depicting resolution as a function of aperture size for various wavelengths was presented earlier in Fig. B-28. By choosing the largest mirror compatible with the ATM, $D_p = 80$ cm, we have (as in the one-axis case) a Rayleigh limit of 0.15 arc sec at $\lambda = 5000$ Å, 0.07 arc sec at $\lambda = 2000$ Å and approximately 0.2 arc sec at $\lambda = 6563$ Å (H_α).

b. Maximum value of tube length (L). The maximum tube length for the telescope is dictated by the size of the ATM and is

$$L_{max} = 350 \text{ cm}$$

c. Maximum value of primary focal ratio (F_p). The first fundamental formula for the off-axis system (Section III-B-1) may be rewritten as

$$F_p = \frac{L}{2(D_p + \omega)}$$

Since $D_p = 80$ cm and $L_{max} = 350$ cm,

$$F_p \leqq \frac{350}{2(80 + \omega)} < \frac{350}{2 \times 80} = 2.19$$

where ω is a positive value.

d. Maximum value of back focus distance ($L + d$). A study of operating characteristics for the inflight system resulted in an optimum location of the cameras around the mouth of the telescope. Hence the appropriate constraint on the back focus distance is

$$L + d \leqq 2L + 100$$

since $L_{max} = 350$ cm, we have

$$L + d \leqq 800 \text{ cm}$$

e. Maximum value of heating factor (H). Studies involving thermal considerations have resulted in establishing a maximum value of the heating factor equal to 10. Thus

$$H \leqq 10$$

f. Minimum value of focal length (f). An expression for the minimum value of f is based on grain size considerations for the emulsion used. It is identical to the expression derived for the m-axis configuration in Section IV-B-1-g which is

$$f_{min} = \frac{g_s}{0.07 \tan s}$$

for a resolution of 0.07 arc sec. Thus, for

$$g = 14\mu$$

and

$$s = 1920 \text{ sec}$$

$$f \geqq 4086 \text{ cm}$$

g. Summary, off-axis system. The design constraints developed in the preceding sections are shown as limiting values on the graphs in Figs. B-32 and B-33.

The situation depicted in Fig. B-33 shows that the off-axis Cassegrain system is not a good candidate for the design of this telescope. That is, in order to have an

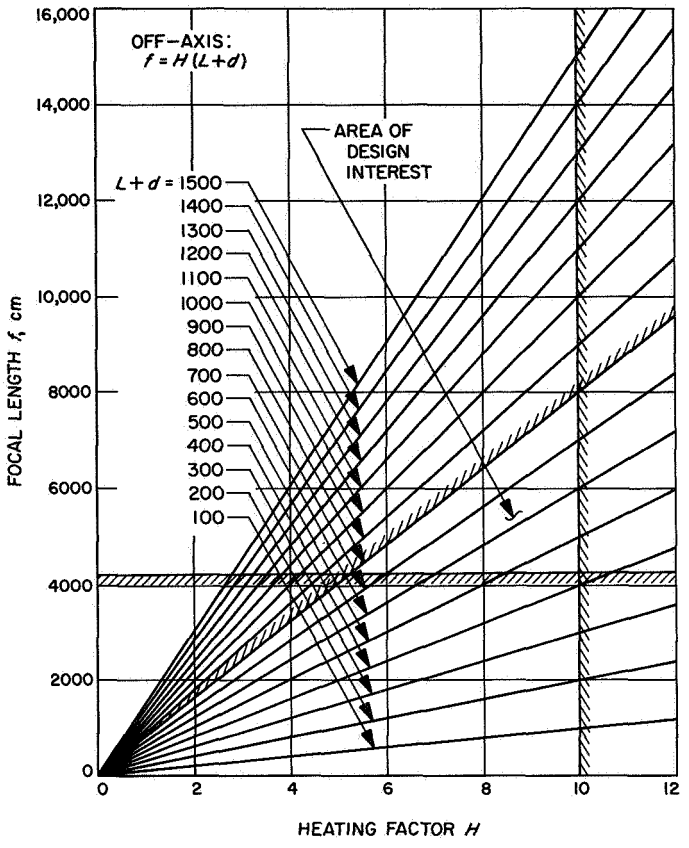

Fig. B-32. Design constraint (1), off-axis system

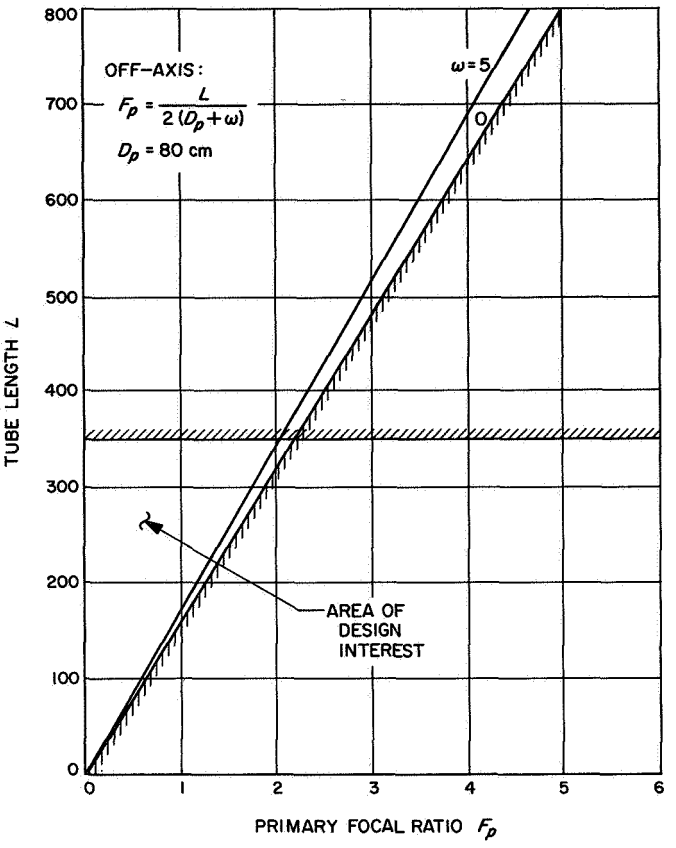

Fig. B-33. Design constraint (2), off-axis system

acceptable tube length of less than 350 cm the primary focal ratio would have to be less than 2.19. The difficulties encountered in the manufacture of such a fast surface ($D_p = 80$ cm) all but preclude this possibility.

Other aspects of the off-axis design, such as the possibility of an unsymmetrical bright area on the primary due to re-reflected radiation, are considered undesirable, and hence support the decision not to use the off-axis design.

Nomenclature

D_a	diameter of re-reflected radiation on primary mirror
D_h	diameter of hole in primary mirror
D_m	diameter of mask
D_0	diameter of paraboloid (off-axis system)
D_p	diameter of primary mirror
D_s	diameter of secondary mirror
D'_s	diameter of illuminated portion of secondary
d	back focus distance
F	focal ratio of telescope
FOV	field of view $= \tan^{-1}(1/F)$
F_p	focal ratio of primary
FS	frame size, film camera
FS'	frame size corresponding to FS at prime focus
FST	frame size, television camera
f	equivalent focal length of telescope
f_p	focal length of primary mirror
H	heating factor
I	image size at focal plane
I_p	image size at prime focus
L	tube length of telescope
m	magnification due to secondary mirror
MTF	modulation transfer function
P	object distance, secondary mirror
q	image distance, secondary mirror
R_a	radius of re-reflected radiation on primary mirror
R_h	off-axis distance of primary mirror
R_m	radius of mask
R_s	radius of secondary mirror
R'_s	radius of illuminated portion of secondary
RL	Rayleigh limit (linear)
$\overrightarrow{RL}$	Rayleigh limit (angular)
s	angular measure of solar disc (1920 seconds = 0.0093 radians)
s'	angular measure of individual solar granule
β_0	radius of entrance pupil
δ_s	diameter of spherical aberration, radians
λ	spectral wavelength
ν	spatial frequency
$\bar{\nu}$	normalized spatial frequency

References

1. "Proposal for Photographic Exploration of the Sun: High Resolution Solar Telescope for the *Apollo* Telescope Mount," Technical Section, Submitted by Calif. Inst. of Tech. and Jet Propulsion Laboratory, 1967.
2. "Surface Distortion Study for Orbiting Solar Telescope Mirrors," JPL IOM, B. K. Wada to L. M. Michal, April 4, 1967.
3. "Optical Technology—*Apollo* Extension System—Part I," Final Technical Report, Vol. I, Contract NAS 8-20256, Space Division, Chrysler Corp., 1966.
4. "Handbook of Physical Constants," Special Paper No. 36, *Geol. Soc. of Am.*, Jan. 31, 1962.
5. "Metallic Materials and Elements for Aerospace Vehicle Structures," MIL-HDBK-5A, D.O.D., Feb. 8, 1966.

References (contd)

6. "Handbook of Thermophysical Properties of Solid Materials," Pergamon Press, WADC Tech. Rept. 58-476, 1960.
7. "Cryogenic Materials Data Handbook," ML-TDR-64-280, PB171809 (Rev.), A. F. Materials Lab., Wright-Patterson AFB, Ohio, 1960.
8. "Beryllium Design Data," LMSD-48472, Lockheed MSD, Sunnyvale, Calif., 1962.
9. "Strength, Efficiency, and Design Data for Beryllium Structures," PB 181324, U. S. Dept. of Commerce, Office of Technical Services, 1963.
10. Brochure, "Beryllium in Aero/Space Structures," The Brush Beryllium Co., 1966.
11. Letter, L. M. Donley, Owens-Illinois Development Center to L. M. Michal, JPL, March 27, 1967.
12. Brochure, "Owens-Illinois Mirror Blanks Made of Low Expansion CER-VIT Material," RO-2, 3-67, 1967.
13. "Invar, 36% Nickel Alloy for Low Temperature Service," Data Sheet 5M 1-67, 4434, International Nickel Co., 1967.
14. Letter, E. A. Bye of Simonds Saw and Steel Co., Lockport, N.Y. to R. A. Happe, JPL, March 30, 1967.
15. Telecon, R. A. Happe, JPL, and W. A. Morgan and D. Hillery of Satellite Experiment Laboratory, ESSA National Environmental Satellite Center, Washington, D.C., April 7, 1967.
16. Telecon, R. A. Happe, JPL, and K. Pierce of Kitt Peak Observatory, April 21, 1967.
17. Telecon, R. A. Happe, JPL, and J. Vern Muffoletto, Muffoletto Optical Co., April 20, 1967.
18. Hale, G. E., "Some Tests of the Snow Telescope," *Contributions from Mount Wilson Solar Observatory,* Vol. 1, p. 57, 1905–1908.
19. Masumoto, Hakar, "On the Thermal Expansion of the Alloys of Iron, Nickel, and Cobalt, and the Cause of the Small Expansibility of Alloys of the Invar Type," *Science Reports,* Tohoku Imp. University, Vol. 20, p. 101, 1932.
20. Letter, W. A. Morgan, ESSA National Environment Satellite Center to R. A. Happe, JPL, April 27, 1967.
21. Bennett, H. E., Silver, M., and Ashley, E. J., "Infrared Reflectance of Aluminum Evaporated in Ultra-High Vacuum," *Journal of the Optical Society of America,* Vol. 53, No. 9, Sept. 1963.
22. Chart, "The Solar Spectrum," Compiled by H. H. Malitson, Calif. Inst. of Tech., 1966.
23. "Metals Handbook," 8th Ed., *Am. Soc. for Metals,* Vol. 2, 1964.
24. Happe, R. A., "Some Materials Problems in Spacecraft," *Mechanical Design of Spacecraft Seminar Proceedings, March 28–May 23, 1962,* JPL Astronautics Information Publication, Aug. 1, 1962.

References (contd)

25. Plunkett, J. D., "NASA Contributions to the Technology of Inorganic Coatings," NASA SP-5014, 1963.

26. Heath, D. F., and Sacher, P. A., "Effects of Simulated High Energy Space Environment of the Ultraviolet Transmittance of Optical Materials between 1050 Å and 3000 Å," *Applied Optics*, Vol. 5, No. 6, June 1966.

27. "Polymers for Spacecraft Hardware: Materials Characterization," Stanford Research Institute, JPL Contract No. 950745 (NAS 7-100), Interim Report #3, March to December 1966.

28. Sears, F. W., and Zemanski, L. P., *College Physics*, Addison-Wesley Press, 1951.

29. Scott, R. M., "Optics for Infrared Systems," Proc. of IRE, p. 1530, Sept. 1959.

30. Wood, R. W., "Physical Optics," Macmillan Co., p. 326, 1936.

31. Brewer, S. H., "Image Evaluation Program," Aerospace Corporation, Report No. TDR-469 (5540-20)-3, pp. 1–4, June 1, 1965.

Bibliography

"Dimensional Stability of Beryllium for High-Precision O Optical Components," Technical Proposal L-0414501-R, General Precision, Inc., Little Falls, N. J., 1966.

Hughel, T. J., "An Investigation of the Precision Mechanical Properties of Several Types of Beryllium," The Institute of Metals 1961 Conference on the Metallurgy of Beryllium, Res. Labs. Gen'l Motors Corp., 1962.

Lement, B. S., Averbach, B. L., and Cohen, Morris, "The Dimensional Behavior of Invar," *Trans. A.S.M.*, pp. 1072–1097, 1951.

Lement, B. S., and Averbach, B. L., "Measurement and Control of the Dimensional Behavior of Metals," Report L-95, Mass. Inst. of Tech., Dec. 1955.

"Mechanical and Physical Properties of Invar and Invar-Type Alloys," Defense Metals Information Center (DMIC), Memorandum 207, Aug. 31, 1965.

"Physical Metallurgy of Beryllium," DMIC Report 230, June 24, 1966.

Principles of Optics, The Perkin-Elmer Corp., Norwalk, Connecticut, 1958.

"Properties of Some Metals and Alloys," Int. Ni Co., 1962.

"Review of Dimensional Instability in Metals," Defense Metals Information Center (DMIC), Memorandum 189, 1964.

"Review of Dimensional Instability in Metals," Defense Metals Information Center (DMIC), Memorandum 213, 1965.

Scott, H., "Expansion Properties of Low Expansion Fe-Ni-Co Alloys," *Trans. A.I.M.E.*, Inst. of Metals Div., p. 506, 1930.

Witherall, C. E., "Welding Nickel-Iron Alloys of the Invar Type," International Nickel Co., Reprinted from *Welding Journal Research Supplement*, April 1964.